THERMAL AND ALKALINE ACTIVATION OF MODEL CLAYS FOR THE PRODUCTION OF GEOPOLYMER BINDERS

Zur Erlangung des akademischen Grades einer

DOKTORIN DER NATURWISSENSCHAFTEN

(Dr. rer. nat.)

von der KIT Fakultät für

Bauingenieur-, Geo- und Umweltwissenschaften

des Karlsruher Instituts für Technologie (KIT)

genehmigte

DISSERTATION

von

M.Sc. Nadja Werling

aus Kandel

Tag der mündlichen Prüfung: 17.11.2022

Referentin: Prof. Dr. Katja Emmerich

Korreferent: PD Dr. Peter Thissen

Karlsruhe 2022

Abstract

Geopolymers are a suitable alternative to cement. The cement and construction industry is responsible for 5 – 8% of the annual global CO_2 emissions. To reduce this negative impact on global warming, it is necessary to reduce the emissions. By using geopolymers as binders in the construction industry, 40 – 80% of the CO_2 emissions could be prevented.

Geopolymers are inorganic binders with a 3-dimensional network of $Si[OH]_4$ and $Al[OH]_4^-$ oligomers. They are formed by the reaction of aluminosilicates with a highly alkaline activator solution. Suitable starting materials are, for example, calcined clay minerals, fly ashes, or blast furnace slags, since they contain large amounts of silicon (Si) and aluminum (Al). NaOH or KOH can be used as activator solutions. Waterglass ($Na_{2x}Si_yO_{2y+x}$) solutions are suitable as well.

Since the availability of fly ash and blast furnace slag will decrease in the coming years, for example due to the reduction of coal-fired power, calcined clay minerals appear to be the most suitable precursor. Clay deposits are widespread worldwide in sufficiently large quantities. By using so-called common clays, which contain a mixture of different clay minerals, geopolymers can be produced economically. The production of geopolymers with pure calcined clay minerals (e.g. metakaolinite) leads to significantly higher costs, compared to cement. Since the various clay minerals differ significantly in their properties (e.g. dehydroxylation temperature, Si:Al ratio, etc.), it is necessary to first investigate the production of geopolymers with different model clay minerals. Based on the findings regarding optimal activation, reaction mechanism and influencing factors of the different clay minerals, statements can be made about the suitability of mixtures of clay minerals.

The subject of this work was the investigation of three different clay minerals (kaolinite, montmorillonite and illite). These were investigated for their thermal activation, called calcination. It is particularly important to determine the optimum activation temperature, which depends on the dehydroxylation behavior of the clay mineral. At the optimum thermal activation, the reactivity of the clay mineral is increased to the maximum. In combination with thermal analyses, the solubility of clay minerals at different calcination temperatures and concentrations of activator solution was investigated. Temperatures of 700 – 750 °C were determined for optimum calcination. The highest solubilities were obtained in the highest concentration of activator solution (10.79 mol/L NaOH). It was found that the solubility was not complete for any of the calcined clay minerals and lay below 90%. Incomplete dissolution would lead to unreacted material, remaining in the cured geopolymers. If the amount of unreacted material is too large, there could be a negative effect on the mechanical properties of a geopolymer.

Besides the experiments on optimal calcination and solubility, investigations on the rehydroxylation behavior of swellable clay minerals were conducted. From the age determination of ancient ceramics, it is known that metakaolinite can recover parts of the structural water after dehydroxylation. In swellable clay minerals, such as montmorillonite, this process occurs as well. It has been shown that rehydroxylation under ambient conditions and slightly increased temperatures (22, 40 & 60 °C, 75% relative humidity) starts after a few hours. The reincorporation of structural water may decrease the reactivity of calcined clay minerals during prolonged storage after calcination. This aspect needs to be investigated in more detail in the future, as it may have an impact on the mechanical properties of geopolymers produced with rehydroxylated calcined clay minerals.

In additional experiments, various blend ratios for geopolymer production were calculated. The Na:Al ratio was fixed at 1:1 and the NaOH concentration and Si:Al ratios were varied. Some mixing ratios were found to be not processable, mostly due to the high solid/liquid ratio. Small discs were prepared from the suitable mixing ratios and used to determine the mechanical properties. Nanoindentation was used to determine Young's modulus and hardness of the geopolymer discs. The results (hardness up to 1.09 GPa) were in the same order of magnitude as already determined for cement. In addition, mercury porosimetry was used to determine the porosity and pore radius of the cured geopolymers. The porosities (20.3 – 31.6%) were comparable to the porosity of cement paste.

Based on the knowledge gained from the investigations carried out, it was concluded that all three investigated calcined clay minerals are suitable as precursor for geopolymers. Furthermore, it can be assumed that a mixture of the calcined clay minerals can be used as a starting material as well.

Kurzfassung

Geopolymere sind eine geeignete Alternative zu Zement. Die Zement- und Bauindustrie ist verantwortlich für 5 – 8% der jährlichen, weltweiten CO_2-Emissionen. Um diesen negativen Einfluss auf die Klimaerwärmung zu verringern, ist es nötig die Emissionen zu reduzieren. Durch die Verwendung von Geopolymeren als Bindemittel in der Bauindustrie, könnten 40 – 80% der CO_2-Emissionen verhindert werden.

Geopolymere sind anorganische Bindemittel mit einem 3-dimensionalen Netzwerk aus $Si[OH]_4$ und $Al[OH]_4^-$ Oligomeren. Sie entstehen durch die Reaktion von Aluminosilicaten mit einer hochalkalischen Aktivatorlösung. Als Ausgangsstoff sind beispielsweise kalzinierte Tonminerale, Flugaschen, oder Hochofenschlacken geeignet, da sie große Mengen Silicium (Si) und Aluminium (Al) enthalten. Als Aktivatorlösung können NaOH oder KOH genutzt werden. Wasserglas ($Na_{2x}Si_yO_{2y+x}$) Lösungen sind ebenfalls geeignet.

Da die Verfügbarkeit von Flugasche und Hochofenschlacke in den kommenden Jahren sinken wird, beispielsweise aufgrund der Reduktion von Kohlestrom, erscheinen kalzinierte Tonminerale als der am besten geeignete Ausgangsstoff. Tonvorkommen sind weltweit in ausreichend großen Mengen vorhanden. Durch die Nutzung sogenannter gemeiner Tone, die eine Mischung verschiedener Tonminerale enthalten, können Geopolymere wirtschaftlich hergestellt werden. Die Herstellung von Geopolymeren mit reinen kalzinierten Tonmineralen (z.B. Metakaolinit) führt zu deutlich höheren Kosten im Vergleich zu Zement. Da die unterschiedlichen Tonminerale sich deutlich in ihren Eigenschaften unterscheiden (z.B. Dehydroxylierungstemperatur, Si:Al Gehalt, etc.) ist es notwendig, zunächst die Herstellung von Geopolymeren mit unterschiedlichen kalzinierten Modelltonmineralen zu untersuchen. Anhand der Erkenntnisse bezüglich optimaler Aktivierung, Reaktionsmechanismus und Einfluss der verschiedenen Tonminerale können Aussagen über die Eignung von Mischungen der kalzinierten Tonminerale getroffen werden.

Gegenstand dieser Arbeit ist die Untersuchung von drei unterschiedlichen Tonmineralen (Kaolinit, Montmorillonit und Illit). Diese wurden auf ihre thermische Aktivierung, auch Kalzinierung genannt, untersucht. Die optimale Aktivierungstemperatur, die abhängig vom Dehydroxylierungsverhalten des Tonminerals ist, muss ermittelt werden. Bei der optimalen thermischen Aktivierung wird die Reaktivität des Tonminerals auf das Maximum gesteigert. In Kombination mit der Analyse des thermischen Verhaltens wurde die Löslichkeit der kalzinierten Tonminerale untersucht. Dabei wurden verschiedene Kalzinierungstemperaturen und Aktivatorlösungen mit unterschiedlichen Konzentrationen verwendet. Eine optimale Kalzinierung wurde bei Temperaturen von 700 – 750 °C erreicht. Die höchsten Löslichkeiten wurden in der höchsten Konzentration der Aktivatorlösung (10.79 mol/L NaOH) erreicht. Jedoch konnte festgestellt werden, dass die Löslichkeit bei keinem der kalzinierten Tonminerale

vollständig war und für alle Proben unter 90% lag. Daraus konnte abgeleitet werden, dass in ausgehärteten Geopolymeren unreagiertes Material zurückbleibt. Zu große Mengen von unreagiertem Material können negative Auswirkungen auf die mechanischen Eigenschaften eines Geopolymers haben.

Neben den Experimenten zur optimalen Kalzinierung und Löslichkeit wurde das Rehydroxylierungsverhalten quellfähiger Tonminerale untersucht. Aus der Altersbestimmung antiker Keramiken ist bekannt, dass Metakaolinit nach der Dehydroxylierung Teile des strukturellen Wassers wieder einbauen kann. Bei quellfähigen Tonmineralen, wie z.B. Montmorillonit, läuft dieser Prozess ebenfalls ab. Es konnte gezeigt werden, dass eine Rehydroxylierung unter Normalbedingungen und leicht erhöhten Temperaturen (22, 40 & 60 °C, 75% relative Luftfeuchtigkeit) bereits nach wenigen Stunden einsetzt. Bei längerer Lagerung nach der Kalzinierung kann der Wiedereinbau strukturellen Wassers die Reaktivität der kalzinierten Tonminerale senken. Dieser Aspekt muss in Zukunft detaillierter untersucht werden, da Auswirkungen auf die mechanischen Eigenschaften der Geopolymere, die mit diesen kalzinierten Tonmineralen hergestellt werden, zu erwaten sind.

Für weitere Versuche wurden verschiedene Mischungsverhältnisse zur Geopolymerherstellung berechnet. Das Na:Al Verhältnis wurde auf 1:1 festgelegt, die NaOH Konzentration und die Si:Al Verhältnisse wurden variiert. Einige Mischungsverhältnisse erwiesen sich als nicht verarbeitbar. Dies lag meist am hohen Feststoff/Aktivatorlösungs Verhältnis. Mit den geeigneten Mischungsverhältnissen wurden kleine Scheiben hergestellt, die zur Ermittlung der mechanischen Eigenschaften genutzt wurden. Mittels Nanoindentation wurden E-Modul und Härte der Geopolymerscheiben bestimmt. Sowohl Härte als auch E-Modul der Geopolymere (Härte bis 1.09 GPa) lagen in der Größenordnung von Zement. Zusätzlich wurden mittels Quecksilberdruckporosimetrie die Porosität und der Porenradius der ausgehärteten Geopolymere bestimmt. Die Porositäten (20.3 – 31.6%) waren vergleichbar mit der Porosität von Zementleim.

Aufgrund der gewonnen Erkenntnisse aus den durchgeführten Untersuchungen wurde geschlussfolgert, dass alle drei untersuchten kalzinierten Tonminerale als Ausgangsstoff für Geopolymere geeignet sind. Außerdem ist anzunehmen, dass auch eine Mischung der kalzinierten Tonminerale als Ausgangsstoff verwendet werden kann.

Table of Contents

1. Introduction

Geopolymers are inorganic binders with a 3-dimensional network which forms due to the reaction of aluminosilicates with a highly alkaline solution. The alkaline activation of aluminosilicates to form a binder material was first described by Gluchovskij (1959). Further research about geopolymers was conducted by Davidovits (1988) who introduced the term "geopolymer". This term refers to the structure which evolves due to polycondensation as "polymer", similar to those in organic chemistry, and "geo" as description of the natural origin of the precursors. In the context of geopolymers, polycondensation is referred to as geopolymerization. (Dehn et al. 2017).

The construction industry is responsible for 5 – 8% of the annual global CO_2 emissions (McLellan et al., 2011). The production of cement clinker contributes to a large extent. Mainly due to the high CO_2 emissions during combustion of limestone ($CaCO_3$) for clinker production and high energy demand for firing of the raw materials at 1400 °C. Geopolymers and supplementary cementitious materials (SCM) are potential substitutes for ordinary Portland cement (OPC). SCM can substitute OPC only partially and show either hydraulic activity like OPC or pozzolanic activity. Geopolymers are OPC free, alkaline activated binders. Alkaline activated binders are subdivided in high Ca and low Ca/Ca-free types (Dehn et al., 2017). Geopolymers are low Ca/Ca-free alkaline activated binders. To reduce the worldwide CO_2 emissions and limit climate change in the future, the CO_2 footprint of the construction industry needs to be reduced. Geopolymers could be the answer to this challenge. The application of geopolymers as binder could reduce the CO_2 emissions of construction industry by 40 – 80% (McLellan et al., 2011; Davidovits, 2013). One of the key points will be making geopolymers competitive concerning properties and costs. The use of calcined common clays as precursors has the potential to reduce the costs for geopolymers significantly compared to the use of calcined mostly pure clay minerals like metakaolinite, since they are available in sufficient amounts in a wide range of regions. Therefore, research on geopolymers produced with calcined common clays is necessary.

Before calcined common clays, which are a mixture of different calcined clay minerals, can be used it is necessary to investigate the behavior of model calcined clay minerals. The dehydroxylation behavior of clay minerals is crucial concerning the reactivity and influences the suitability as a precursor for geopolymers. Clay minerals have varying natural Si:Al ratios, which influences the evolving geopolymer structure and mechanical properties. The knowledge of the behavior of each clay mineral (in its calcined form) as precursor, will help to predict the behavior of mixtures of calcined clay minerals. The aim of this work is to investigate three different clay minerals, which are commonly components of natural common clays, concerning their thermal and alkaline activation and the impact on the produced geopolymers.

1.1 Construction Materials

The term “construction materials” describes different materials used for the construction of buildings and infrastructure. There are natural construction materials (e.g. clay, wood, sand, and natural stone) and processed construction materials (e.g. steel, glass, cement, concrete, and ceramics).

The percentage of concrete used in total construction projects in Germany is larger than for other construction materials (e.g. wood). In 2021 concrete was most used (about 32%) as construction material for residential buildings, followed by bricks (30%) and wood (20%; Statistisches Bundesamt, 2021). In the case of non-residential buildings, such as office and administrative buildings, hotels, agricultural buildings, factory or commercial buildings, reinforced concrete dominated in 2021 with a share of 35% of the approximately 22,358 building permits. Wood was used to about 21% and brick to 11% (Statistisches Bundesamt, 2021).

1.1.1 Cement & Concrete

The term “cement” is used to describe the solid powder after combustion and grinding of the raw materials. “Clinker” is used to describe the intermediate product after combustion, before the endproduct is obtained. The cement hydrates by the addition of water and thus solidifies. Cement paste refers to the hydrated product. The reaction depends on the original composition of the cement. The five main components of OPC are C_3S (Ca_3SiO_5), C_2S (Ca_2SiO_4), C_3A ($Ca_3Al_2O_6$), C_4AF ($Ca_4Al_2Fe_2O_{10}$), and a sulphate phase like gypsum (Wesselsky & Jensen, 2009). Different constituents like limestone, clay, and marl can be used as raw materials. To produce clinker, the raw materials are ground and mixed homogeneously. Subsequently, a combustion step is required in the production of clinker, mostly using rotary kilns. During firing at 1400 °C limestone ($CaCO_3$) is decomposed to lime (CaO). Depending on the requirements for the cement, additional raw materials like quartzsand can be added before grinding. During the mixing step of cement and water, it is possible to add pozzolans or SCM. Gyspsum and anhydrite are widely used to regulate the setting time of cement.

According to DIN EN 197-1 six types of cement are distinguished (Fig. 1). CEM I stands for pure OPC, CEM II for Portland composite cement, CEM III for blast furnace cement, CEM IV for pozzolanic cement, CEM V for ground granulated blast furnace slag pozzolanic cement, and CEM VI for composite cement. Only a composition of 95 – 100% clinker is called OPC.

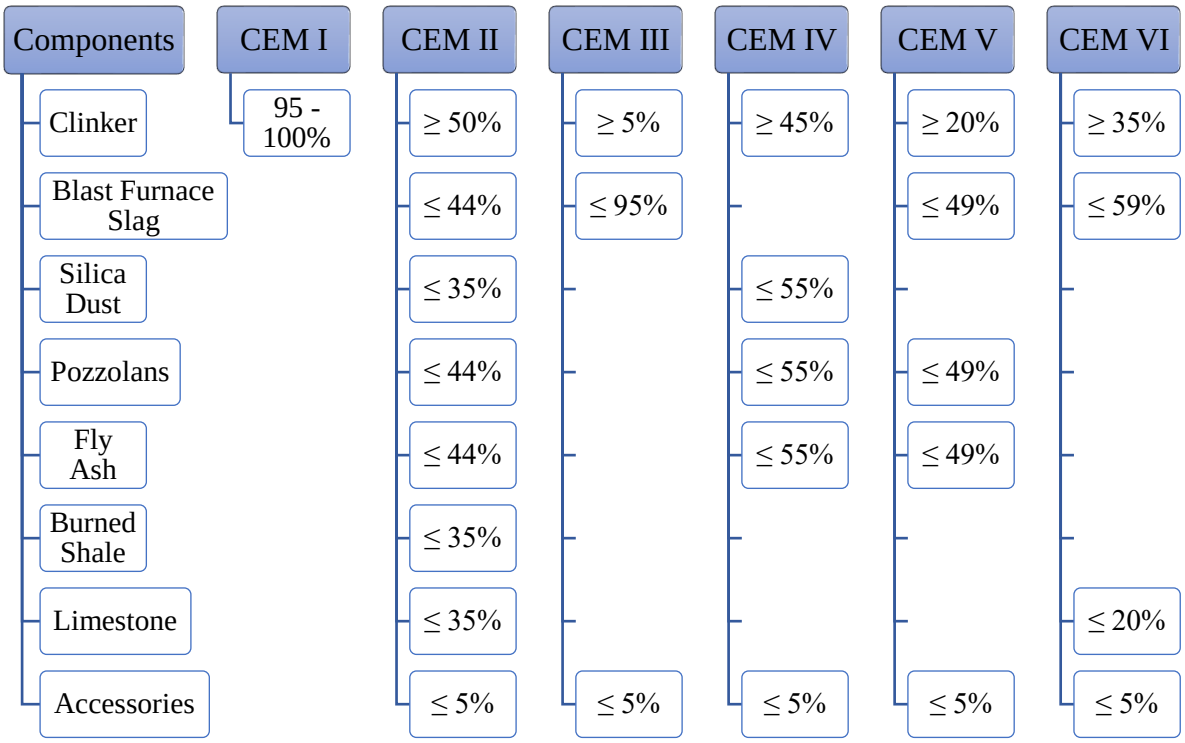

Fig. 1. Products of cements, named according to composition (according to DIN EN 197-1).

By mixing cement with sand, mortar can be obtained. By adding aggregates concrete is produced. During production of cement paste and concrete, additives can be used to regulate the properties of the mixture. Suitable additives (e.g. retarder, superplasticizer, foaming agent, etc.) are described in DIN EN 934-2.

1.1.2 Pozzolans, SCM, and LC[3]

Pozzolans are widely used during mortar or concrete production and contribute to the strength (Achternbosch et al., 2011). Natural pozzolans (e.g. tuff) or technical/artificial pozzolans (e.g. calcined clays, slag, fly ash) can be used. After the formation of calciumhydroxide during hydration of cement (Cement + Water → CSH + $Ca(OH)_2$) the pozzolanic reaction takes place. Pozzolans show a hydraulic reaction with calciumhydroxide and water ($Ca(OH)_2$ + Pozzolan + Water → CSH; ≙ $CaO \cdot SiO_2 \cdot H_2O$; Dodson, 1990). This formation of calciumsilicatehydrates (CSH) and/or calciumaluminatehydrates (CAH) is called pozzolanic reaction. The pozzolanic reaction is important for the long-term strength development.

SCM can be used as a replacement for cement (Lothenbach et al., 2011). Blast furnace slag, fly ash, silica fume, calcined clays, or natural pozzolans are suitable as SCM (Juenger & Siddique, 2015). No additional clinkering process is needed, which can reduce the CO_2 emissions associated with construction industry. Further possible advantages are lower costs, higher long-term strength, and improved durability (Juenger & Siddique, 2015). The use of waste/byproducts can help with waste

treatment in industry. The hydration of cement and hydraulic reaction of SCM occur simultaneously (Lothenbach et al., 2011).

The topic of limestone calcined clay cement (LC^3) has been widely studied recently. The amount of cement clinker is reduced by substituting 50% cement clinker with 30% calcined clay, 15% limestone, and 5% gypsum (LC^3-50; Scrivener et al., 2018). Other mixing proportions are known as well, e.g. LC^3-65 with a clinker content of 65% (Scrivener et al., 2018). Due to the composition and the substitution by a natural pozzolan and limestone, LC^3 could be classified as Portland composite cement (CEMII). In the system various reactions take place, such as cement hydration, pozzonlanic reaction of the calcined clay, and formation of carboaluminates by the reaction of the limestone with alumina phases of cement and calcined clay. Nevertheless, the main proportion of the limestone stays unreacted and acts as a filler (Sharma et al., 2021). One advantage of the use of LC^3 is that the available technologies and procedures can be used for production. LC^3 is already commercially available in several countries (e.g., India).

1.1.3 Geopolymers & Geopolymer Concrete

The term "geopolymer" refers to the binder, after activation of a solid precursor with an alkaline solution. "Geopolymer concrete" refers to the mixture of the binder and aggregates (e.g., gravel), equally to concrete which is a mixture of cement and aggregates.

Geopolymers can be used as replacement for cement paste. In oil extraction industry geopolymers already replace cement paste (Balet-Gouedard et al., 2009). Geopolymers can enclose heavy metals and toxic waste materials (Davidovits, 1989). Geopolymer foams can function as insulating materials (Zhang et al., 2015), e.g. as a replacement for materials containing asbestos. Due to the absence of chemically bound water, geopolymers show good fire resistance. In construction industry geopolymers can, therefore, be used for fire protection (Duxson et al., 2005; Yaseri et al., 2017)

As precursors for geopolymers a wide variety of materials can be used, such as calcined clay minerals, fly ash (waste product of burning coal), furnace slag (waste product from processing of metallic ores), or other aluminosilicate waste materials. Commonly NaOH, KOH, sodium silicate solutions or a combination is used for alkaline activation. Geopolymerization takes place in three subsequent reaction steps. First, dissolution of the aluminosilicate source due to addition of the alkaline solution and, therefore, formation of monomers. Second, reorganization and diffusion of the monomers and formation of a gel. Third, emerging of a 3-dimensional network (Heah et al. 2013; Dehn et al. 2017) with $Si[OH]_4$ and $Al[OH]_4^-$ oligomers which form the framework (Gharzouni et al. 2015). There are three different chemical structures, which can be formed – namely polysialate (PS), polysialate-siloxo (PSS) and polysialate-disiloxo (PSDS) (Davidovits 1989).

Fly ash or blast furnace slag are known as potential precursors for geopolymers. But, as their availability in the upcoming years will decrease, the focus should be on calcined clays as precursors. The availability of fly ash from Germany, for example, will decrease from 2 Mio. tons in 2019 to 0 t in 2035, due to

withdrawal from coal-fired power plants for electricity production. Blast furnace slag availability from Germany will decrease up to one third (Bundesverband Baustoffe – Steine und Erden e.V., 2022). Huge amounts of clays, which can be economically mined, are common clays. Therefore, the costs of geopolymers could be reduced by the use of calcined common clays.

1.1.4 Cement vs. Geopolymer

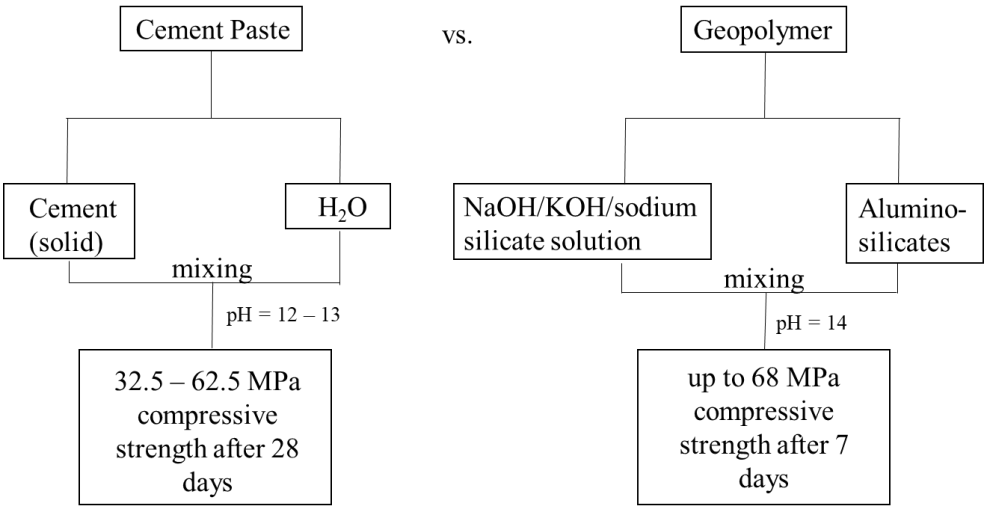

Fig 2. Production of OPC paste and geopolymer and compressive strengths.

The compressive strength of cement pastes after 28 days (DIN EN 197-1) and of geopolymers after 7 days (Yaseri et al., 2017) are in the same order of magnitude (Fig. 2). While in OPC paste the solid cement is mixed with water, in geopolymers the solid precursor is mixed with a highly alkaline solution. This leads to a higher pH value in geopolymer production.

The fire resistance of geopolymers is superior compared to OPC. The spalling resistance of geopolymers is higher and there is no breakdown of the chemical structure (Lahoti et al., 2019). Geopolymers have a superior resistance against chemical attacks (Albitar et al., 2017). The exposure to sulphuric acid up to 9 months has a significant negative impact on OPC with a reduction of compressive strength up to 25%, while the compressive strength of geopolymers is only reduced by 10% after 9 months.

1.2 Environmental Impact

The reduction of CO_2 emissions in construction industry is urged in many ways. The Global Cement and Concrete Association (GCCA; https://gccassociation.org/) is an alliance of international companies with the aim of reducing CO_2 emissions associated with cement and concrete production to net zero in 2050.

1.2.1 Cement & Concrete

The combustion of limestone for clinker production takes place at 1400 °C. During the decomposition of limestone CO_2 is emitted ($CaCO_3$ → $CaO + CO_2$). 100 g of $CaCO_3$ emit 44 g CO_2, which equals 440 kg CO_2 per ton of lime production. Assuming that clinker consists of around 77% $CaCO_3$ (Hökfors et al., 2015), 338.8 kg CO_2 emissions due to $CaCO_3$ combustion for 1 ton of clinker would be emitted. There are additional CO_2 emissions due to the high energy demand for the combustion process. In addition to the release of structural CO_2, about 370 kg CO_2 are produced due to the use of fuels (e.g. gas) and electricity usage. Therefore, a sum of about 709 kg CO_2 per ton of OPC are emitted. According to a mixing ratio of 1:4 (cement to aggregrate), 1 t of concrete would lead to 177.25 kg CO_2 emissions due to the use of cement as binder.

Based on an average value, about 110 kWh electricity per ton cement are needed (Verein Deutscher Zementwerke e.V., 2016). An annual total production of 32,674,000 tons of cement would lead to a total electricity demand of 3.59 TWh. Using an electricity mix with 0.366 kg(CO_2)/kWh (in Germany for 2020; Umweltbundesamt, 2021) a total of about 1.32 Mio t CO_2 would be emitted annually by the electricity demand of cement industry.

1.2.2 Pozzolans, SCM, LC^3

Pozzolans and SCM can reduce the CO_2 emissions associated with the use of cement. The reduction depends on the percentage at which clinker is replaced. For example, in CEM IV (pozzolan cement) clinker can be reduced up to 55%. The reduction of CO_2 emissions by using LC^3 is limited, as a maximum of 50% of the clinker can be replaced without negative impact on the binder properties.

Besides LC^3, the use of oxyfuel technology is being driven forward. During combustion the fuel is burned with nearly pure oxygen instead of air. Parts of the waste gas are recycled and fed back to the furnace (Stanger et al., 2015). With this technology the amount of CO_2 in the waste gas is increased. The CO_2 is then captured and stored after the process. By carbon capture and storage (CCS), cement producing companies want to reach net zero CO_2 emissions for their production. CCS is a promising technology to reduce or prevent further CO_2 emissions into the atmosphere. Limitations of oxyfuel technology result from the fact that changes in the production steps have to be investigated further. For example, higher operation temperatures in the kiln could be necessary and pollutants (e.g., mercury) could be enriched in the gas which is refed to the kiln (Carrasco-Maldonado et al., 2016). An enrichment of pollutants would make an additional removal step necessary. Ongoing research about worldwide storage capacities will be necessary, as well.

The GCCA aims to reach net zero emissions by savings in clinker production (11%), savings in cement and binders (9%), efficiency in concrete production (11%), decarbonization of electricity (5%), CO_2 sink by recarbonation (6%), efficiency in design and contruction (22%), and carbon capture and utilization/storage (36%). During the first decades from 1990 – 2020 a reduction of emissions by around

a fifth, mainly by clinker substitution and fuel side measures, was reached. From 2020 – 2030 an acceleration of reduction of emissions by increasing clinker substitutions, use of alternative fuels, improved efficiency, carbon capture, et cetera is planned. As milestones for this period, 25% of the emissions attributed to concrete and 20% attributed to cement (CO_2 emissions per m^3) are supposed to be avoided by 2030. From 2030 – 2050 the GCCA plans a continuing progress to reach net zero emissions in 2050 (GCCA, 2022).

1.2.3 Geopolymers

As mentioned before geopolymers could save up to 40 – 80% CO_2 emissions in the context of cement industry (McLellan et al., 2011; Davidovits, 2013). In comparison to limestone, clay minerals do not contain structural CO_2. The temperature and, therefore, the energy demand needed for the calcination of clay minerals is lower than for the combustion of limestone. Temperatures in a range of 700 – 800 °C are sufficient for the activation of the clay minerals. For the calcination about 22 kg CO_2 per ton of natural clays are emitted (Beuntner, 2019). The CO_2 emissions associated with the use of fly ash or blast furnace slag as precursors are considered to be zero, as both are waste materials from industry. However, it should be remembered that fly ash will only be available as long as electricity is still generated by coal-fired power plants, which emit non-negligible amounts of CO_2.

It is important to notice that the environmental benefits of geopolymers are reduced by the use of waterglass. During the production of waterglass ($Na_{2x}Si_yO_{2y+x}$) CO_2 is emitted due to the combustion of sodium carbonates, comparable to the emissions during combustion of limestone ($Na_2CO_3 + SiO_2 \rightarrow Na_2SiO_3 + CO_2$; production temperatures around 1200 °C). Therefore, other alkaline solutions should be favored for geopolymer production. The use of NaOH, KOH or sodium silicate solutions produced in the lab emit less CO_2. Sodium silicate solutions can be produced by mixing amorphous silica with NaOH.

Chlor-alkali electrolysis is used to produce potassium-/sodiumhydroxides. The precursors are potassium-/sodiumchloride and water which react to potassium-/sodiumhydroxide, hydrogen, and chlor (anode reaction: $2\ Cl^- \rightarrow Cl_2 + 2\ e^-$; cathode reaction: $2\ H_2O + 2\ e^- \rightarrow H_2 + 2\ OH^-$; $2\ Na^+ + 2\ OH^- \rightarrow 2$ NaOH). This process has an energy demand of 1500 kWh per t NaOH (Staab, 1987). Using the german electricity mix of 2020 (0.366 kg(CO_2)/kWH; Umweltbundesamt, 2021) this energy demand would lead to 549 kg CO_2 per t NaOH. Increased use of electricity from renewable sources could significantly reduce these CO_2 emissions.

Amorphous silica can have different origins, for example, fumed silica is produced at temperatures > 2000 °C in a flame. The precursors are quartzsand and Na-/K-carbonates, which emit CO_2 during firing ($SiO_2 + Me_2CO_3 \rightarrow Me_2SiO_3 + CO_2$). Due to these emissions, fumed silica should not be used as a source of amorphous silica. Silica fume is more sustainable, as it is a byproduct in silicon-/ferrosilicon alloy

production. Furthermore, other waste materials like rice husk ash are suitable as SiO_2 sources (Tchakouté et al., 2016).

In addition, aluminumhydroxide ($Al(OH)_3$) can be used to adjust the Si:Al ratio of geopolymers. $Al(OH)_3$ occurs naturally in form of minerals, e.g. gibbsite. No additional energy is needed for calcination or further treatment. It is also a byproduct during Bayer process, after the main portion of Al from bauxite is extracted. Industrial waste or byproducts are considered to have no additional environmental impact when used for geopolymer production, since they are obtained anyway.

By applying the mixing ratio of 1:4 (binder to aggregate) for OPC concrete, 1 t of geopolymer concrete would lead to 71.38 kg CO_2 emissions (if produced with calcined clay and NaOH). Compared to OPC concrete a reduction of 59.7% of the CO_2 emissions could be reached.

1.3 Geopolymers of Calcined Clays

Clays are naturally occurring materials with different mineral compositions. The main component of a clay is one or several clay minerals. There are four types of clays. First type is kaolin which contains kaolinite as main clay mineral. Second type is bentonite in which the dominating clay minerals are smectites. Third type are so called special clays which contain particular clay minerals (e.g. sepiolite). Fourth type are so called common clays which contain a mixture of different clay minerals.

In many studies calcined clay minerals were proposed as precursors for geopolymers. Most of these studies investigated kaolin bulk material or (quite) pure kaolinite (Duxson et al., 2005; Heah et al., 2013; Lahoti et al., 2017). There are lesser studies where other clay minerals were used (Buchwald et al., 2009; Marsh et al., 2018). Clay minerals differ significantly in their properties, such as chemical composition, thermal behavior, layer charge, swelling capacity, and others. Due to the impact of the properties on the geopolymer production and evolving geopolymer structure, it is necessary to investigate the different clay minerals as precursors separately, before mixtures should be used.

1.3.1 Clay Minerals and Si:Al Ratio

Kaolinite Group

Clay minerals belonging to the kaolinite group are halloysite, dickite, nacrite, and kaolinite. The minerals of the kaolinite group are polytypes, which means that the chemistry is the same, but the stacking is different. The minerals of this group are dioctahedral 1:1 layer silicates with a structural formula of $Si_2Al_2O_5(OH)_4$. All 1:1 layer silicates show recurrent sequences of a tetrahedral sheet followed by an octahedral sheet (Fig. 3). The natural Si:Al ratio is 1:1. The layer silicates of this group are non-swellable.

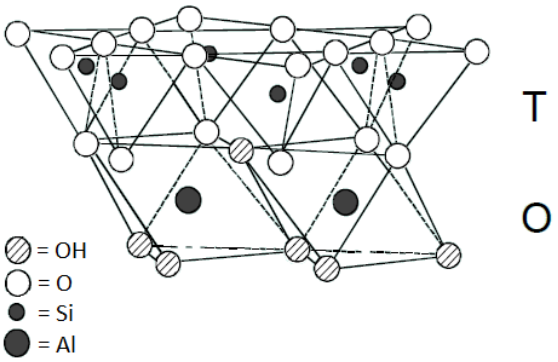

Fig. 3. Crystal structure of minerals from the kaolinite group (modified from Brindley & MacEwan, 1953).

Kaolinite and dickite are based on a 1M stacking sequence with three octahedral sites (A, B, C). In well ordered kaolinite, each layer is identical and has a vacant site B (Brigatti & Mottana, 2011). In dickite the vacant site alternates between B and C in successive layers (Brindley & Brown, 1980). Layers with the vacant site B are called B layers, C layers show the vacant site C. Kaolinites can show defects in their structure, well ordered kaolinites are rare (Izadifar et al., 2020). The disorder can be described by the Hinckley index (Hinckley, 1962). Hinckley index of kaolinites can vary significantly, a Hinckley index around 0.43 indicates a moderate abundance of defects (Plançon et al., 1989). Disorder can be caused, for example, by different tetrahedral and octahedral rotations. The major defect is caused by the translation between adjacent layers. Between the B layers of kaolinite, the existence of some C layers can cause minor defects. It is possible that a kaolinite contains a small amount of dickite layers (Plançon et al., 1989).

Smectite Group

The smectite group includes a large number of dioctahedral and trioctahedral swellable clay minerals, such as montmorillonite, beidellite, nontronite, and others. Smectites are 2:1 layer silicates. Two tetrahedral sheets enclose one octahedral sheet (Fig. 4).

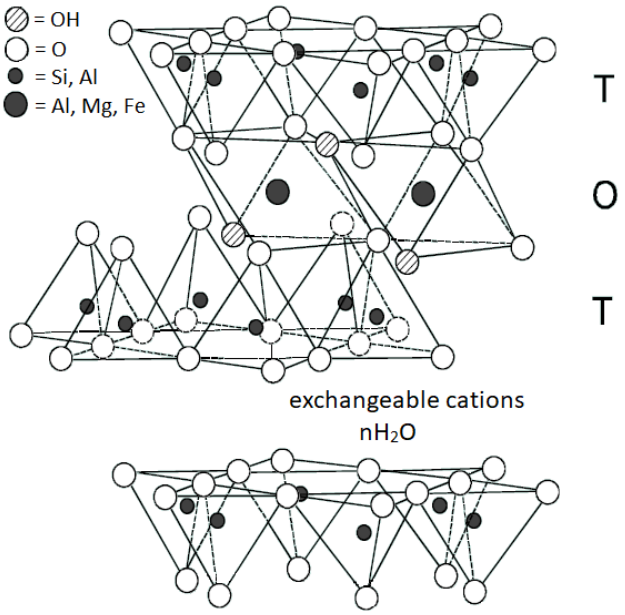

Fig. 4. Crystal structure of minerals from the smectite group (modified from Brindley & MacEwan, 1953 and Borchardt, 1989).

The trioctahedral varieties of smectites are not further discussed here, because the experiments conducted in this work were exclusively with dioctahedral clay minerals. The main difference is that for trioctahedral varieties 3/3 of the octahedron sites are occupied by bivalent cations, while for dioctahedral varieties only 2/3 octahedron sites are occupied by trivalent cations. Due to one unoccupied octahedron site, the distribution of the trivalent cations in dioctahedral clay minerals can be either cis- or trans-vacant (Fig. 5).

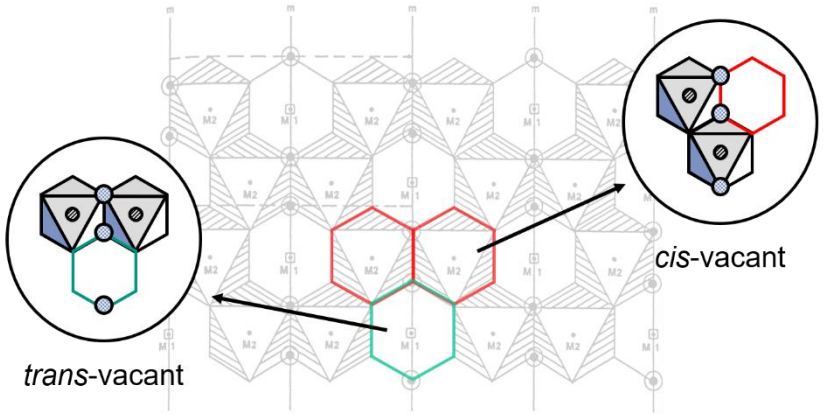

Fig. 5. Distribution of the octahedral vacancies (according to Emmerich, 2000).

Pure cis-vacant (cv) varieties are rare, even if classified as cv they can contain up to 25% trans-vacant (tv) sites (Emmerich et al., 2009). Mixtures of cv/tv sites are most common (Wolters et al., 2009). The general structural formula for dioctahedral clay minerals of this group is $M^{z}_{(x+y)/z}(Si_{4-x}Al_x)(Al_{2-y}Mg_y)O_{10}(OH)_2$ (x+y = 0.2 – 0.6; z = 1 or 2). The natural Si:Al ratio is about 2:1, depending on substitutions of Al^{3+} for Si^{4+} in the tetrahedral sheet and Mg^{2+} or $Fe^{2+/3+}$ for Al^{3+} in the octahedral sheet. Due to these substitutions the clay minerals of this group have a layer charge. The layer charge of minerals from this group lies between 0.2 and 0.6 negative charges per formula unit. In contrast to the kaolinite minerals, smectites contain interlayer cations (Na^+, Ca^{2+}, or Mg^{2+}) to compensate for layer charge. The capacity to exchange those interlayer cations can be determined by cation exchange capacity measurements (see Chapter 3.2) and, subsequently, it is possible to determine which interlayer cations were present.

Illite Group

Illites are di- or trioctahedral, non swellable 2:1 layer silicates. Illite and glauconite are members of the illite group. The difference to the minerals from the smectite group are layer charge and the interlayer cations. The layer charge of illites lies between 0.6 and 0.9 negative charges per formula unit. The interlayer cations of illite are K^+ ions without additional water in the interlayers. As for smectites, two tetrahedral sheets enclose one octahedral sheet (Fig. 6).

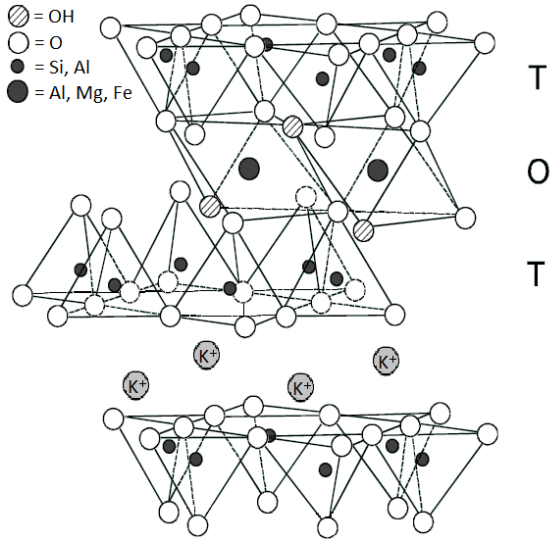

Fig. 6. Crystal structure of minerals from the illite group (modified from Brindley & MacEwan, 1953).

The structural formula of dioctahedral illite is $K_{\zeta=x+y}(Si_{4-x}Al_x)(Al_{2-y}Mg_y)O_{10}(OH)_2$ (ζ = layer charge = x+y = 0.6 – 0.9). The natural Si:Al ratio of illite is 2:1 depending on substitutions.

Besides the described clay mineral groups, there are the mica group, chlorite group, vermiculite group, and others. Which are not further described as they were not included in the conducted experiments.

Micas frequently occur as impurities or accessories in natural clays. In the investigated materials mainly muscovite $K(AlSi_3)(Al_2)O_{10}(OH)_2$ could be found as an impurity.

Si:Al Ratio

The Si:Al ratio (in the range between 1:1 and 3:1) is known to affect the structure of a geopolymer (Fig. 7). The compressive strength of geopolymers can be increased by adjusting the Si:Al ratio. But, Si:Al ratios higher than the optimum (e.g. Si:Al = 4.2 for a solid/liquid ratio = 1.8; Yaseri et al., 2017) can reduce the compressive strength. The setting time of geopolymers is influenced by the Si:Al ratio as well. Higher Si:Al ratios retard the setting, because Si reacts slower compared to Al during geopolymerization (Yaseri et al., 2017). An adjustment of the Si:Al ratio, which differs from the natural Si:Al ratio of the calcined clay mineral precursor, can be made by using waterglass solutions or by adding other Si or Al sources, e.g. silica fume or aluminumhydroxide powders.

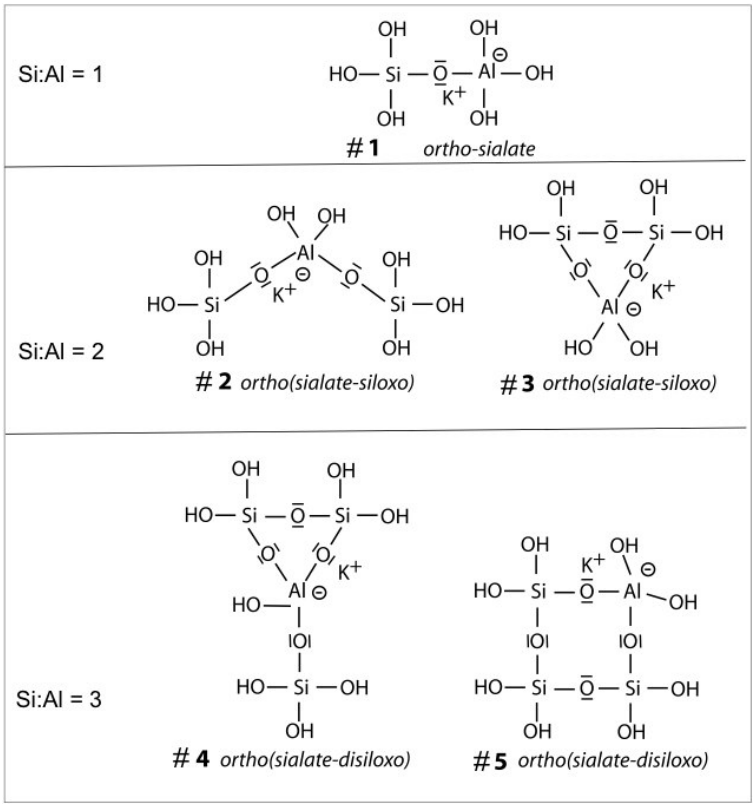

Fig. 7. Geopolymer oligomers in dependence of the Si:Al ratio (Davidovits, 2013).

1.3.2 Thermal Reactions of Clay Minerals and Thermal Activation

Thermal reactions of all clay minerals during heating are dehydration, dehydroxylation, decomposition and recrystallization. During dehydration up to 200 °C the adsorbed water is released. Simultaneously, the interlayer cations of swellable clay minerals are dehydrated up to 300 °C. Due to dehydroxylation,

clay minerals lose their structural water between 450 – 850 °C. Decomposition and recrystallization take place at temperatures > 800 °C.

During dehydroxylation minerals of the kaolinite group lose the structural OH-groups starting at around 500 °C and ending around 700 °C. The following reaction takes place:

$Si_2Al_2O_5(OH)_4 \rightarrow Si_2Al_2O_7 + 2H_2O \uparrow$

Kaolinite minerals have the ability to rehydroxylate after dehydroxylation. During rehydroxylation the structural OH^- groups can be restored to a certain extent. Rehydroxylation of kaolinite minerals can be used for dating of ancient ceramics (Hamilton & Hall, 2012).

The dehydroxylation of minerals of the smectite group strongly depends on the structure. Cis- and trans-vacant varieties of smectites release the structural OH^- groups at different temperatures. Trans-vacant smectites dehydroxylate at temperatures below 600 °C and cis-vacant ones above 600 °C (Emmerich et al., 2009). During dehydroxylation of a smectite, the structural water is released according to the following reaction:

$M^z_{(x+y)/z}(Si_{4-x}Al_x)(Al_{2-y}Mg_y)O_{10}(OH)_2 \rightarrow M^z_{(x+y)/z}(Si_{4-x}Al_x)(Al_{2-y}Mg_y)O_{11} + H_2O \uparrow$

Due to the interlayer cations and swelling ability of smectite minerals, rehydroxylation of minerals of this group can take place under ambient conditions (Derkowski et al., 2012; see chapter 7 for experiments on rehydroxylation).

Minerals from the illite group mainly dehydroxylate at temperatures between 550 – 750 °C. The reaction is similar to other 2:1 layer silicates (e.g. from the smectite group):

$K_{\zeta=x+y}(Si_{4-x}Al_x)(Al_{2-y}Mg_y)O_{10}(OH)_2 \rightarrow K_{\zeta=x+y}(Si_{4-x}Al_x)(Al_{2-y}Mg_y)O_{11} + H_2O \uparrow$

Illites can slowly rehydroxylate, depending on the firing history (Hamilton & Hall, 2012).

By thermal treatment the reactivity of clay minerals can be increased significantly. While uncalcined clay minerals react only to a small amount with alkaline solutions, fully dehydroxylated clay minerals dissolve to around 80% (Werling et al., 2022). There is an optimal temperature range for thermal activation, which depends on the clay mineral type. Thermal activation should be conducted at temperatures between the starting temperature for dehydroxylation and the start of recrystallization. Optimal temperature for calcination of kaolinites lies mostly around 700 °C, for montmorillonites around 800 °C, and between 750 – 800 °C for illites (Garg & Skibsted, 2015; Seiffarth et al., 2013). If temperatures significantly higher than dehydroxylation are used, the reactivity decreases. This happens due to formation of less soluble, less reactive phases when recrystallization starts.

It has to be mentioned that an increase of reactivity of clay minerals was also obtained by mechanical treatment (grinding) which can lead to an amorphization of the material (Sanchez-Soto et al., 2000) and,

therefore, higher reactivity (Balek et al., 2007). But to elevate the reactivity before geopolymer production, thermal activation is the most widely used method.

1.3.3 Alkaline Activation

For alkaline activation either pure NaOH or KOH solutions can be used, which can influence the geopolymer production and properties. Several studies detected a higher solubility of calcined clay minerals in NaOH solutions (Xu & Van Deventer, 2000; Poulesquen et al., 2011). KOH solutions were found to induce higher compressive strengths of the hardened geopolymers (Xu & Van Deventer, 2003). A higher extent of dissolution of the precursor increases the compressive strength for geopolymers prepared with the same alkaline solution, but even higher dissolution rates in NaOH cannot compensate for the higher strength development when KOH is used (Xu & Van Deventer, 2000). Many studies were conducted using sodium silicate solutions with a general structural formula of $Na_{2x}Si_yO_{2y+x}$ ($x = 1 – 3$; $y = 1 – 4$) which is commonly known as waterglass (Duxson et al., 2005; Poulesquen et al., 2011). Alkaline solutions (NaOH, KOH) or mixtures of waterglass and NaOH or KOH were used as well (Buchwald et al., 2009; Provis & Bernal, 2014; Marsh et al., 2018). The cations of the alkaline activator solution (Na^+ or K^+) balance the negative charge resulting from the charge difference of Si^{4+} and Al^{3+} in the emerging geopolymer structure. Nevertheless, if there is an excess of cations, carbonation is induced (Werling et al., 2020), which can influence the properties of the geopolymer binder. The concentration of the alkaline activator solution influences workability, stability and emerging compressive strength. While the compressive strength increases proportionally with the concentration due to a higher extent of dissolution, the workability decreases and vice versa. Geopolymers produced with NaOH show a faster setting time, than those produced with KOH, which can also reduce the workability (Poulesquen et al., 2011).

1.3.4 (Heat-)Curing

After mixing the solid precursors with the alkaline activator, geopolymers harden at ambient conditions (room temperature, ambient pressure, and a relative humidity of about 50%). But for some solid precursors an enhanced performance for the geopolymers was observed at elevated temperatures (60 – 90 °C). Especially in case of fly ash precursors, elevated curing temperatures are used to increase the compressive strength (Patankar et al., 2014). In case of temperatures above 90 °C, increased shrinkage and cracking was observed and, consequently, lower compressive strengths (Patankar et al. 2014). For clay precursors curing of the geopolymers at elevated temperatures is not necessary (Rovanik, 2010).

The same precursors can be used to either produce geopolymers or zeolites. Geopolymer production and zeolite synthesis differ in terms of temperature and pressure used during the synthesis process. Hydrothermal synthesis in aqueous solutions is used for zeolite production. For hydrothermal synthesis high temperatures (> 100 °C up to 1000 °C) and high pressures (> 1 bar up to 3000 bar) in a closed system (e.g. autoclave) are used (Milton, 1989; Yu, 2007).

If curing takes place in unsealed containers the initial water loss/evaporation is larger, compared to curing in sealed containers for 24 h. But, most of the excess water leaves the geopolymer structure during aging (up to 21 days) independently from un-/sealed curing during the first 24 h (Lizcano et al., 2012). Therefore, curing in un-/sealed containers does not change the water content in the final geopolymer. The main advantage of curing in sealed containers is the inhibited formation of efflorescence, which takes place due to carbonation of the alkali ion in the activator solution, during the hardening of the geopolymer.

1.3.5 Additives

The cement industry can offer a wide range of additives. For geopolymers especially superplasticizers are needed to enhance the workability. For example, PCE superplasticizers are incompatible with high basic media like the activator solutions of geopolymers. Investigations on the manufacturing of bio-based plasticizers customized for the use in geopolymers indicated that starch-superplasticizers showed promising improvements (Tutal et al., 2020).

References

Achternbosch, M., Kupsch, C., Nieke, E., & Sardemann, G. (2011). Climate-Friendly Production of Cement: A Utopian Vision? *GAIA-Ecological Perspectives for Science and Society, 20(1),* 31-40.

Albitar, M., Ali, M. M., Visintin, P., & Drechsler, M. (2017). Durability evaluation of geopolymer and conventional concretes. *Construction and Building Materials, 136,* 374-385.

Balek, V., Pérez-Maqueda, L., Poyato, J., Černý, Z., Ramírez-Valle, V., Buntseva, I., & Pérez-Rodríguez, J. (2007). Effect of grinding on thermal reactivity of ceramic clay minerals. *Journal of Thermal Analysis and calorimetry, 88(1),* 87-91.

Barlet-Gouedard, V., Porcherie, O., & Pershikova, E. (2009). Pumpable geopolymer formulation for oilfield application. *World Patent WO/2009/103480,* 28.

Beuntner, N. (2019). Zur Eignung und Wirkungsweise Calcinierter Tone als Reaktive Bindemittelkomponente im Zement. *Dissertation,* Neubiberg, Universität der Bundeswehr München, 2017.

Borchardt, G. (1989). Smectites. *Minerals in soil environments, 1,* 675-727.

Brigatti, M. F., & Mottana, A. (Eds.). (2011). *Layered mineral structures and their application in advanced technologies (Vol. 11).* The Mineralogical Society of Great Britain and Ireland.

Brindley, G.W., & Brown, G. (editors) (1980). *Crystal structures of clay minerals and their X-ray identification (Vol. 5).* Mineralogical Society, Monograph 5, London.

Brindley, G. W., & MacEwan, D. M. (1953). Structural aspects of the mineralogy of clays and related silicates. *Ceramics: A Symposium,* The British Ceramic Society, 15-59.

Buchwald, A., Hohmann, M., Posern, K., & Brendler, E. (2009). The suitability of thermally activated illite/smectite clay as raw material for geopolymer binders. *Applied Clay Science, 46(3),* 300-304.

Bundesverband Baustoffe – Steine und Erden e.V. (2022). Die Nachfrage nach Primär- und Sekundärrohstoffen der Steine-und-Erden-Industrie bis 2040 in Deutschland. https://www.baustoffindustrie.de/fileadmin/user_upload/bbs/Dateien/Downloadarchiv/Rohstoffe/2022-04-20_BBS_Rohstoffstudie_01_ONLINE.pdf

Carrasco-Maldonado, F., Spörl, R., Fleiger, K., Hoenig, V., Maier, J., & Scheffknecht, G. (2016). Oxy-fuel combustion technology for cement production–state of the art research and technology development. *International journal of greenhouse gas control, 45,* 189-199.

Davidovits, J. (1988). Geopolymer chemistry and properties. *Geopolymer, Vol. 88,* No.1.

Davidovits, J. (1989). Geopolymers and geopolymeric materials. *Journal of thermal analysis, 35(2),* 429-441.

Davidovits, J. (2013). Geopolymer cement. A review. *Geopolymer Institute, Technical papers, 21,* 1-11.

Dehn, F., Koenig, A., & Herrmann, A. (2017). Alkalisch-aktivierte Bindemittel und Geopolymer-Bindemittel als Alternative zu Zement. *Neue Herausforderungen im Betonbau,* 155-170

Derkowski, A., Drits, V. A., & McCarty, D. K. (2012). Nature of rehydroxylation in dioctahedral 2: 1 layer clay minerals. *American Mineralogist, 97(4),* 610-629.

DIN e.V. (Hrsg.) (DIN EN 197-1:2014, 2016-11): DIN EN 197-1:2014, Zement – Teil 1: Zusammensetzung, Anforderungen und Konformitätskriterien von Normalzement, Beuth-Verlag, Berlin.

DIN e.V. (Hrsg.) (DIN EN 934-2:2009+A1:2012, 2016-11): DIN 934-2:2009+A1:2012, Zusatzmittel für Beton, Mörtel und Einpressmörtel – Teil 2: Betonzusatzmittel – Definitionen, Anforderungen, Konformität, Kennzeichnung und Beschriftung, Beuth-Verlag, Berlin.

Dodson, V. H. (1990). Pozzolans and the pozzolanic reaction. *Concrete admixtures*, Springer, Boston, MA, 159-201.

Duxson, P., Provis, J. L., Lukey, G. C., Mallicoat, S. W., Kriven, W. M., & Van Deventer, J. S. (2005). Understanding the relationship between geopolymer composition, microstructure and mechanical properties. *Colloids and Surfaces A: Physicochemical and Engineering Aspects, 269(1-3),* 47-58.

Emmerich, K. (2000). Die geotechnische Bedeutung des Dehydroxylierungsverhaltens quellfähiger Tonminerale. *Doctoral dissertation (Vol. 13508),* Veröffentlichung des Instituts für Geotechnik (IGT) der ETH Zuerich.

Emmerich, K., Wolters, F., Kahr, G., & Lagaly, G. (2009). Clay profiling: the classification of montmorillonites. *Clays and Clay Minerals, 57(1),* 104-114.

Garg, N., & Skibsted, J. (2015). Heated montmorillonite: structure, reactivity, and dissolution. *In Calcined Clays for Sustainable Concrete*, 117-124.

GCCA – Global Cement and Concrete Association (2022). GCCS Concrete Future – Roadmap to Net Zero. https://gccassociation.org/concretefuture/wp-content/uploads/2021/10/GCCA-Concrete-Future-Roadmap-Document-AW.pdf

Gharzouni, A., Joussein, E., Samet, B., Baklouti, S., & Rossignol, S. (2015). Effect of the reactivity of alkaline solution and metakaolin on geopolymer formation. *Journal of Non-Crystalline Solids, 410*, 127-134.

Gluchovskij, V.D. (1959): Gruntosilikaty. Grosstrojizdat Kiev, Patent USSR 245627 (1967), Patent USSR 449894.

Hamilton, A., & Hall, C. (2012). A review of rehydroxylation in fired-clay ceramics. *Journal of the American Ceramic Society, 95(9), 2673-2678.*

Heah, C. Y., Kamarudin, H., Mustafa Al Bakri, A. M., Bnhussain, M., Luqman, M., Khairul Nizar, I., Ruzaidi, M., & Liew, Y. M. (2013). Kaolin-based geopolymers with various NaOH concentrations. *International Journal of Minerals, Metallurgy, and Materials, 20(3),* 313-322.

Hinckley, D. N. (1962). Variability in "crystallinity" values among the kaolin deposits of the coastal plain of Georgia and South Carolina. *Clays and clay minerals, 11(1),* 229-235.

Hökfors, B., Boström, D., Viggh, E., & Backman, R. (2015). On the phase chemistry of Portland cement clinker. *Advances in Cement Research, 27(1),* 50-60.

Izadifar, M., Thissen, P., Steudel, A., Kleeberg, R., Kaufhold, S., Kaltenbach, J., Schuhmann, R., Dehn, F., & Emmerich, K. (2020) Comprehensive examination of dehydroxylation of kaolinite, disordered kaolinite, and dickite: Experimental studies and Density Functional Theory. *Clays and Clay Minerals, 68(4),* 319-333.

Juenger, M. C. G., & Siddique, R. (2015). Recent advances in understanding the role of supplementary cementitious materials in concrete. *Cement and Concrete Research, 78*, 71-80.

Lahoti, M., Narang, P., Tan, K. H., & Yang, E.-H. (2017). Mix design factors and strength prediction of metakaolin-based geopolymer. *Ceramics International, 43(14),* 11433-11441.

Lahoti, M., Tan, K. H., & Yang, E.-H. (2019). A critical review of geopolymer properties for structural fire-resistance applications. *Construction and Building Materials, 221,* 514-526.

Lizcano, M., Gonzalez, A., Basu, S., Lozano, K., & Radovic, M. (2012). Effects of water content and chemical composition on structural properties of alkaline activated metakaolin-based geopolymers. *Journal of the American Ceramic Society, 95(7),* 2169-2177.

Lothenbach, B., Scrivener, K., & Hooton, R. D. (2011). Supplementary cementitious materials. *Cement and Concrete Research, 41(12),* 1244-1256.

Marsh, A., Heath, A., Patureau, P., Evernden, M., & Walker, P. (2018). Alkali activation behaviour of un-calcined montmorillonite and illite clay minerals. *Applied Clay Science, 166,* 250-261.

McLellan, B. C., Williams, R. P., Lay, J., van Riessen, A., & Corder, G. D. (2011). Costs and carbon emissions for geopolymer pastes in comparison to ordinary portland cement. *Journal of Cleaner Production, 19(9),* 1080-1090.

Milton, R. M. (1989). Zeolite synthesis. *In ACS Symposium Series, Vol. 398,* 1-10.

Patankar, S. V., Ghugal, Y. M., & Jamkar, S. S. (2014). Effect of concentration of sodium hydroxide and degree of heat curing on fly ash-based geopolymer mortar. *Indian Journal of Materials Science,* 2014.

Plançon, A., Giese, R., Snyder, R., Drits, V., & Bookin, A. (1989). Stacking faults in the kaolin-group minerals: Defect structures of kaolinite. *Clays and Clay Minerals, 37(3),* 203-210.

Poulesquen, A., Frizon, F., & Lambertin, D. (2011). Rheological behavior of alkali-activated metakaolin during geopolymerization. *Journal of Non-Crystalline Solids, 357(21),* 3565-3571.

Provis, J. L., & Bernal, S. A. (2014). Geopolymers and related alkali-activated materials. *Annual Review of Materials Research, 44,* 299-327.

Rovnaník, P. (2010). Effect of curing temperature on the development of hard structure of metakaolin-based geopolymer. *Construction and Building Materials, 24(7),* 1176-1183.

Sánchez-Soto, P. J., del Carmen Jiménez de Haro, M., Pérez-Maqueda, L. A., Varona, I., & Pérez-Rodríguez, J. L. (2000). Effects of dry grinding on the structural changes of kaolinite powders. *Journal of the American Ceramic Society, 83(7),* 1649-1657.

Scrivener, K., Martirena, F., Bishnoi, S., & Maity, S. (2018). Calcined clay limestone cements (LC3). *Cement and Concrete Research, 114,* 49-56.

Seiffarth, T., Hohmann, M., Posern, K., & Kaps, C. (2013). Effect of thermal pre-treatment conditions of common clays on the performance of clay-based geopolymeric binders. *Applied Clay Science, 73,* 35-41.

Sharma, M., Bishnoi, S., Martirena, F., & Scrivener, K. (2021). Limestone calcined clay cement and concrete: A state-of-the-art review. *Cement and Concrete Research, 149,* 106564.

Staab, R. (1987). Alkalichlorid-Elektrolyse mit Sauerstoff-Verzehrkathode–ein Verfahren zur Energie-Einsparung. *Chemie Ingenieur Technik, 59(4),* 316-319.

Stanger, R., Wall, T., Spörl, R., Paneru, M., Grathwohl, S., Weidmann, M., Scheffknecht, G., McDonald, D., Myöhänen, K., Ritvanen, J., Rahiala, S., Hyppänen, T., Mletzko, J., Kather, A., & Santos, S. (2015). Oxyfuel combustion for CO2 capture in power plants. *International journal of greenhouse gas control, 40,* 55-125.

Tchakouté, H. K., Rüscher, C. H., Kong, S., Kamseu, E., & Leonelli, C. (2016). Geopolymer binders from metakaolin using sodium waterglass from waste glass and rice husk ash as alternative activators: a comparative study. *Construction and Building Materials, 114,* 276-289.

Statistisches Bundesamt (2021). Baufertigstellungen von Wohn- und Nichtwohngebäuden (Neubau) nach überwiegend verwendetem Baustoff Lange Reihen ab 2000.

www.destatis.de/DE/Themen/Branchen-Unternehmen/Bauen/Publikationen/Downloads-Bautaetigkeit/baufertigstellungen-baustoff-pdf-5311202.pdf?__blob=publicationFile

Tutal, A., Partschefeld, S., Schneider, J., & Osburg, A. (2020). Effects of bio-based plasticizers, made from starch, on the properties of fresh and hardened Metakaolin-Geopolymer Mortar: basic investigations. *Clays and Clay Minerals, 68(5),* 413-427.

Umweltbundesamt (2021). Entwicklung der spezifischen Kohlendioxid-Emissionen des deutschen Strommix in den Jahren 1990 – 2020. https://www.umweltbundesamt.de/sites/default/files/medien/5750/publikationen/2021-05-26_cc-45-2021_strommix_2021_0.pdf

Verein Deutscher Zementwerke e.V. (2016) Umweltdaten der deutschen Zementindustrie: Environmental Data of the German Cement Industry. https://www.vdz-online.de/fileadmin/wissensportal/publikationen/umweltschutz/Umweltdaten/VDZ_Umweltdaten_Environmental_Data_2016.pdf

Werling, N., Dehn, F., Krause, F., Steudel, A., Schuhmann, R., & Emmerich, K. (2020). Solubility of precursors and carbonation of waterglass-free geopolymers. *Clays and Clay Minerals, 68(5),* 524-531.

Werling, N., Kaltenbach, J., Weidler, P. G., Schuhmann, R., Dehn, F., & Emmerich, K. (2022). Solubility of Calcined Kaolinite, Montmorillonite, and Illite in High Molar NaOH and Suitability as Precursors for Geopolymers. *Clays and Clay Minerals, 70,* 270-289.

Wesselsky, A., & Jensen, O. M. (2009). Synthesis of pure Portland cement phases. *Cement and concrete research, 39(11),* 973-980.

Wolters, F., Lagaly, G., Kahr, G., Nueesch, R., & Emmerich, K. (2009). A comprehensive characterization of dioctahedral smectites. *Clays and Clay Minerals, 57(1),* 115–133. .

Xu, H., & Van Deventer, J. (2000). The geopolymerisation of alumino-silicate minerals. *International journal of mineral processing, 59(3),* 247-266.

Xu, H., & van Deventer, J. S. (2003). The effect of alkali metals on the formation of geopolymeric gels from alkali-feldspars. *Colloids and Surfaces A: Physicochemical and Engineering Aspects, 216(1-3),* 27-44.

Yaseri, S., Hajiaghaei, G., Mohammadi, F., Mahdikhani, M., & Farokhzad, R. (2017). The role of synthesis parameters on the workability, setting and strength properties of binary binder based geopolymer paste. *Construction and Building Materials, 157,* 534-545.

Yu, J. (2007). Synthesis of zeolites. *Introduction to zeolite science and practice, 168,* 39.

Zhang, Z., Provis, J. L., Reid, A., & Wang, H. (2015). Mechanical, thermal insulation, thermal resistance and acoustic absorption properties of geopolymer foam concrete. *Cement and Concrete Composites, 62,* 97-105.

2. Materials

The Bavarian kaolin KBE-1 (Amberger Kaolinwerke Eduard Kick GmbH & Co. KG, Germany), the Bavarian bentonite Ceratosil® WG (Clariant AG, Germany) and the illitic clay Arginotec INX (Arginotec GmbH & Co. KG, Germany) were used for the different experiments.

A low b-axis error-ordered kaolinite, which consisted of 46–47 mass% ordered kaolinite and 50–51 mass% disordered kaolinite, was the main mineral in KBE-1 (≥ 93 wt.%). The disordered kaolinite was characterized by 93% BB/7% BC stacking sequences. 88% of BB sequences had no additional ~b/3 stacking errors (Izadifar et al., 2020). The kaolinite had a Hinckley Index of 1.63, which was characteristic for a well-ordered kaolinite (Izadifar et al., 2020). As accessory minerals dioctahedral mica (muscovite), quartz and anatase were present (Table 1). The specific surface area (BET surface) of the bulk material was 9 m^2/g. The initial Si:Al ratio was 1.09 for the bulk material of KBE-1 and 1.0 for the kaolinite.

Table 1. Mineral phases (in wt.%).

Phase	KBE-1	Ceratosil WG	Arginotec INX
Kaolinite	93.0 (± 0.5)	-	5.4 (± 0.2)
Montmorillonite	-	67.1 (± 0.4)	-
Dioctahedral illite	-	-	76.4 (± 0.6)
Dioctahedral mica	5.5 (± 0.5)	2.4 (± 0.1)	-
Biotite (Phlogopite)	-	-	7.8 (± 0.3)
Zeolite (Heulandite)	-	0.9 (± 0.1)	-
Quartz	1.0 (± 0.5)	-	0.4 (± 0.2)
Cristobalite/Opal-C	-	13.3 (± 0.1)	-
K-Feldspar	-	10.4 (± 0.1)	4.4 (± 0.3)
Plagioclase	-	4.1 (± 0.3)	1.1 (± 0.5)
Calcite	-	1.9 (± 0.1)	2.4 (± 0.2)
Anatase	< 0.5	-	-
Anhydrite	-	-	1.4 (± 0.1)
Apatite	-	-	0.7 (± 0.1)

Dioctahedral smectite (montmorillonite) was the main phase of Ceratosil® WG. The bulk material contained accessories such as silicates, cristobalite/opal-C and carbonates (Table 1). The cation exchange capacity (CEC) of the bulk material was 81 cmol(+)/kg. Ca^{2+} accounted for the largest amount

of the exchangeable cations (Table 2). The specific surface area (BET surface) was 58 m^2/g. The structural formula for montmorillonite was $Ca_{0.1}Na_{0.1}Mg_{0.01}(Si_{3.96}\ Al_{0.04})(Al_{1.48}Fe_{0.09}Mg_{0.51})O_{10}(OH)_2$ (calculated according to Stevens, 1946) from XRF data (Table 3). The initial Si:Al ratio was 3.55 for the bulk material of Ceratosil WG and 2.6 for the montmorillonite. The montmorillonite was classified as a medium-charged cis-vacant montmorillonite (according to Emmerich et al., 2009) from composition and by dehydroxylation behavior (Drits et al., 1995; Wolters & Emmerich, 2007).

Table 2. Percentage of exchangeable cations of Ceratosil WG (in %).

Cation	Ca^{2+}	Mg^{2+}	Na^+	K^+
	59	21	17	3

A dioctahedral trans-vacant interlayer-deficient mica ($2M_1$ polytype with its specific peaks in X-ray diffraction patterns, see Grathoff & Moore (1996) for distinction of illite polytypes) was the dominating clay mineral in Arginotec INX. Small amounts (≤ 10 wt.%) of other clay minerals (kaolinite and trioctahedral mica) and accessory silicates, quartz, carbonates, sulphates, and phosphates (Table 1) were present. The bulk material had a specific surface area (BET surface) of 110 m^2/g. The structural formula for illite $K_{0.75}(Si_{3.5}\ Al_{0.5})(Al_{1.25}Fe_{0.5}Mg_{0.25})O_{10}(OH)_2$ was calculated (according to Stevens, 1946) from XRF data (Table 3). The initial Si:Al ratio was 1.91 for the bulk material of Arginotec INX and 2 for the illite.

An industrial produced crystalline aluminum hydroxide powder (Table 3) (Hydrafil®, HPF – The Minerals Engineers, Germany) and an amorphous SiO_2 powder (Amosil®, HPF – The Minerals Engineers, Germany) were analyzed as well. The $Al(OH)_3$ was supposed to be used to lower the Si:Al ratio of solid geopolymer precursors, the amorphous SiO_2 for increasing the Si:Al ratio.

For solubility experiments and geopolymer production NaOH solutions with different concentrations were purchased (Carl Roth GmbH & Co.KG, Germany). Ultrapure NaOH solutions with 10.79 mol/L, 7.96 mol/L, 6.10 mol/L, 5 mol/L and 4 mol/L were used. Additionally, solutions with 1 mol/L, 0.1 mol/L and 0.01 mol/L were prepared for the solubility experiments. The activity of the solutions represents the effective molarity of the solutions. It can be calculated by multiplication of activity coefficient and molarity of the solution. For NaOH concentrations higher than 1 mol/L activity coefficients increase (Table 4).

Table 3. Oxide and element compositions (in wt.%, normalized to ignited state).

	KBE-1	Ceratosil WG	Arginotec NX	Hydrafil®	Amosil®
SiO_2	54.12	71.10	52.43	-	99
Al_2O_3	43.93	17.71	24.28	99.50	0.3
Fe_2O_3	0.40	1.31	8.74	0.01	0.03
MnO	-	0.07	-	-	-
MgO	-	3.91	4.02	-	0.015
CaO	0.10	2.72	1.46	0.10	0.015
Na_2O	-	1.08	-	-	0.015
K_2O	-	1.92	6.82	-	0.015
TiO_2	-	0.18	0.88	-	-
Si	25.32	33.24	24.74	-	46.26
Al	23.27	9.37	12.97	58.87	0.16
Fe	0.28	0.91	6.17	0.01	0.02
Mn	-	0.05	-	-	-
Mg	0.06	2.36	2.45	-	0.01
Ca	0.09	1.94	1.05	0.07	0.01
Na	0.01	0.80	-	-	0.01
K	0.47	1.59	5.71	-	0.01
Ti	0.38	0.11	0.53	-	-
O	50.11	49.62	46.38	47.05	-

Table 4. NaOH solutions.

Molarity	[mol/L]	0.01	0.1	1	4	5	6.1	7.96	10.79
Concentration	[%]	0.038	0.38	3.80	13.90	16.88	20	25	32
pH	-	12	13	13.99	14.55	14.60	14.63	14.68	14.73
Molality	[mol/kg]	0.01	0.10	0.99	3.5	4	5	6	8
Activity coefficient*	-	-	0.777	0.668	-	0.900	1.065	1.287	1.992
Activity	[mol/L]	0.01	0.08	0.67	-	4.5	6.5	10.3	21.5

*) Pabalan and Pitzer 1987

References

Drits, V., Besson, G., & Muller, F. (1995). An improved model for structural transformation of heat-treated aluminous dioctahedral 2: 1 layer silicates. *Clays and Clay Minerals, 43(6),* 718-731.

Emmerich, K., Wolters, F., Kahr, G., & Lagaly, G. (2009). Clay profiling: the classification of montmorillonites. *Clays and Clay Minerals, 57(1),* 104-114.

Grathoff, G. H., & Moore, D. (1996). Illite polytype quantification using WILDFIRE [C] calculated X-ray diffraction patterns. *Clays and Clay Minerals, 44(6),* 835-842.

Izadifar, M., Thissen, P., Steudel, A., Kleeberg, R., Kaufhold, S., Kaltenbach, J., Schuhmann, R., Dehn, F., & Emmerich, K. (2020) Comprehensive examination of dehydroxylation of kaolinite, disordered kaolinite, and dickite: Experimental studies and Density Functional Theory. *Clays and Clay Minerals, 68(4),* 319-333.

Pabalan, R. T., & Pitzer, K. S. (1987). Thermodynamics of NaOH (aq) in hydrothermal solutions. *Geochimica et Cosmochimica Acta, 51(4),* 829-837.

Stevens, R. (1946). A system for calculating analyses of micas and related minerals to end members. *US Geol. Surv. Bull, 950,* 101-119.

Wolters, F., & Emmerich, K. (2007). Thermal reactions of smectites—Relation of dehydroxylation temperature to octahedral structure. *Thermochimica Acta, 462(1-2),* 80-88.

3. Methods

Both intrinsic and extrinsic material properties were investigated in the course of the research conducted. Most of the methods described were used to determine both intrinsic and extrinsic properties.

3.1 X-Ray Diffraction (XRD)

XRD is used for the determination of the phase content of a sample, e.g. natural clay. The method is based on the diffraction of X-rays by a crystal (e.g., clay minerals). The diffraction is explained by Bragg's law.

$$n \cdot \lambda = 2 \cdot d \cdot \sin(\theta)$$

with n = natural number indicating the diffraction order; λ = wavelength [Å]; d = lattice spacing; θ = diffraction angle [°]

By XRD measurements of powder and oriented samples, it is possible to distinguish between clay minerals. Other minerals contained in natural clays like quartz, feldspars, etc. are also identifiable. The different clay minerals show specific layer spacing (d_{001} reflections: kaolinite 7 Å, smectite 12 – 14 Å, illite 10 Å). The differentiation between di- and trioctahedral clay minerals can be done by interpreting the d_{060} reflection (Moore & Reynolds, 1997). Values between 1.48 – 1.50 Å indicate dioctahedral and 1.52 – 1.53 Å trioctahedral smectites (Brindley & Brown, 1984). A quantitative phase analysis of the sample, without a standard, is possible by Rietveld analysis.

Oriented samples of the raw clays were prepared by dispersing about 100 mg (tip of a spatula) powder (< 20 µm) in 3 mL deionized water. The dispersion was treated with an ultrasonic finger (UP 200s, Dr Hielscher GmbH, Germany) for 30 s to ensure homogeneous mixing. The sample dispersions were applied on glass slides (2.5 cm x 2.5 cm) and dried in lab atmosphere (21 °C, 50 – 60% r.H.) over night. The air-dried samples were measured by XRD. Subsequently, the samples were stored over ethylene glycol in a desiccator which was put into an oven at 60 °C for a minimum of 3 days before another XRD measurement. Last measurements were done with the oriented samples which were heated up to 550 °C. By the treatment with ethylene glycol, swellable clay minerals can be detected. With the treatment at 550 °C thermal reactions of the clay minerals can be detected, e.g. the amorphization of kaolinite. By oriented samples especially the d_{001} reflections are investigated for qualitative analysis of the clay minerals. For the powdered samples the material (< 20 µm) was loosely filled in the sample holder from the top (top loading). The powder was then pressed into the sample holder by a glass slide without pressure. During this step surplus powder was removed, as well. After the sample holder was fully filled with sample material, a sandpaper was used for roughening of the surface. The aim of this preparation

is to prevent a preferred orientation of the clay minerals. Powdered samples are used for quantitative phase analysis.

XRD was measured with a Bruker D8 Advance A25 diffractometer (Bruker Corporation, Massachusetts, USA). A LYNXEYE XE Detector (2.94° opening degree) was used. Powdered and oriented samples of the raw clay materials (ground by McCrone mill, < 20 µm), ground geopolymers powders, and solid geopolymers discs were analyzed. The measuring range for powdered samples and solid geopolymers was 5 to 80° 2θ, the step size 0.02° and scan rate was 2 s per step. For the oriented samples the measuring range was 2 to 35° 2θ, step size and scan rate did not change. Automatic slit (primary side), soller collimators of 2.5° (primary and secondary side) and automatic knife edge were used. CuKα radiation (1.54 Å) was generated at 40 kV and 35 mA. Qualitative phase analysis was carried out using Brindley & Brown (1980). Quantitative analysis was performed using Rietveld software Profex (Doebelin & Kleeberg 2015; www.profex-xrd.org).

3.2 Cation Exchange Capacity (CEC)

CEC includes the exchangeable cations of the interlayers and the exchangeable cations from the edges of the clay mineral. The interlayer CEC is set by layer charge, independent from the pH. The CEC of the edges is dependent from the pH, it contributes to 10% – 20% of the CEC (if pH ≥ $pH_{PZC,edge}$; Delavernhe et al., 2015).

The Cu-trien method was used to determine CEC (Meier & Kahr, 1999). 15 mL centrifuge tubes were used to mix 50 mg of the powdered sample with 10 mL deionized water and 5 mL of a 0.01 mol/L copper-triethylentetramine (Cu-trien) solution. The sample was shaken by hand briefly and, subsequently, placed on a shaking table for 3 h. Afterwards, the sample was centrifuged at 4500 rpm (4347*x*g) for 10 min (Heraeus Multifuge 3 S-R, Thermo Heraeus, Thermo Fisher Scientific Inc., Massachusetts, USA). A UV-Vis spectrophotometer (Genesys 10 UV, Thermo Electron Corporation, Massachusetts, USA) was used at a wavelength (λ) of 580 nm to measure the absorbance of the supernatants using polystyrene microcuvettes (path length 1 cm; Lab Logistics Groups GmbH, Germany). The concentration of Cu-trien of the supernatants was determined by a calibration curve. By the depletion of the supernatant due to the exchange of interlayer cations by Cu-trien the CEC [cmol(+)/kg] was calculated. Subsequently to CEC measurements, the exchanged cations in the sample solution were determined. For the analysis, 5 mL of the solution prepared for CEC measurements were diluted with 4.8 mL deionized water and acidified with 0.2 mL HNO_3 (1 mol/L). The amount of cations (in mg/L) which were exchanged (e.g., Na^+, K^+, Ca^{2+}, Mg^{2+}) were determined by ICP-OES. By the total amount of exchanged cations, a verficiation of the measured CEC is possible.

3.3 Inductively Coupled Plasma Optic Emission Spectrometry (ICP-OES)

This method is used for the determination of elements in a solution. The solution is vaporized and fed into a plasma as an aerosol. For the plasma argon is used, which reaches temperatures of 5000 – 7000

K. Due to the high temperatures, the elements in the sample solution are ionized and thus excited to emit light pulses. The characteristic wavelengths of light pulses are measured (Table 5).

Table 5. Characteristic wavelengths of analyzed cations.

Cation	Ca^{2+}	Mg^{2+}	Na^{+}	K^{+}	Si^{4+}	Al^{3+}
Wavelength [nm]	396.847	279.553	589.529	766.491	251.611	396.153

ICP-OES was carried out with an Optima 8300DV (PerkinElmer, Massachusetts, USA). Liquid samples from solubility experiments were acidified and diluted according to a measuring range of Si and Al concentrations in solution of 30 mg/L. The sample preparation for solubility experiments is described in chapter 4. The exchanged cations (Na^{+}, K^{+}, Ca^{2+}, Mg^{2+}) of the clay minerals were also analyzed by ICP-OES, the sample preparation was conducted according to the description in chapter 3.2. By this analysis the ratio of the exchanged cations relative to each other could be determined.

3.4 Simultaneous Thermal Analysis (STA)

STA includes several methods for the investigation of thermal behavior of materials. These investigations include thermogravimetry (TG) which determines the change in weight during a fixed temperature-time-program in a defined atmosphere (Hemminger & Cammenga, 1989). The changes in weight take place due to thermal reactions of the sample. Thermal flow Differential Scanning Calorimetry (DSC) determines endo- and exothermal reactions (e.g., thermal decomposition, dehydroxylation, oxidation, recrystallization). In thermal flow DSC, equal heat flows are applied to a sample and an inert reference. The temperature gradients, evolving due to reactions in the sample, are measured and used to detect phase transformations or differences in heat capacities. The determination of the reaction heat and specific heat capacities is possible. A mass spectrometer can be added to the measurements setup to detect gases escaping from the sample (e.g., water during dehydroxylation) by their ionized mass fragments.

STA can be used to determine thermal reactions like water release, phase transformation, decomposition reactions, and recrystallization. By the determination of water release, information about the type and structure of clay minerals can be gathered. Clay minerals release different kinds of water, namely adsorbed water on their surface and in pores, interlayer water (depending on the clay mineral type), and structural water. The structural water is released at different temperatures depending on the clay mineral. Smectites dehydroxylate, for example, between 500 – 700 °C (Wolters & Emmerich, 2007). The vacancies in the octahedral sheet of smectites can be determined, as trans-vacant smectites dehydroxylate at temperatures 150 – 200 °C lower than cis-vacant varieties (Emmerich, 2000).

For STA a Jupiter 449 (Netzsch, Germany) coupled with a mass spectrometer (Quadrupol 409 Aeolos, Netzsch, Germany) was used. The samples were stored under ambient conditions (21 °C, 50 – 60% r.H.)

prior to measurements. About 100 mg of the powdered raw materials were heated from 35 – 1000 °C with a heating rate of 10 K/min in a Pt-Rh crucible with a loose lid. As reference an empty crucible with lid was used. The measurements were carried out under an atmosphere of synthetic air (50 ml/min, purge gas) and nitrogen (25 ml/min, protective gas). An isothermal segment of 10 min at 35 °C was performed before the dynamic heating, to ensure stabilization of the measurement atmosphere.

3.5 Specific surface area

To determine the specific surface area by BET method (Brunauer et al. 1938), the gas adsorption of a sample can be measured. The method is based on the assumed monolayer adsorption at material surfaces of the measurement gas. The measurement takes place under vacuum.

Specific surface area was determined by Argon adsorption measurements at 87 K with a Quantachrome Autosorb 1-MP (Anton Paar GmbH, Germany). Specific surface area was calculated with the Quantachrome program ASiQwin 4.0, according to BET method on raw and calcined bulk materials. The powdered samples were outgassed at 95 °C for 24 h in vacuum before adsorption measurements.

3.6 Atomic force microscopy (AFM)

AFM is based on the mechanical scanning of the surface of a sample. A nanoscale needle is pressed against the sample by a spring called cantilever. Atomic forces bend the spring. The extent to which the spring is bend can be measured by light.

AFM was used for determination of the height of particles (according to Delavernhe et al., 2015). A Bruker Dimension Icon (Bruker Corporation, Massachusetts, USA) was used to investigate a grid of 1 µm x 1 µm. For the measurements a cantilever type MikroMasch (HQ:NSC15 AL/Bx: 320 kHz; 40 N/m) was used (MikroMasch, Estonia). For each sample a dispersion of 50 mg/L (40 mL total dispersion volume) was prepared in ethanol (99.9%) in a 50 mL centrifuge tube. The dispersions were ultrasonicated (37 kHz) for 15 min in an ultrasonic bath and, subsequently, deposited on silica wafers by spin coating at 2000 rpm (WS-650MZ-23NPP, Laurell Technologies Corporation, Pennsylvania, USA). To ensure a sufficient coverage with sample material spin coating was performed twice (about 0.5 mL each time).

3.7 Mercury Porosimetry

By mercury porosimetry, the total pore area, average pore radius, porosity, and bulk density of a sample can be determined. The method is based on the penetration of mercury into a solid sample. The pores of solids can be penetrated by a non-wetting liquid (mercury) applying pressure. The volume of mercury penetrating the pores can be measured as a function of the applied hydraulic pressure from which intrusion/extrusion curves are obtained (Porcheron & Monson, 2004). The connection to the pore radius distribution is given by the Washburn equation (Porcheron & Monson, 2004):

$P_h r = -2\gamma\cos\theta$

where P_h is the hydraulic pressure, r is the pore radius, γ is the surface tension of mercury, and θ is the contact angle between mercury and the solid pore. The Washburn equation is, equally to the Kelvin equation, based on the pressure difference developed at a curved vapor-liquid interface and the assumption that liquids in pores have bulklike properties (Porcheron & Monson, 2004).

For mercury porosimetry an AutoPore V 9600 (Micrometrics Instrument Corporation, Georgia, USA) was used. The results were evaluated using the associated software MicroActive. The measurement contact angle was 141.3° and the maximum injection pressure was 420.6 MPa.

3.8 Environmental Scanning Electron Microscopy (ESEM)

Using electron microscopy, the surface of a sample is scanned by an electron beam, producing a two-dimensional image. Signals generated by interactions of the primary electron beam with the material are detected. The intensities of secondary electrons, backscattered electrons, X-rays, and photons that are specific to the material are measured. Accompanying EDX can be used to investigate the chemical composition of the sample.

Electron microscopy was carried out using a Philips XL 30 environmental scanning electron microscope (Thermo Fisher Scientific Inc., Massachusetts, USA) or a VEGA 3 instrument (TESCAN, Czech Republic). The measurements were conducted at 15 – 20 kV and the low-vacuum mode. The SE-detector was used. The solid geopolymer discs were used to study the sample surface without prior polishing. Additionally, the cross sections of the discs were embedded in epoxy resin (Epoxy2000 from Cloeren Technology GmbH, Germany) and polished for further investigations. The analysis of the solid geopolymers were complemented by EDX analysis (measuring field of 250 µm x 250 µm). Furthermore, about 2 – 3 mg/cm^2 of the powders of the raw clay samples, calcined clay samples and the dried residues were scattered on the sample holders for investigations. Prior to analysis, a coating of 5 nm platinum was applied on the sample surfaces.

3.9 Nanoindentation

A typical nanoindentation test consists of a loading and an unloading phase. The indentation results are represented by a P - h curve (load to indentation depth; Fig. 8) (Constantinides et al., 2003). By nanoindentation the hardness and Young's modulus of a material can be determined. As indenter, different types of tips can be used. The Berkovich tip is a three-sided pyramid made of diamond. Four-sided pyramids, conical or spherical indenter tips can be used as well (Constantinides et al., 2003). A smooth surface is mandatory for this measurement technique, greater roughness of the sample surface leads to errors.

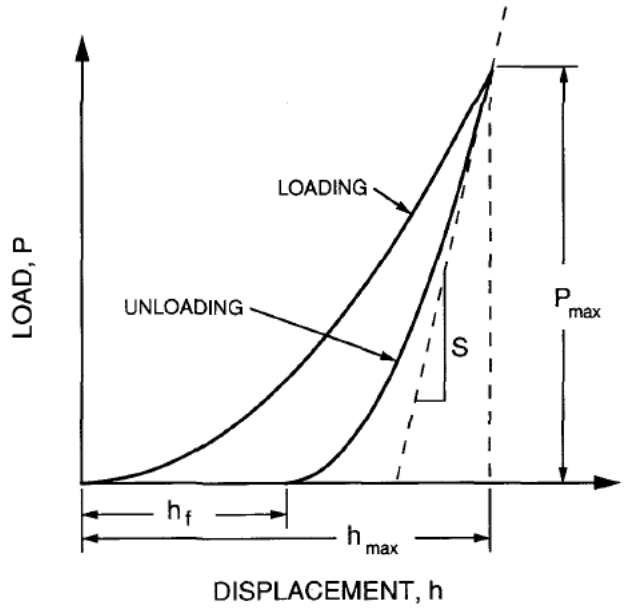

Fig 8. Loading and unloading phase during nanoindentation (Oliver & Pharr, 1992).

The hardness can be determined as followed (Oliver & Pharr, 1992):

$$H = \frac{Pmax}{A}$$

where P_{max} is the peak indentation load and A is the projected area of the indent. By the determination of the stiffness, it is possible to determine the Young's modulus of a sample (Oliver & Pharr, 1992):

$$S = \frac{dP}{dh} = \frac{2}{\sqrt{\pi}} E_r \sqrt{A}$$

where S is the experimentally measured stiffness of the upper portion of the unloading curve, E_r is the reduced modulus, and A is the projected area of the indent, as described before. With E_r Young's modulus can be determined as followed (Oliver & Pharr, 1992):

$$\frac{1}{E_r} = \frac{(1-v^2)}{E} + \frac{(1-v_i^2)}{E_i}$$

where E is Young's modulus and v is the Poission's ratio, E_i and v_i are the same parameters for the indenter.

Nanoindentation was carried out using a Nano Indenter® G200 X (KLA, California, USA). The test method NanoBlitz3D was used. The measurements were performed with a diamond Berkovich indenter. Hardness and Young's modulus were determined according to Oliver & Pharr (1992). 28 x 28 indents within a test area of 30 µm x 30 µm and with an indentation load of 3 mN were conducted per test. For each geopolymer sample between 400 and 800 tests were carried out.

References

Brunauer, S., Emmett, P. H., & Teller, E. (1938). Adsorption of Gases in Multimolecular Layers. *Journal of the American Chemical Society, 60(2),* 309-319.

Brindley, G.W. & Brown, G. (1984). Crystal structures of clay minerals and their X-Ray identifikation. *Mineralogical Society Monograph No. 5*, 41 Queen's Gate, London SW7 5HR.

Constantinides, G., Ulm, F.-J., & Van Vliet, K. (2003). On the use of nanoindentation for cementitious materials. *Materials and Structures, 36(3),* 191-196.

Delavernhe, L., Steudel, A., Darbha, G., Schäfer, T., Schuhmann, R., Wöll, C., Geckeis, H., & Emmerich, K. (2015). Influence of mineralogical and morphological properties on the cation exchange behavior of dioctahedral smectites. *Colloids and Surfaces A: Physicochemical and Engineering Aspects, 481*, 591-599.

Doebelin, N., & Kleeberg, R. (2015). Profex: a graphical user interface for the Rietveld refinement program BGMN. *Journal of applied crystallography, 48(5),* 1573-1580.

Emmerich, K. (2000). Spontaneous rehydroxylation of a dehydroxylated cis-vacant montmorillonite. *Clays and Clay Minerals, 48(3),* 405-408.

Hemminger, W., & Cammenga, H. (1989). Methods of thermal analysis. *Heidelberg, Germany: Springer Co, 1(9),* 8.

Meier, L., & Kahr, G. (1999). Determination of the cation exchange capacity (CEC) of clay minerals using the complexes of copper (II) ion with triethylenetetramine and tetraethylenepentamine. *Clays and Clay Minerals, 47(3),* 386-388.

Moore, D.M. & Reynolds Jr., R.C. (1997). X-Ray Diffraction and the Identifiaction and analysis of Clay Minerals. *Oxford University Press,* Oxford.

Oliver, W. C., & Pharr, G. M. (1992). An improved technique for determining hardness and elastic modulus using load and displacement sensing indentation experiments. *Journal of materials research, 7(6),* 1564-1583.

Porcheron, F., Monson, P. A., & Thommes, M. (2004). Modeling Mercury Porosimetry Using Statistical Mechanics. *Langmuir, 20(15),* 6482-6489.

Wolters, F., & Emmerich, K. (2007). Thermal reactions of smectites—Relation of dehydroxylation temperature to octahedral structure. *Thermochimica Acta, 462(1-2),* 80-88.

4. Experimental Procedure

4.1 Calcination

The calcination process to produce metaclay minerals was carried out in a L9/12/B180 furnace in air (Nabertherm, Germany) with a heating rate of 10 K/min. 5 g of raw clay were heated in unglazed ceramic crucibles to the final temperature and immediately placed in a desiccator for cooling down to room temperature. The calcination temperatures were selected based on STA results, starting at the onset of dehydroxylation and ending prior to recrystallization. Kaolinite was calcined at 480, 555, 615, 700, and 900 °C. For montmorillonite calcination temperatures of 550, 670, 750, and 900 °C were selected. The same criteria were applied to select the calcination temperatures for illite (300, 510, 650, 750, and 900 °C). After calcination all samples were stored in a desiccator until the preparation for experiments.

4.2 Sample Preparation for Solubility Experiments

The solubility of the raw and calcined clay minerals was investigated. The powdered samples (0.1 g) were mixed with NaOH solution (5 g) in 50 ml polypropylene centrifuge tubes. This corresponded to a solid/liquid (s/l) ratio of 0.02. Concentrations of NaOH solutions were 0.01 to 10.79 mol/L, reflecting a pH value ranging between 12 and 14.73. The reaction time for the solubility experiments was 24 h or 7 d, during which the samples were placed horizontally on a shaking table (Edmund Buehler GmbH, Germany). Subsequently, the samples were centrifuged (Heraeus Multifuge 3 S-R, Thermo Heraeus, Thermo Fisher Scientific Inc., Massachusetts, USA) for 25 min at 4500 rpm (rotations per minute). The supernatant was decanted and 0.5 ml were acidified (with 7.5 mL 1 mol/L HNO_3) and diluted (with 17 mL deionized water). Subsequently, 2.5 mL of the diluted solution were diluted again with 7.5 mL deionized water (final dilution factor 1:200) for ICP-OES measurement.

4.2.1 Preparation of Residues

The solid residues of the solubility experiments were washed several times until pH was equal to the deionized water used for washing (pH = 5.5). Afterwards the samples were dried at room temperature and gently ground before the measurements to determine the morphology (ESEM) and the phase content (XRD).

4.3 Geopolymer Production

Geopolymers with varying Si:Al ratios between 1 – 3 were produced according to stoichiometric mixing ratios. The mixing was carried out manually and with a Roti®-Speed stirrer (Proxxon S.A., Luxembourg). Stirring was started with 5000 rpm and gradually increased to a maximum of 10.000 rpm. The Na:Al ratio for all geopolymers was fixed at 1:1, which resulted in varying s/l ratios dependent on the concentration of the used NaOH. Pretests revealed that some of the mixing ratios were not

producible, mainly because homogeneous mixing was not possible. The major limitation in production was poor workability due to the high viscosity of the mixtures. The s/l ratios in the range of 0.8 – 1.44 showed a good workability and, therefore, were used for further experiments (Table 6).

Table 6. Si:Al ratio, solid/liquid (s/l) ratio and NaOH concentration of studied geopolymers.

Sample	Si:Al [mol/mol]	s/l [g/g]	NaOH [mol/L]
K1	1:1	0.89	10.79
K2	2:1	0.86	6.1
K3	2:1	1.07	7.96
K4	3:1	0.80	4
K5	3:1	0.98	5
K6	3:1	1.16	6.1
K7	3:1	1.44	7.96
C3	1:1	0.83	6.1
C6	2:1	1.0	4
C5	2:1	1.24	5
C4	2:1	1.25	6.1
I3	1:1	0.97	4
I2	1:1	1.08	5

Mixtures with Si:Al ratios deviating from the natural Si:Al ratio of the calcined clay mineral were produced by adding amorphous SiO_2 or $Al(OH)_3$. In this case, a pre-dissolution was performed by mixing the powdered SiO_2 or $Al(OH)_3$ with NaOH 24 h before the production of the geopolymer. Subsequently, the pre-prepared SiO_2/NaOH, $Al(OH)_3$/NaOH solutions or pure NaOH were mixed with the powdered calcined clay minerals and stirred for 5 minutes. The geopolymers were cast in cylindric plastic molds (PE cylinders, Kulzer GmbH, Germany) with a diameter of 2.5 cm, after homogeneous mixtures were obtained. To release macroscopic air bubbles, the molds were put on a vibration table (Vortex Genie 2, Scientific Industries Inc., New York, USA) for 2 minutes. Especially the more viscous mixtures showed a large quantity of trapped air, which made a vibration step necessary. The geopolymers were stored at room temperature for hardening. The molds were sealed with lids to prevent carbonation during the hardening process. Demolding was carried out after 3 days. The height of the hardened geopolymer discs was about 5 mm.

4.4 Sample Preparation for Nanoindentation

The hardened geopolymer discs were left in lab atmosphere (21 °C, 50 – 60% r.H.) for additional 7 days to reduce the residual moisture. The surface of the geopolymer cylinders was ground and polished in multiple steps which was necessary to reach a smooth sample surface for nanoindentation. Different abrasive papers were used on a MetaServ 250 grinder and polisher (Buehler, Germany). First a rougher abrasive paper (P2500; 8 µm) was used for grinding. Subsequently, polishing was finished with a P6000 (2 µm) abrasive paper. The surface of the geopolymers was cleaned from loose particles with compressed air after polishing. The use of diamond suspensions (or similar) for polishing has been avoided, because afterwards an ultrasonic treatment would have been necessary to remove residual suspension particles.

4.5 Sample Preparation for Mercury Porosimetry

After demolding and hardening for 7 days in lab atmosphere, one of each of the prepared geopolymer discs was crushed manually. A total of 2 – 3 g of fragments with a size between 2 – 4 mm were used for mercury porosimetry. Before the measurement, the fragments were dried at 105 °C for 24 h.

5. Solubility of metakaolinite and carbonation of waterglass-free geopolymers

The following study was published in Clays and Clay minerals and is a reprint of:

Werling, N., Dehn, F., Krause, F., Steudel, A., Schuhmann, R., & Emmerich, K. (2020). Solubility of precursors and carbonation of waterglass-free geopolymers. *Clays and Clay Minerals*, *68*(5), 524-531. https://doi.org/10.1007/s42860-020-00096-4

Sequences which were edited are marked in italics.

Abstract – Geopolymers have the potential to function as an environmentally friendly substitute for ordinary Portland cement, with up to 80% less CO_2 emission during production. The effect is best utilized for geopolymers prepared with amorphous silica instead of waterglass ($Na_{2x}Si_yO_{2y+x}$) to adjust the Si:Al ratio. The reactivity of the precursors with the alkaline activator affects the final mineralogical properties of the binder. The purpose of the present study was to investigate the amount of different phases formed during geopolymerization and to understand the quantitative evolution of carbonation during geopolymer synthesis by determining the solubility of metakaolinite and amorphous SiO_2 in NaOH at various concentrations. The solubility was studied by ICP-OES measurements. X-ray diffraction was used for qualitative and quantitative phase analysis of the geopolymers. The solubility of the precursors increased with calcination temperature of metakaolinite, reaction time for amorphous SiO_2, and at higher NaOH concentrations. Partial dissolution resulted in free Na^+, which is a source for the formation of carbonates in the geopolymers. Thermonatrite occurred prior to trona formation in all samples.

Keywords – Amorphous silica, Carbonation, Geopolymers, Metakaolinite

5.1 Introduction

Geopolymer binders are inorganic polymers with a 3-dimensional framework structure of oligomers with various ratios of Si, Al, O, and OH^-. The negative charge created by Si:Al substitutions is balanced by the cation of the alkaline activator solution. As well as supplementary cementitious materials (SCM), geopolymer binders are potential substitutes for ordinary Portland cement (OPC), and emit up to 40 – 80% less CO_2 than OPC during their production (McLellan et al. 2011; Davidovits 2013). The lower emissions are mainly due to the fact that the raw materials contain no structural CO2. In contrast to SCM, which replace only a certain amount of OPC, geopolymers are ideally OPC-free binders. OPC is a hydraulic binder, while geopolymers are alkaline-activated binders. High-Ca and low-Ca/Ca-free types of alkaline-activated binders differ from one another (Herrmann et al. 2018) in that geopolymers contain little or no Ca. Aluminosilicates (fly ash, furnace slag, silica fume, or calcined clays) function as

precursors and are activated with a highly alkaline solution (waterglass and/or highly concentrated alkali brines), which leads to a geopolymerization reaction (Davidovits 1991). The polymerization takes place in three successive reactions: the dissolution of the precursors in the alkaline activator solution; the reorganization and diffusion of monomers; and, afterwards, the formation of the 3-dimensional network and hardening of the binder (Heah et al. 2013; Esaifan et al. 2015). The mechanical properties of geopolymers are comparable to those of binders prepared with OPC (Oh et al. 2010; Gao et al. 2014; Djobo et al. 2016; Yaseri et al. 2017; Hàjkovà 2018). When calcined clay minerals such as metakaolinite (Si:Al = 1:1) are used as a precursor, adjusting the Si:Al ratio may be necessary to optimize the mechanical performance of the geopolymers (Duxson et al. 2005; Ozer and Soyer-Uzun 2015; Yaseri et al. 2017). A Si:Al ratio of 3:1 is given as a suitable ratio (Davidovits 1982; Yaseri et al. 2017). For this purpose, commercial waterglass solutions are mostly used for the production of geopolymers. The term waterglass describes aqueous solutions of the glassy frozen melts of alkali silicates, mostly sodium silicates, with varying SiO_2:M_2O (M: Na, K, or Li) ratios (e.g., Na_2SiO_3). In the production of geopolymers, however, waterglass accounts for most of the CO_2 emissions. The environmental benefit is reduced by commercial waterglass, therefore, in comparison with OPC cements. The usage of alkaline brines (e.g. NaOH) can lead to a reduction in CO_2 emissions of up to 50% and the Si:Al ratio can be adjusted by alternative SiO_2 sources (Mellado et al. 2014). Microcrystalline or amorphous SiO_2 can be obtained by combustion of organic materials or by technical manufacturing (e.g. silica fume). Rice husk ash appeared to be suitable for producing an alkaline activator solution in combination with NaOH (He et al. 2013; Tchakouté et al. 2016). Furthermore, waste glass and sugar cane bagasse ash performed well in terms of geopolymer production (Tchakouté et al. 2016, 2017). The solubility of any other alternative SiO_2 sources in NaOH was not considered here. The solubility of SiO_2 in alkaline solutions was investigated only up to a pH value of 12 (Alexander et al. 1954; Crundwell 2017). In addition, unreacted metakaolinite remains following the production of geopolymers (Rowles and O'Connor 2003; Duxson et al. 2005; Heah et al. 2013; Esaifan et al. 2015; Faisal et al. 2015), but usually the amount of unreacted material and the range of the solubility of metakaolinite in the alkaline activator have not been investigated further. The solubility of clay minerals increases with the concentration of NaOH (Xu and Van Deventer 2003). In addition, geopolymers produced with more concentrated NaOH show greater compressive strengths (Heah et al. 2013). Research on clay-mineral solubility in alkaline environments is carried out mainly in the field of nuclear-waste storage. The highest concentration of alkaline solution used is 4 mol/L (Chermak 1992; Bauer and Berger 1998; Cuevas et al. 2006). The solubility of metakaolinite and SiO_2 at pH = 14 and at high NaOH concentrations should be investigated with respect to the amount of unreacted material left after geopolymerization. Unreacted material must be considered because of its impact on the compressive strength and carbonation (formation of carbonates) of geopolymers. While unreacted material can act as a filler and increase mechanical strength (Xu and Van Deventer 2000; Moosberg-Bustnes et al. 2004), a non-stoichiometric conversion of precursors and activator will lead to unreacted Na^+ and carbonation. Carbonation was observed in various geopolymers

(e.g. Fletcher et al. 2005; Zaharaki et al. 2010; Nikolov et al. 2017), but a quantitative description was not given. The present study investigated geopolymers prepared using metakaolinite and NaOH but without commercial waterglass. The Si:Al ratio was adjusted by amorphous SiO_2. The objective was first to determine quantitatively the solubility of metakaolinite and amorphous SiO_2 and second to study the carbonation of geopolymers prepared with the initial Si:Al:Na ratio ranging from 1:1:1 to 3:1:1 with the expected incomplete dissolution of the precursors.

5.2 Materials and Methods

5.2.1 Raw Materials

The investigated Bavarian kaolin KBE-1 was described in chapter 2. The material was calcined according to the procedure described in chapter 4.1.

These temperature steps were selected based on the dehydroxylation of kaolinite (beginning at the onset of DHX and ending prior to recrystallization) determined by thermal analysis (see supplementary material, Fig. S1). Samples were heated at a rate of 10 K/min in air without forced recirculation. No holding time at maximum temperature was applied.

The metakaolin consisted mainly of metakaolinite, therefore. This term will be used through the manuscript to describe the samples.

5.2.2 Analytical Techniques

X-ray diffraction, ICP-OES, and electron microscopy were conducted according to the descriptions in chapters 3.1, 3.3, and 3.8.

5.3 Experimental Procedure

5.3.1 Determination of Dissolution Characteristics

The samples to determine the dissolution characteristics were prepared according to the description in chapter 4.2.

5.3.2 Geopolymer Production

The geopolymers were manufactured with the metakaolinite calcined at 700 °C, to ensure fully dehydroxylated material (see supplementary material, Fig. S1). After calcination, the metakaolinite was ground manually and gently to destroy small aggregates which were formed during calcination. Metakaolinite has a natural Si:Al ratio of 1:1. The Si:Al ratio was increased to the supposed optimum of 3:1 by adding amorphous silica as a solid powder in various amounts (*Table 7*). The Na:Al ratio was fixed at 1:1 and, thus, the s/l ratio varied (*Table 7*).

Table 7. Composition of blends

Geopolymer sample	Si:Al ratio	NaOH concentration (mol/L)	s/l	l/s	Metakaolinite (g)	Amorphous silica (g)	NaOH (g)
GP1	1:1	10.79	0.89	1.13	5	-	5.63
GP2	2:1	6.1	0.86	1.17	3.25	1.76	5.85
GP3	2:1	7.96	1.07	0.94	3.25	1.76	4.68
GP4	3:1	4	0.8	1.24	2.45	2.65	6.34
GP5	3:1	5	0.98	1.03	2.45	2.65	5.23
GP6	3:1	6.1	1.16	0.86	2.45	2.65	4.41
GP7	3:1	7.96	1.44	0.69	2.45	2.65	3.53

In preliminary tests, s/l ratios of between 0.8 and 2 yielded sufficient hardening and good workability. S/l ratios of <0.8 led to mixtures with very low viscosity and insufficient hardening. If the NaOH concentration was too high, its volume in the formulation was too low (s/l > 2) and workability was lost. The solids were mixed with the NaOH solutions for several minutes at 10,000 rpm using a Roti-Speed-Stirrer (Xenox MHX/E from Proxxon, Wecker, Luxembourg) operated at 40 W. Next, the stirred material was placed on a vibration table (Vortex Genie 2 from Scientific Industries Inc., Bohemia, New York, USA) for several more minutes to avoid trapped air in the hardening samples. The hardening took place in open PE cylinders (from Kulzer GmbH, Hanau, Germany) with 30 mm diameter under ambient conditions (~21 °C, ~50% relative humidity). Three days after preparation, the geopolymer discs were subjected to XRD for qualitative phase analysis. For quantitative analysis, powdered samples were prepared from a second set of geopolymer discs prepared in parallel. They were crushed after 1 day of hardening and ground gently after the second day. After 3 days, the samples were ground again and sieved (<32 μm). As an internal standard, 10 wt.% ZnO was added. XRD analysis of the powdered samples also started at a sample age of 3 days.

5.4 Results and Discussion

5.4.1 Solubility of Metakaolinite and Amorphous Silica

Kaolinite and metakaolinite showed a congruent solubility of Si and Al (for solubility of Al see supplementary material, Fig. S2). Non-congruent solubility would lead to an excess or a deficit of Al in the geopolymer matrix. The samples that were not calcined presented the lowest solubility (<5%, *Fig. 8*). The solubility increased by >20% after the calcination temperature was increased from 480 to 555 °C. At calcination temperatures of >555 °C the increase in solubility declined (≤10%). The maximum solubility (e.g. 65% in 4 mol/L and 71.5% in 10.79 mol/L NaOH) was reached in sample KBE-1 calcined at 900 °C (*Fig. 8*). This trend was observed in all NaOH concentrations. The solubility of samples calcined at 700 and 900 °C differed only slightly (0–5%). Calcination to 700 °C is sufficient, therefore,

for geopolymer production. The solubility of metakaolinite calcined at 700 °C increased with the concentration of NaOH (*Fig. 9*).

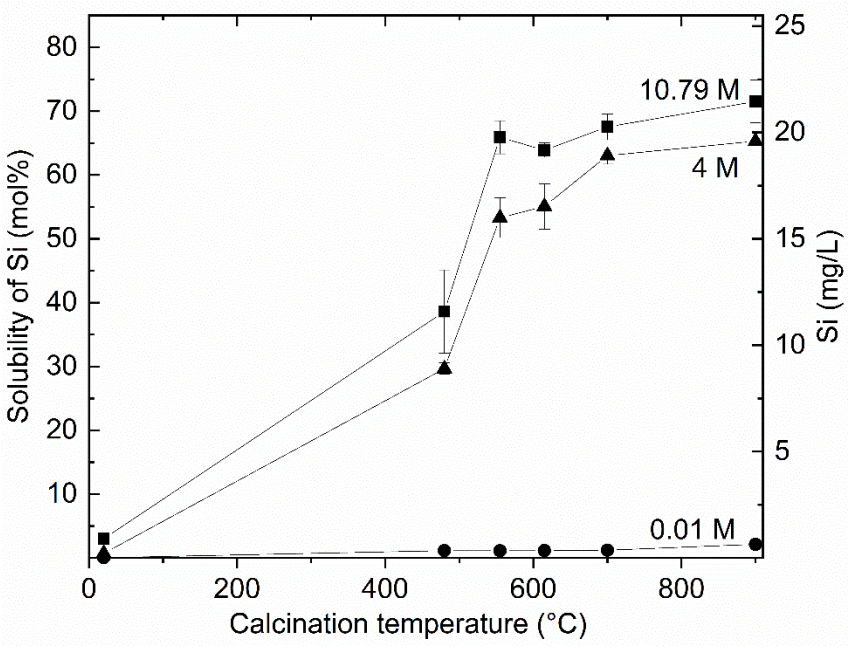

Fig. 8. Solubility of KBE-1 in NaOH (10.79 mol/L, 4 mol/L, 1 mol/L) as a function of calcination temperature (reaction time 24 h).

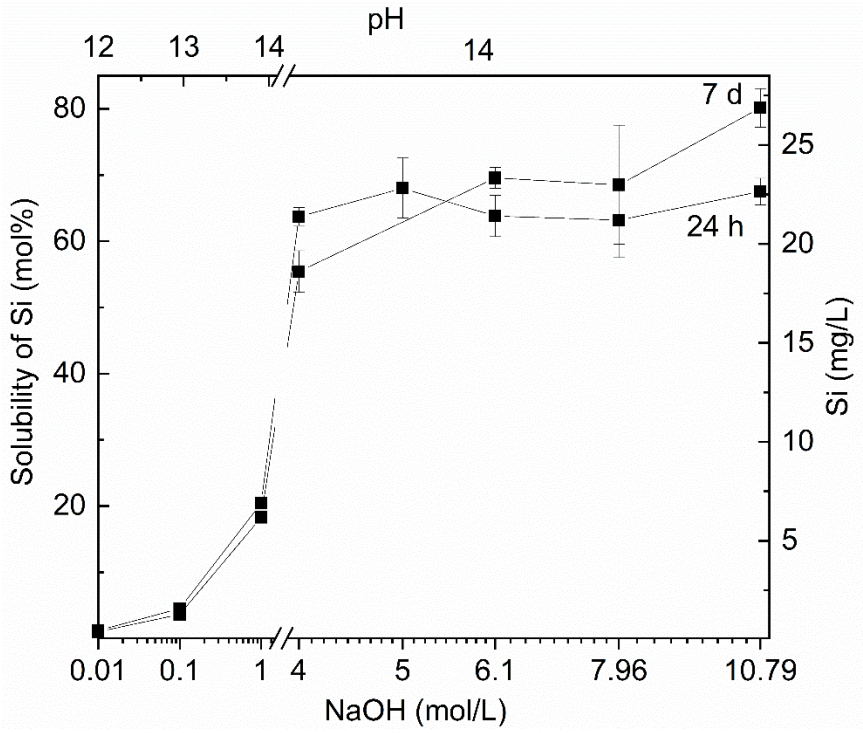

Fig. 9. Solubility of metakaolinite (KBE-1 calcined at 700°C) at various NaOH concentrations (reaction time 24 h and 7 days).

In 0.01 and 0.1mol/L, solubilities of <5% were reached even after 7 days. The greatest solubility for the same metakaolinite was reached in 10.79 mol/L NaOH after 7 days (80%, *Fig. 9*). Note that none of the samples reached a solubility of 100%. At the beginning of geopolymer formation, the incomplete dissolution of metakaolinite in NaOH led to an excess of unreacted Na^+ in the mixture. This unreacted Na^+ formed carbonates (thermonatrite at first) from reaction with airborne CO_2. Theoretical amounts of free Na^+ and thermonatrite (*Table 8*) were estimated based on the solubility of metakaolinite after 24 h (*Fig. 9*) and the assumption that the solubility of metakaolinite is not influenced by the dissolution of amorphous SiO_2 in geopolymer formulation. Excess Na^+ is determined by the amount of metakaolinite (s/l) and its solubility in the specific NaOH in the geopolymer formulation. As solubility of metakaolinite in NaOH with a concentration of ≥ 4 mol/L varies only slightly, the samples with higher s/l (with the same amount of metakaolinite) must contain a larger amount of thermonatrite.

Table 8. Estimated amounts of free Na^+ and thermonatrite.

Geopolymer sample	Surplus Na^+ [mol]	Thermonatrite [wt.%]
GP1	0.015	11.2
GP2	0.010	8.2
GP3	0.011	8.5
GP4	0.008	7
GP5	0.007	6.4
GP6	0.008	7.5
GP7	0.008	7.9

GP2 has a calculated amount of thermonatrite of 8.17 wt.% (s/l 0.86) while that of GP3 is slightly larger with 8.50 wt.% (s/l 1.07). The same goes for GP4 – 7 (s/l 0.80–1.44). The slightly smaller amount of thermonatrite calculated for GP5 compared to GP4 is a result of the greater solubility of metakaolinite measured at 5 mol/L NaOH. The largest amount of thermonatrite at the beginning of the geopolymerization was found in GP1. The solubility of amorphous silica was between 20 and 25% after 24 h and up to 55% after 7 days at a s/l ratio of 0.02 (*Fig. 10*). The solubility in 10.79 mol/L NaOH was slightly less than in 7.96 mol/L NaOH. By lowering the s/l to 0.005, the solubility had already increased after 24 h. At 7 days, a maximum of 70% was reached in 5 mol/L NaOH (*Fig. 10*). Because the solubility of amorphous silica at a s/l ratio of 0.02 was only 20 – 25% in NaOH of 4 – 7.96 mol/L after 24 h, even less SiO_2 dissolution after 24 h could be assumed during geopolymer production with a much higher s/l ratio of 0.8 – 1.44. To estimate the resulting Si:Al of the geopolymer matrix after 24 h, however, a solubility of 25% was considered (*Table 9*).

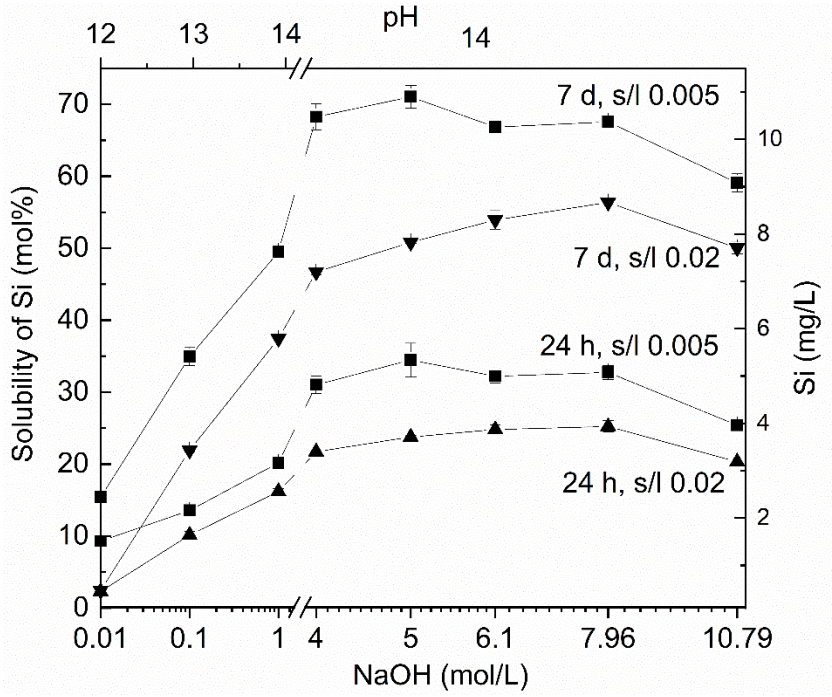

Fig. 10. Solubility of amorphous silica at various NaOH concentrations (reaction times of 24 h and 7 days).

Table 9. Si:Al ratios of GP, calculated by solubilities of metakaolinite and amorphous SiO_2.

Geopolymer	dissolved Si ≙ Al (metakaolinite)[a] (mol)	dissolved Si (amorphous SiO_2)[a,b] (mol)	total Si in GP[c] (mol)	Si:Al in GP (after 24 h)
GP1	0.675	-	0.675	1:1
GP2	0.638	0.25	0.888	1.39:1
GP3	0.632	0.25	0.882	1.4:1
GP4	0.637	0.5	1.137	1.79:1
GP5	0.680	0.5	1.18	1.74:1
GP6	0.638	0.5	1.138	1.78:1
GP7	0.632	0.5	1.132	1.79:1

[a]normalized solubility of metakaolinite; [b]0.25y Si (y = 1 oder 2); [c]x Si + 0.25y Si (x: normalized solubility of metakaolinite)

5.4.2 Phase Composition of Geopolymers

All the geopolymers described in this study hardened, and those prepared with NaOH concentrations of >5 mol/L showed compressive strengths of a few MPa. Further study and the optimization of mechanical properties were not the aim of the present study, however. The formation of carbonates during the early

stages of hardening was evident from the appearance of white efflorescence at the surface of the geopolymer discs and confirmed by XRD (*Fig. 11*).

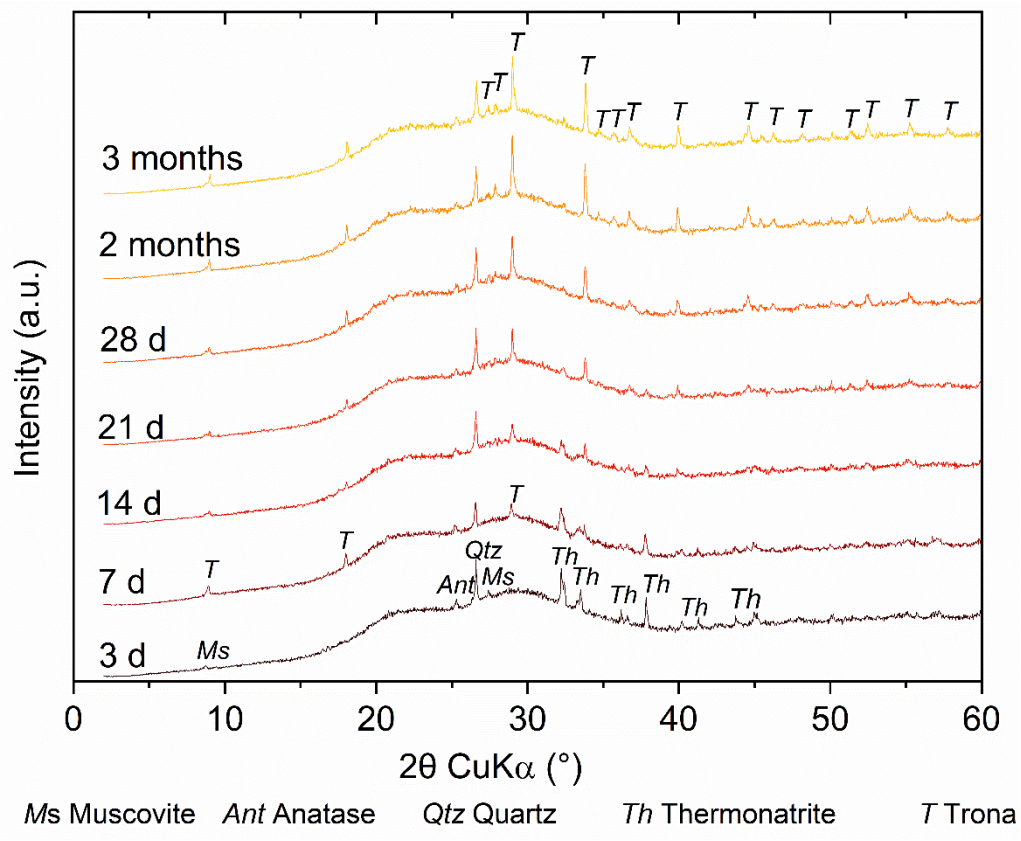

Fig. 11. Qualitative phase analysis of GP7 over a period of 3 months.

First, thermonatrite ($Na_2CO_3 \cdot H2O$) and, shortly afterward, trona ($Na_3(HCO_3)(CO_3) \cdot 2H_2O$) were formed. For GP1, GP3, and GP7 the carbonation started after 3 days; for the other GP samples, carbonates first appeared at a sample age of 7 days (*Table 10*).

Table 10. First appearance of carbonates in geopolymers discs (determined by XRD).

	GP1	GP2	GP3	GP4	GP5	GP6	GP7
Occurrence of Carbonates (determined by XRD) (d)							
Thermonatrite	3	7	3	7	7	7	3
Trona	14	14	7	14	7	14	7

While the amount of trona increased for up to 3 months, thermonatrite disappeared with time; after 28 days, thermonatrite could no longer be detected (*Fig. 11*). In the powdered samples, small amounts of trona (1.13 – 3.59 wt.%) could be observed after 3 days in all geopolymers (*Table 11*).

Table 11. Amounts of minerals present in powdered geopolymers (wt.% after 3 days, 28 days, and 3 months; measured by XRD and calculated using Autoquan).

	GP1	GP2	GP3	GP4	GP5	GP6	GP7
3 d							
Thermonatrite	22	8	7	5	7.5	8	5
Trona	3.5	2	3	1	1	2	1.5
Quartz	1.5	1	1	0.5	0.5	0.8	1
Anatase	1	0.5	0.2	0.1	0.1	0.1	0.1
Muscovite	1.5	1	3	2	2	2	2.5
Amorphous phase	71	87.5	85	92	89	87	90
28 d							
Thermonatrite	15	0	0	0	0	0	0.5
Trona	2	2	2	1	3	2	2
Quartz	1	1	1	0.5	1	1	1
Anatase	0.5	0.1	0.1	0.1	0.1	0.1	0.1
Muscovite	2.5	1	1	1	1	2	2
Amorphous phase	78	96	96	98	95	95	94
3 months							
Thermonatrite	0	0	0	0	0	0	0
Trona	2	2	2	1	3	2	2
Quartz	1	1	1	0.5	1	1	1
Anatase	0.1	0.1	0.1	0.1	0.1	0.1	0.1
Muscovite	1	1	1	1	1	2	2
Amorphous phase	95	96	96	98	95	95	94

The reduction of thermonatrite over time, which was already detected in the discs, was confirmed with the powders. The largest amount of thermonatrite at the beginning of geopolymerization was calculated and observed in GP1 (theoretical amount = 11.19 wt.%; measured amount = 22.11 wt.%). The large deviation between the theoretical and measured amounts of thermonatrite for GP1 was explained by the larger s/l ratio in the geopolymer and, therefore, a larger surplus of Na^+ than estimated. The measured amounts of thermonatrite in GP2 to GP6 were within the range of estimation and measurement error. The increasing amount of thermonatrite with increasing s/l could be confirmed at least for GP4 to GP6. The amount of thermonatrite measured in GP7 (5.28 wt.%) was less than the estimated amount (7.9

wt.%). The largest s/l ratio in GP7 of all samples could result in a denser fabric with trapping of free Na^+ and hindered air exposure and, thus, reduced carbonation. While the quantity of thermonatrite decreased over time, the amorphous content increased (*Fig. 12*).

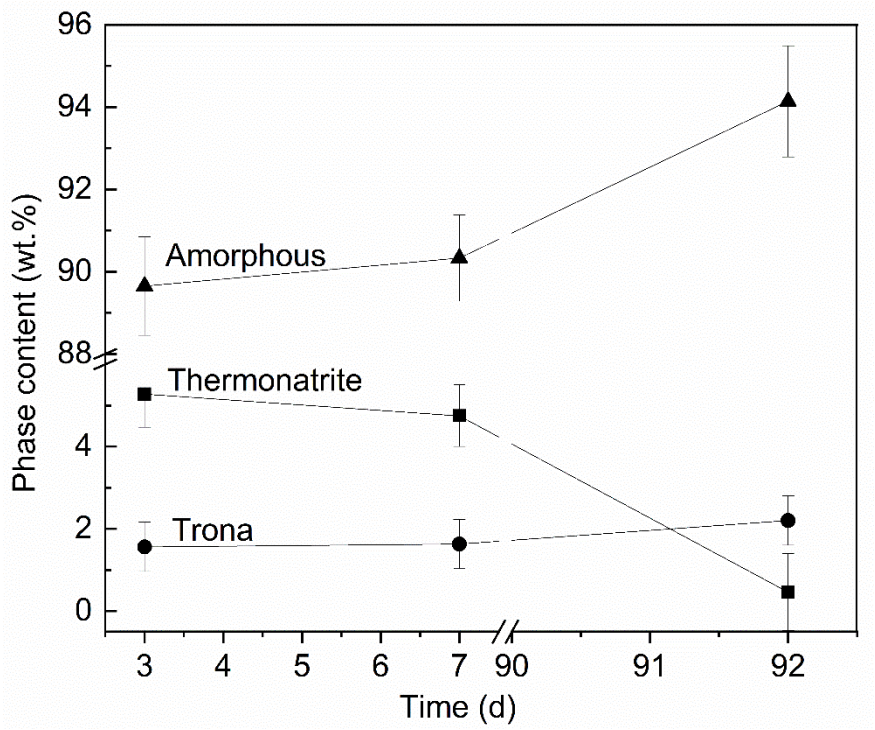

Fig. 12. Time-dependent change in mineralogical content of GP7 (from 3 days to 3 months).

The amount of trona remained approximately the same (variation of <1%). The decrease in the amount of thermonatrite and a nearly constant, small amount of trona in the powder samples, combined with the increase in amorphous phase, indicated that geopolymerization took place for far longer than 24 h. The continuing dissolution of metakaolinite led to the subsequent binding of free Na^+ and, therefore, a reduction of thermonatrite. After 28 days, GP1 still contained 15.13 wt.% thermonatrite, GP7 contained <0.5 wt.%. After 3 months, thermonatrite could be detected in none of the powder samples. After 28 days, the increase in the amorphous phase was marginal for GP2 – 7, but GP1 showed a significant increase until 3 months. Geopolymerization in the discs could have been inhibited by the fast hardening, but, in the solid samples, thermonatrite also disappeared and the amount of amorphous material increased over time.

5.4.3 Microstructural Properties of Geopolymers

The unpolished samples showed a rough surface (e.g. GP4; 4 months; *Fig. 13*). The element ratios reflected the components added at geopolymer production (Na:Al 1:1 and Si:Al 3:1), but spots with a surplus of Na were observed up to Na:Al ratios of 2.25:1, indicating remaining trona deposits at the surface. The micrographs of the polished cross sections revealed that the geopolymers consisted of a fine-grained matrix with a homogeneous distribution of bigger particles throughout the entire sample thickness. No reaction front of carbonates was detected at the surface of the samples (*Fig. 14*), by which

the penetration depth of the carbonates within the geopolymer could be examined. The Si:Al ratio was ~1.5:1 for the bigger particles (X1 and X2, *Fig. 14*) and ~2.5:1 for the matrix (X3 and X4, *Fig. 14*). Both the particles and the matrix showed a Na:Al ratio of only 0.5:1, however. A few spots with Si:Al ratios up to 7:1 were found, which indicate agglomerated, unreacted SiO_2 attached to the geopolymer matrix. Aggregates of unreacted SiO_2, together with a geopolymer matrix of about stoichiometric composition, showed that the raw materials were not converted completely into geopolymers.

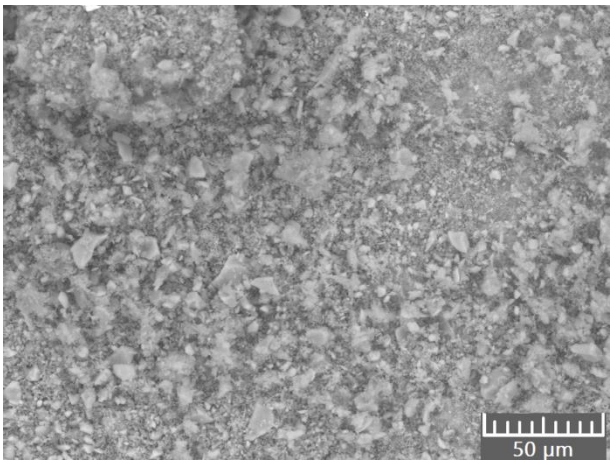

Fig. 13. SEM image of an air-exposed surface of GP4.

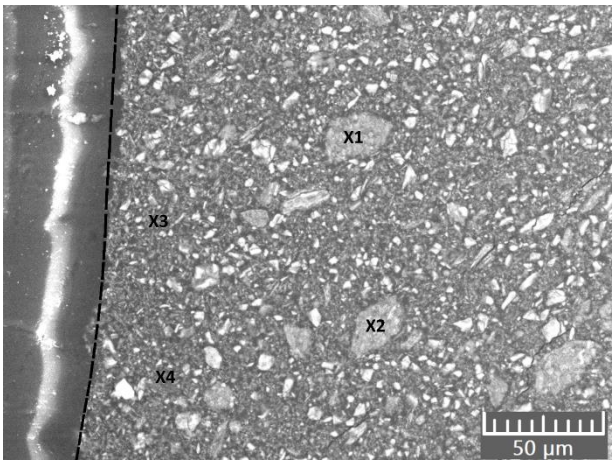

Fig. 14. SEM image of a polished section of GP4 (the dashed line marks the edge of the sample).

5.5 Summary and Conclusion

Incomplete and/or delayed dissolution of metakaolinite in NaOH resulted in a surplus of reactive Na^+ of stoichiometrically mixed educts. Na^+ reacted with airborne CO_2 to form thermonatrite during the early stage of hardening. Ongoing exposure to the atmosphere of the freshly prepared geopolymer caused an increase in CO_2 incorporation during consumption of thermonatrite and the formation of trona. The progressive dissolution of the metakaolinite and geopolymerization reduced the formation of trona. Further studies are needed to show the influence of carbonation on mechanical strength and durability of geopolymers as well as on the pH value of geopolymers and its impact on steel corrosion.

Furthermore, the s/l ratio at the same metakaolinite content had an impact on carbonation. The coupled influence on workability, extent of thermonatrite formation, and mechanical strength also require study. The incomplete dissolution of the amorphous silica added resulted in smaller Si:Al ratios within the geopolymers in relation to the initial stoichiometric calculations with no influence on carbonation but with a possible influence on mechanical strength. While a reduced Si:Al ratio reduces the mechanical strengths of geopolymers, amorphous SiO_2 fillers could increase the mechanical strength of construction materials by increasing bulk density and decreasing porosity. The combined influence needs to be studied in detail for practical applications. The presolution of amorphous SiO_2 in NaOH, e.g. at moderate temperatures, prior to mixing with metakaolinite should be considered.

Acknowledgements

This project was funded by Deutsche Forschungsgemeinschaft under EM79/8-1. The ICP-OES measurements were performed by Marita Heinle, Institute of Functional Interfaces, Karlsruhe Institute of Technology (KIT), Karlsruhe, Germany.

References

Alexander, G. B., Heston, W., & Iler, R. K. (1954). The solubility of amorphous silica in water. *The Journal of Physical Chemistry, 58,* 453–455.

Bauer, A., & Berger, G. (1998). Kaolinite and smectite dissolution rate in high molar KOH solutions at 35 and 80 °C. *Applied Geochemistry, 13,* 905–916.

Chermak, J. (1992). Low temperature experimental investigation of the effect of high pH NaOH solutions on the Opalinus Shale, Switzerland. *Clays and Clay Minerals, 40,* 650–658.

Crundwell, F. K. (2017).On the mechanismof the dissolution of quartz and silica in aqueous solutions. *ACS Omega, 2,* 1116–1127.

Cuevas, J., De LaVilla, R.V., Ramírez, S., Sánchez, L., Fernández, R., & Leguey, S. (2006). The alkaline reaction of FEBEX bentonite: a contribution to the study of the performance of bentonite/concrete engineered barrier systems. *Journal of Iberian Geology, 32,* 151–174.

Davidovits, J. (1982). U.S. Patent No. 4,349,386. Washington, DC: U.S. Patent and Trademark Office.

Davidovits, J. (1991). Geopolymers: inorganic polymeric new materials. *Journal of Thermal Analysis and Calorimetry, 37,* 1633–1656.

Davidovits, J. (2013). Geopolymer cement. *Geopolymer Science and Technics,* Technical Paper #21, Geopolymer Institute Library, France.

Djobo, J. N. Y., Elimbi, A., Tchakouté, H. K., & Kumar, S. (2016). Mechanical activation of volcanic ash for geopolymer synthesis: effect on reaction kinetics, gel characteristics, physical and mechanical properties. *RSC Advances, 6,* 39106–39117.

Duxson, P., Provis, J. L., Lukey, G. C., Mallicoat, S. W., Kriven, W. M., & Van Deventer, J. S. (2005). Understanding the relationship between geopolymer composition, microstructure and mechanical properties. *Colloids and Surfaces A: Physicochemical and Engineering Aspects, 269,* 47–58.

Esaifan, M., Rahier, H., Barhoum, A., Khoury, H., Hourani, M., & Wastiels, J. (2015). Development of inorganic polymer by alkaliactivation of untreated kaolinitic clay: Reaction stoichiometry, strength and dimensional stability. *Construction and Building Materials, 91,* 251–259.

Faisal, M., Muhammad, K., & Amin, W. (2015). Geopolymerization with bagasse bottom ash and china clay, effect of calcination temperature and silica to alumina ratio. *RSC Advances, 5,* 67814–67819.

Fletcher, R. A., MacKenzie, K. J., Nicholson, C. L., & Shimada, S. (2005). The composition range of aluminosilicate geopolymers. *Journal of the European Ceramic Society, 25,* 1471–1477.

Gao, X., Joussein, E.,Michaud, P., & Rossignol, S. (2014). Role of the synthesis method on the microstructure and mechanical properties of metakaolin-based potassium geopolymers. *Ceramics–Silikáty, 58,* 215–222.

Hájková, P. (2018). Kaolinite claystone-based geopolymer materials: Effect of chemical composition and curing conditions. *Minerals, 8,* 444.

He, J., Jie, Y., Zhang, J., Yu, Y., & Zhang, G. (2013). Synthesis and characterization of red mud and rice husk ash-based geopolymer composites. *Cement and Concrete Composites, 37,* 108–118.

Heah, C. Y., Kamarudin, H., Mustafa Al Bakri, A. M., Bnhussain, M., Luqman, M., Khairul Nizar, I., et al. (2013). Kaolin-based geopolymers with various NaOH concentrations. *International Journal of Minerals, Metallurgy, and Materials, 20,* 313–322.

Herrmann, A., Koenig, A., & Dehn, F. (2018). Structural concrete based on alkali-activated binders: Terminology, reaction mechanisms, mix designs and performance. *Structural Concrete, 19(3),* 918–929.

Izadifar, M., Thissen, P., Steudel, A., Kleeberg, R., Kaufhold, S., Kaltenbach, J., Schuhmann, R., Dehn, F., & Emmerich, K. (2020) Comprehensive examination of dehydroxylation of kaolinite, disordered kaolinite, and dickite: Experimental studies and Density Functional Theory. *Clays and Clay Minerals, 68(4),* 319-333.

McLellan, B. C., Williams, R. P., Lay, J., van Riessen, A., & Corder, G. D. (2011). Costs and carbon emissions for geopolymer pastes in comparison to ordinary portland cement. *Journal of Cleaner Production, 19,* 1080–1090.

Mellado, A., Catalán, C., Bouzón, N., Borrachero, M., Monzó, J., & Payá, J. (2014). Carbon footprint of geopolymeric mortar: study of the contribution of the alkaline activating solution and assessment of an alternative route. *RSC Advances, 4,* 23846–23852.

Moosberg-Bustnes, H., Lagerblad, B., & Forssberg, E. (2004). The function of fillers in concrete. *Materials and Structures, 37,* 74.

Nikolov, A., Rostovsky, I., & Nugteren, H. (2017). Geopolymer materials based on natural zeolite. *Case Studies in Construction Materials, 6,* 198–205.

Oh, J. E., Monteiro, P. J.M., Jun, S. S., Choi, S.,&Clark, S.M. (2010). The evolution of strength and crystalline phases for alkali-activated ground blast furnace slag and fly ash-based geopolymers. *Cement and Concrete Research, 40,* 189–196.

Ozer, I., & Soyer-Uzun, S. (2015). Relations between the structural characteristics and compressive strength in metakaolin based geopolymers with different molar Si/Al ratios. *Ceramics International, 418,* 10192–10198.

Rowles, M., & O'Connor, B. (2003). Chemical optimisation of the compressive strength of aluminosilicate geopolymers synthesized by sodium silicate activation of metakaolinite. *Journal of Materials Chemistry, 13,* 1161–1165.

Tchakouté, H. K., Rüscher, C. H., Kong, S., Kamseu, E., & Leonelli, C. (2016). Geopolymer binders from metakaolin using sodium waterglass from waste glass and rice husk ash as alternative activators: a comparative study. *Construction and Building Materials, 114,* 276–289.

Tchakouté, H. K., Rüscher, C. H., Hinsch, M., Djobo, J. N. Y., Kamseu, E., & Leonelli, C. (2017). Utilization of sodium waterglass from sugar cane bagasse ash as a new alternative hardener for producing metakaolin-based geopolymer cement. *Geochemistry, 77(2),* 257–266.

Xu, H., & Van Deventer, J. S. J. (2000). The geopolymerisation of alumino-silicate minerals. *International Journal of Mineral Processing, 59,* 247–266.

Xu, H., & van Deventer, J. S. J. (2003). The effect of alkali metals on the formation of geopolymeric gels from alkali-feldspars. *Colloids and Surfaces A: Physicochemical and Engineering Aspects, 216,* 27–44.

Yaseri, S., Hajiaghaei, G., Mohammadi, F., Mahdikhani, M., & Farokhzad, R. (2017). The role of synthesis parameters on the workability, setting and strength properties of binary binder based geopolymer paste. *Construction and Building Materials, 157,* 534–545.

Zaharaki, D., Komnitsas, K., & Perdikatsis, V. (2010). Use of analytical techniques for identification of inorganic polymer gel composition. *Journal of Materials Science, 45,* 2715–2724.

(Received 14 April 2020; revised 5 August 2020; AE: Andrey G. Kalinichev)

6. Solubility of calcined clay minerals and suitability as geopolymer precursors

The following study was published in Clays and Clay minerals and is a reprint of:

Werling, N., Kaltenbach, J., Weidler, P. G., Schuhmann, R., Dehn, F., & Emmerich, K. (2022). Solubility of Calcined Kaolinite, Montmorillonite, and Illite in High Molar NaOH and Suitability as Precursors for Geopolymers. Clays and Clay Minerals 70, 270–289. https://doi.org/10.1007/s42860-022-00185-6

Sequences which were edited are marked in italics.

Abstract – Clays and clay minerals dissolve over a broad pH range, such as during sediment diagenesis and in a variety of applications, including nuclear waste storage, landfills, and geopolymer binders in the construction industry. The solubility depends on process parameters (pH, temperature, pressure, etc.) and material properties (phase content, clay mineral composition, particle size, etc.). Pretreatments such as calcination or severe grinding change the material properties and could enhance solubility, which is called activation. The aim of the current study was to determine the solubility of three different clay minerals after calcination (metakaolinite, metamontmorillonite, and metaillite) in high molar alkaline solutions (NaOH) up to 10.79 mol/L and pH = 14.73. Furthermore, the solubility of an $Al(OH)_3$ powder in alkaline solution (NaOH) was analyzed, as it can be used to adjust the Si:Al ratio of geopolymer precursors. The residues of the clay minerals after the alkaline treatment were investigated to disclose potential alterations in their phase contents. Based on the results of the thermal and alkaline activation, conclusions about the suitability as geopolymer precursors were made. All clay minerals showed an increase in solubility proportional to the concentration of the alkaline solution. The solubility decreased in the order metakaolinite > metamontmorillonite > metaillite. Thereby, dissolution was incomplete for all three clay minerals (<90%) after 7 days and congruent for metakaolinite and metaillite but incongruent for metamontmorillonite.

Keywords – Alkaline activation, Calcination, Clay minerals, Geopolymer, Metaillite, Metakaolinite, Metamontmorillonite, Solubility

6.1 Introduction

Clay and clay mineral dissolution over a broad pH range takes place in natural systems, such as during sediment diagenesis and soil (trans)formation, in geotechnical applications including landfill liners (Kayabali, 1997; Rozalén et al., 2008) and geotechnical barriers of nuclear waste deposits (Charlet et al., 2017; Dohrmann et al., 2013; Güven, 1990; Madsen, 1998), in technical production processes or applications including during production of bleaching earths (Steudel et al., 2009a, b; Valenzuela Díaz

& Santos, 2001), and in construction materials (Khalifa et al., 2020; Shubbar et al., 2019). For construction materials, clays in their natural form or after thermal or mechanical activation are used as rheology modifiers (Tregger et al., 2010), supplementary cementitious materials (Badogiannis et al., 2005), or precursors of geopolymers, and are subjected to solutions of various pH (Duxson et al., 2005; Werling et al., 2020). Clay dissolution and formation of new phases is determined by material properties (phase content, clay mineral composition and structure, particle size, and microstructure) and process parameters (pH, activity of protons and hydroxyls, temperature, pressure, and saturation state of solution) (Amram & Ganor, 2005; Köhler et al., 2003; Nagy, 2018; Rozalen et al., 2009; Sato et al., 2005). Pretreatments such as severe grinding or calcination change the clay mineral structure, particle size, and microstructure and represent additional influence on dissolution characteristics. Typically, the temperature-dependent dissolution at a given pH follows the Arrhenius law. Dissolution rates decrease with increasing pH under acidic conditions, minimize at near neutral pH, and increase with increasing pH under basic conditions. This reflects proton-promoted dissolution at low pH, hydrolysis at intermediate pH, and hydroxyl promoted dissolution at high pH (Rozalen et al., 2009). Proton exchange on interlayer positions of swellable clay minerals promotes the dissolution of smectites under acidic conditions (Janek et al., 1997; Steudel et al., 2009a, b). Alkaline dissolution is controlled mainly by dissolution of layer edges, whereas the basal surfaces are unreactive (Bauer & Berger, 1998; Kuwahara, 2006; Sato et al., 2003). To elucidate the dissolution mechanisms and kinetics, research concerning the dissolution characteristics of clay minerals has been performed with a wide variation of different experimental setups in flow-through (Metz et al., 2005; Rozalén et al., 2008; Rozalen et al., 2009) or batch reactors (Bauer & Berger, 1998; Bauer et al., 1998; Carroll-Webb & Walther, 1988; Köhler et al., 2003; Zysset & Schindler, 1996). In batch reactors the solid/liquid ratios are fixed from the beginning until the end of the experiment. In flow-through experiments, fresh solution is fed continuously into the reactor and the reacted phases are collected continuously. The saturation state of the solution, which varies between flow-through and batch experiments, influences the reaction. Consideration must be given to whether the dissolution takes place under equilibrium or far from equilibrium conditions. In any experimental setup, accessory minerals can hardly be avoided and may have non neglectable impact if they are dissolved and affect the overall dissolution.

Previous Studies on Dissolution of Raw and Calcined Clay Minerals in Alkaline Solutions:

Many studies concentrated on the dissolution of various clays and clay minerals and calcined clays or clay minerals under alkaline conditions (*Table 12*). Due to the different approaches in the research areas, the experimental conditions differed significantly, e.g. in concentrations and types of alkaline solution, reaction times, and temperatures. For kaolinite and metakaolinite, congruent dissolution was observed up to concentrations of 4 mol/L NaOH or KOH. Dioctahedral smectites and metasmectites showed mainly incongruent dissolution in concentrations up to 5 mol/L of the alkaline activator solution. At a calcination temperature of 900 °C a congruent dissolution for a metasmectite was observed, which was explained by the formation of a separate, inert SiO_2 phase at that temperature and, therefore, a reduction

of dissolvable silica (Garg & Skibsted, 2015). Studies on illite and metaillite dissolution in alkaline activators with concentrations up to 6 mol/L showed a strong dependence of congruency on the calcination temperature. Uncalcined illite showed incongruent solubility, while for metaillite (calcined at <800 °C) mostly congruent dissolution was observed. While raw and calcined clay minerals in natural and geotechnical applications and even when used as supplementary cementitious materials (SCM) are subjected to pH <14, these materials react with NaOH of up to 18.94 mol/L (50%) when used as precursors for geopolymer binder production. As yet, the solubility characteristics in high molar alkaline solutions are not fully understood. Additional silica or aluminum sources are regularly supplemented in geopolymer production. The aim is to adjust the Si:Al ratio of the evolving geopolymers, which can benefit the mechanical properties. For metakaolinite (with a natural Si:Al of 1:1), silica is used to increase the Si:Al. Metasmectite or metaillite have natural Si:Al ratios of 2:1 or higher, so aluminum can be used to decrease the ratio. Si:Al ratios in the broad range of 2:1–4:1 were mostly determined to be favorable. The aim of the current study was to analyze the solubility of three different calcined clay minerals (metakaolinite, metamontmorillonite, and metaillite) in high molar alkaline solution (NaOH), considering the influence of the preceding calcination and unavoidable mineral impurities. A further objective was to understand better the dissolution of an industrial crystalline aluminum hydroxide powder.

Table 12. Summary of dissolution experiments in alkaline medium in prior studies.

Material	Sample/calcination [°C]	Si:Al	s/l	cNaOH [mol/L]	T [°C]	congruent dissolution	Si:Al after reaction in solution	Reference
Bentonite (La Serrata, Spain)	Bulk/none	2.6	0.3	0.0001 - 0.5	35- 90	No	3.4	Cuevas et al. (2006)
Bentonite (La Serrata, Spain)	Bulk/none	2.6	n.s.*	0.25	25 - 120	n.s.*	n.s.*	Fernandez et al. (2006)
Boom clay (Belgium)	Bulk/none	n.s.*	0.25	0.1	60	No	6	Honty et al. (2010)
Bentonite (MX-80, USA)	Bulk/none	2.4	n.s.*	0.01, 0.3, 1	20	No	2.2	Karnland et al. (2007)
Opalinus clay	Bulk/none	n.s.*	0.02 - 0.2	0.01 - 0.1	150- 200	n.s.*	n.s.*	Chermak (1992)
Kaolinite (from St. Austell, UK	< 2 µm/none	1	0.004 – 0.01	KOH 0.1 - 4	35-80	Yes	1	Bauer et al. (1998)
Kaolinite (from Georgia, USA)	< 1 µm/none	1	0.002 - 0.004	0.001, 0.01	25-60	Yes	1	Carroll-Webb & Walther (1988)
Kaolinite (KGa-1)	Bulk/none	1	0.002	0.001 - 0.1	25	Yes	1	Huertas et al. (1999)
Kaolinite (from St. Austell, UK)	< 2 µm/none	1	0.004 – 0.01	KOH 0.1 - 4	35-80	Yes	1	Bauer & Berger (1998)
Smectite (from industrial bentonites)	< 2 µm/none	2.4, 2.6	0.004 – 0.01	KOH 0.1 - 4	35-80	Yes	2.4, 2.6	Bauer & Berger (1998)
Smectite (from Cabo de Gata and Yunclillos deposits, Spain)	< 2 µm/none	2.5	0.05	5	20	No	3.3	Elert et al. (2015)
Smectite (from natural bentonites)	Bulk/none	2.4	0.1	0.01	150	n.s.*	n.s.*	Mosser-Ruck & Cathelineau (2004)

Table 12. Summary of dissolution experiments in alkaline medium in prior studies (continued).

Material	Sample/calcination [°C]	Si:Al	s/l	cNaOH [mol/L]	T [°C]	congruent dissolution	Si:Al after reaction in solution	Reference
Montmorillonite (from Cabo de Gata bentonite, Spain)	< 4 µm/none	3	n.s.*	KOH 0.005 – 0.5	50-70	No	3.3	Rozalen et al. (2009)
Montmorillonite (from MX-80, USA)	< 2 µm/none	2.4	n.s.*	0.01, 0.3, 1	20	No	2.2	Karnland et al. (2007)
Montmorillonite (n.s*)	Bulk/none	n.s.*	0.005	1	90	n.s.*	2.9	Nakayama et al. (2004)
Illite (Illite de Puy)	< 8 µm/none	2.1	n.s.*	0.03 & 0.05	5- 50	No	1.8 – 3.3	Köhler et al. (2003)
Calcined kaolinite (KGa-2)	Bulk/500-900	1	0.00025	0.1	25	Yes	1	Garg and Skibsted (2019)
Calcined montmorillonite (SAz-2)	Bulk/500-900	2.5	0.00025	0.1	25	No	2.9 – 3.6	Garg and Skibsted (2019)
Calcined Illite (IMt-1)	Bulk/650-930	1.8	0.02	0.5	100	Yes	1.8	He et al. (1995)
Calcined interstratified illite/smectite (natural clay)	Bulk/550-950	n.s.*	0.001	2.77	60	n.s.*	2.5	Buchwald et al. (2009)
Calcined interstratified illite/smectite (Friedland clay, Germany)	Bulk/850°C	2.3	0.001	6	25- 75	No	3.1	Hu et al. (2017)
Calcined common clays (Belgium)	Bulk/700-900	1.45-4.1	0.0125	6	25	n.s.*	n.s.*	Khalifa et al. (2019)

*n.s. = not specified

0

6.2 Materials and Methods

6.2.1 Raw Materials

The investigated Bavarian kaolin KBE-1, Bavarian bentonite Ceratosil®WG, and illitic clay Arginotec INX were described in chapter 2. The crystalline aluminum hydroxide powder was described in chapter 2, as well.

6.2.2 Analytical Techniques

XRD, CEC, *ICP-OES,* STA, *determination of specific surface area, AFM, and ESEM, were conducted according to the descriptions in chapters 3.1, 3.2, 3.3, 3.4, 3.5, 3.6 and 3.8.*

6.3 Experimental Procedure

6.3.1 Calcination of Clay Minerals

The materials were calcined according to the procedure described in chapter 4.1.

6.3.2 Determination of Dissolution characteristics

The samples to determine the dissolution characteristics were prepared according to the description in chapter 4.2. The solid residues after dissolution experiments were treated as explained in chapter 4.2.1.

6.2.3 Differentiation between Silica Polymorphs

In bentonites, opaline silica polymorphs (opal-C and opal-CT) can be mistaken easily for cristobalite. Silica polymorphs such as opal-C and opal-CT show reflections in XRD patterns near those of cristobalite. For opal-C a sharp reflection with a FWHM in a range of 0.222 – 0.453 Å would appear. Opal-CT shows a broader reflection with a FWHM ranging from 0.506 – 0.883 Å (Elzea et al., 1994). To differentiate between opal-C, opal-CT, and cristobalite the bulk sample was heated at 1050 °C for 24 h (Elzea et al., 1994). The change of the d_{101} reflection near 4.0 Å in the XRD pattern indicates the nature of the silica polymorph. As opal-C and opal-CT are hydrated, the d_{101} reflection shifts and sharpens due to heating. Cristobalite does not change the position of its reflection (Elzea et al., 1994). For quantitative analysis of the mixture of cristobalite and an opaline silica polymorph, the raw bulk material of Ceratosil WG was treated in boiling 0.5 mol/L NaOH for 10 min (Hillier & Lumsdon, 2008). By comparing the sample weight before and after dissolution, the silica polymorph and cristobalite could be quantified.

6.4 Results and Discussion

The thermal behavior of kaolinite for calcination as a geopolymer precursor was investigated in preliminary experiments (Werling et al., 2020). Only a small mass loss of 0.32% occurred up to 300 °C due to dehydration. The DHX reached its peak (in the DSC curve) at 576 °C and led to a weight loss of 13.04%. Recrystallization of the material started at 980 °C (*Fig. 15*).

6.4.1 Thermal Behavior of Montmorillonite and Illite

The air-dry montmorillonite showed a mass loss of 11.11% caused by dehydration (DHD) with a peak temperature in the DSC curve of 151 °C. The moisture content was obtained by adding the mass loss during the isothermal heating (100% minus starting mass of the dynamic measurement) to the mass loss during DHD. The moisture of this montmorillonite was 11.60%. A mass loss of 2.96% due to DHX

occurred with the peak of the reaction (in the DSC curve) at 663 °C (*Fig. 15*), which agreed with the DHX of mainly cis-vacant montmorillonites between 650 and 700 °C (Emmerich et al., 2009). Normalized to the dry weight (after loss of moisture), the mass loss for DHX was 3.35%. This result confirmed the quantified amount of montmorillonite (67.1 wt.%) together with traces of mica. The DHX overlapped with the decomposition of calcite, which led to a further mass loss of 0.58% (normalized 0.66%). The mass loss corresponded to a calcite amount of 1.5 wt.%, the quantified amount of calcite was 1.9 wt.%. The deviation was probably caused by challenges in the determination of the mass loss values due to the overlap of the signals from H_2O and CO_2 loss. Recrystallization started at 990 °C. The mass loss (3.48%) of illite during DHD with a peak maximum in the DSC curve at 98 °C was considerably smaller than for montmorillonite (*Fig. 15*). The moisture was 4.41%. During DHX a mass loss of 4.51% was observed with the peak maximum (in the DSC curve) at 504 °C, which was characteristic for trans-vacant dioctahedral illite (Emmerich et al., 2009). Normalized to the dry weight the mass loss for DHX was 4.72%, which confirmed the quantified amount of illite in combination with the DHX of the quantified amount of kaolinite. The sample contained a small amount of calcite, which decomposed at 678 °C with an associated mass loss of 1.10%. The normalized mass loss of 1.15% agreed with a calcite content of 2.6%, which was within the error of the quantification (2.4 ± 0.2 wt.%).

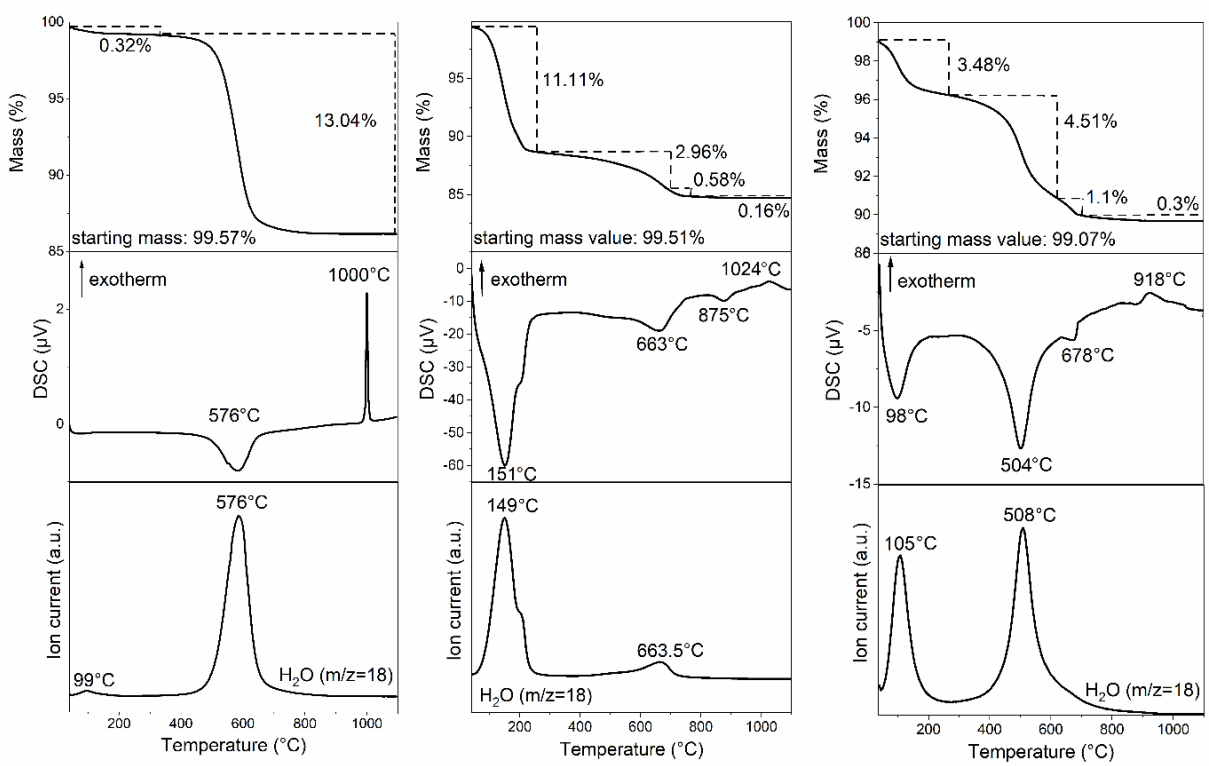

Fig. 15. Thermal behavior of kaolinite (left) from Werling et al. (2020), montmorillonite (middle), and illite (right).

6.4.2 Phase Content of the Calcined Materials

The XRD patterns of KBE-1 with a calcination temperature of 480 °C showed no changes compared to the raw material (for patterns see Supplementary Data). At 555 °C the background increased due to the formation of an amorphous phase. Kaolinite was still detectable, but the intensity of the peaks decreased. At 615 °C kaolinite was completely transformed into amorphous metakaolinite. The broad hump between 15 and 30°2θ in the X-ray pattern due to an amorphous phase increased in intensity by calcination to 700 °C. Kaolinite was already converted into amorphous metakaolinite before; therefore, only the accessories (mica, anatase, and quartz) were still detectable by XRD. The XRD pattern of the material did not change by calcination up to 900 °C. At temperatures of ~1000 °C, recrystallization of a defect spinel followed by mullite formation at ~1400 °C would take place (Glass, 1954; Sonuparlak et al., 1987).

At a calcination temperature of 550 °C for Ceratosil WG the reflections of montmorillonite were still detectable. Only the d_{001} reflection shifted to higher °2θ values due to dehydration of adsorbed water, which was completed at that calcination temperature. At 670 °C the intensity of the montmorillonite reflections decreased. Calcite started to decompose. Further calcination to 750 °C led to a further decrease in the intensity of the montmorillonite reflections. The accessories did not react, except calcite was decomposed completely and lime (CaO) was formed. The background increased, which indicated the formation of amorphous phases. At 900 °C the reflections of montmorillonite were no longer detectable by XRD. No high-temperature phases were observed.

At a calcination temperature of 300 °C for Arginotec NX, no changes compared to raw illite occurred. At 510 °C the kaolinite reflections were reduced in intensity due to the start of the conversion into amorphous metakaolinite. At 650 °C no kaolinite reflections were detectable anymore, which indicated that the total amount of kaolinite was transformed into metakaolinite. The d_{001} of illite was reduced slightly in intensity at that calcination temperature. The decomposition of calcite started, but small amounts of calcite were still detectable. For calcination at 750 °C only slight differences (increase in background) could be observed. Metaillite still displayed similar reflections as illite. Phlogopite was not yet dehydroxylated at that temperature. DHX of phlogopites starts at >800 °C. Therefore, the only layer silicate from which reflections disappeared was kaolinite due to the formation of amorphous metakaolinite. Phosphates, sulfates, quartz, and feldspars did not change. During heating, α-quartz was transformed into β-quartz at 573 °C, but after cooling of the sample, α-quartz was the existing phase again. Calcite was completely decomposed at 750 °C at the expense of CaO formation. By calcination at 900 °C the illite reflections decreased in intensity but were still detectable. No high-temperature phases formed.

6.4.3 Solubility of Clay Minerals

The metakaolinite showed congruent dissolution (Werling et al., 2020). The maximum solubility for the bulk material was reached in 10.79 mol/L NaOH (up to 70 mol.% of Si or Al after 24 h). This corresponded to a solubility of 77 mol.% of the metakaolinite after 24 h. It was increased at longer

reaction times up to 80 mol.% of Si and Al of the bulk material after 7 days (*Fig. 16a–d*), which corresponded to a dissolution of 88% of the metakaolinite, while dissolution of the mica could be ignored. Mica did not contribute significantly to dissolution because it was not yet dehydroxylated during calcination of kaolinite. Assuming that mica (5.5 wt.%) showed a similarly low solubility as the undehydroxylated illite (max. 6 mol.%) studied here, a maximum contribution of 0.4% of mica to the total solubility of the material would be possible.

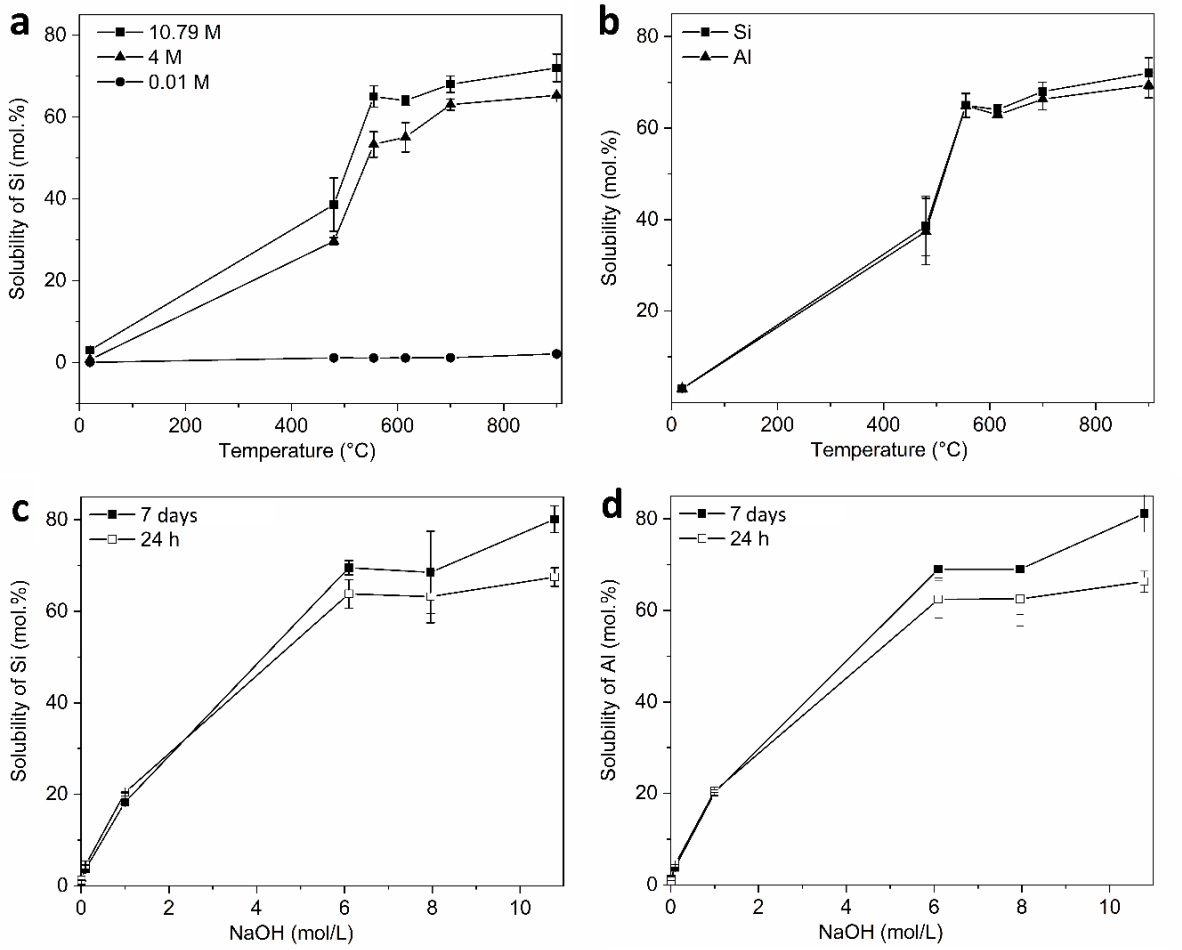

Fig. 16. a Solubility of Si (equal for Al) of metakaolinite in NaOH (10.79 mol/L, 4 mol/L, 0.01 mol/L) as a function of calcination temperature (reaction time 24 h) (from Werling et al., 2020). **b** Solubility of Si and Al of metakaolinite (reaction time 24 h, NaOH 10.79 mol/L). **c** Solubility of Si of metakaolinite as a function of NaOH concentration (reaction time 24 h and 7 days, calcination temperature 700°C) (from Werling et al., 2020). **d** Solubility of Al of metakaolinite as a function of NaOH concentration (reaction time 24 h and 7 days, calcination temperature 700°C).

The first experiments on the solubility of a second kaolinite (KGa-2 (Georgia, USA) from the Source Clays Repository of The Clay Minerals Society; see Supplementary Data) indicated that the specific surface area of the material influenced the dissolution. The solubility experiments were performed according to the same procedure. Kaolinite was the main mineral of KGa-2 with 97.3 wt.% (Izadifar et al., 2020). Only small amounts of mica were present (0.5 wt.%). KGa-2 showed a high degree of

structural disorder and had a significantly lower Hinckley Index (0.5) compared to KBE-1 (Izadifar et al., 2020). The DHX was comparable to KBE-1 and the DHX peak temperature was in the range of 20 °C (Izadifar et al., 2020). Compared to KBE-1 the particle size of KGa-2 was smaller. KGa-2 had a larger BET surface of 18 m^2/g compared to KBE-1. The maximum solubility of KGa-2 for the metakaolinite (at calcination temperatures of 540, 615, and 700 °C) was 86 mol.% Si and 84 mol.% Al in 10.79 mol/L NaOH already after 24 h. Due to particles with a larger specific surface area, the dissolution seemed to be accelerated. But, the influence of disorder and particle size/surface area on dissolution were not clearly distinguishable.

6.4.4 Solubility of Montmorillonite and Metamontmorillonite

The amounts of dissolved Si and Al measured by ICP-OES were used to calculate the solubility of (meta)montmorillonite (for total dissolved values see Supplementary Data). The raw material and the material calcined at 900 °C showed the lowest solubility for metamontmorillonite after 24 h in any concentration of NaOH (*Fig. 17a*). Thereby, the dissolved Si (7.8 mol.%) from metamontmorillonite calcined at 900 °C was even lower than the dissolved Si (24.6 mol.%) from the raw montmorillonite in 10.79 mol/L NaOH. Otherwise, the solubility of the metamontmorillonite increased with increasing the calcination temperature up to 63.5 mol.% after calcination at 750 °C in 10.79 mol/L NaOH (*Fig. 17a*). Dissolution of the raw montmorillonite as well as the metamontmorillonite increased with NaOH concentration from 0.01 to 10.79 mol/L. In 0.01 mol/L NaOH a maximum of 0.4 mol.% Si (for calcination temperatures of 670 and 750 °C) was dissolved. At 4 mol/L NaOH the solubility of Si rose to a maximum of 42.6 mol.% (at a calcination temperature of 750 °C). Due to simplicity of presentation not all of the analyzed NaOH concentrations are shown in the figures (for remaining concentrations see Supplementary Data). Both montmorillonite and metamontmorillonite showed an incongruent dissolution of Si and Al (*Fig. 17b*), which was also observed at low NaOH concentrations by Bauer and Velde (1999) and by Garg and Skibsted (2015). Garg and Skibsted (2015) as well as Khalifa et al. (2020) suggested that Si dissolves faster from the structure than Al at low NaOH concentrations, as in the distorted 2:1 layers of metamontmorillonite Al hexahedra are enclosed by Si tetrahedra. Nevertheless, the solubility of Al in metamontmorillonite increased with increasing concentration of NaOH. The highest solubility for Al of the metamontmorillonite (42.1 mol.%) was reached in 10.79 mol/L NaOH for a calcination temperature of 750 °C. Calcination temperatures significantly greater than DHX can lead to the formation of segregated SiO_2 and crystalline silicates (Grim & Kulbicki, 1961), which are less soluble. This changes the Si:Al in the still soluble phases of the metamontmorillonite and can lead to reduced leaching of Si and, therefore, apparent congruent dissolution of metamontmorillonite. However, X-ray diffraction of the material calcined at 900 °C did not show newly formed crystalline silicates. The reduction of the solubility could be explained by sintering of metamontmorillonite. Due to the formation of large particles (and the reduction of specific surface area), particles within the agglomerates were less accessible for the alkaline activator solution and, therefore, the amounts of dissolved Si and Al decreased (Dietel et al., 2017). In subsequent experiments the reaction time was

increased to 7 days, to determine whether the reaction was completed after 24 h. The samples with a calcination temperature of 750 °C, which showed the greatest solubility after 24 h, were leached in the different NaOH concentrations (*Fig. 17c*). The maximum solubility for metamontmorillonite was increased by 20.6 mol.% up to 84.1 mol.% Si at a reaction time of 7 days. For Al the increase in solubility after 7 days was even higher (25.8 mol.%), a maximum of 67.9 mol.% Al was reached (*Fig. 17d*). The Si:Al ratio (in solution) for the metamontmorillonite in the different NaOH concentrations ranged from 1.6 – 3.0 after 24 h, and from 1.2 – 2.1 after 7 days. The Si:Al ratios showed that the dissolution was more incongruent after 24 h compared to dissolution after 7 days. To determine the dissolved Si from metamontmorillonite, the amount of dissolved Si from the accessory minerals must be considered, especially in the case of the nature of the accessory SiO_2 in Ceratosil WG, the solubility of which plays an important role. The FWHM of the d_{101} reflection of 0.309 was in the range of that for opal-C (0.222 – 0.453; Elzea et al., 1994). After heating, the reflection sharpened (see Supplementary Data for XRD pattern) and the FWHM decreased to 0.208. The mass loss of the sample due to the dissolution procedure (Hillier & Lumsdon, 2008) indicated that Cerastosil WG contained 54% opal-C and 46% cristobalite. The total solubility of Si was, therefore, increased by the simultaneous dissolution of opal- C with metamontmorillonite. While cristobalite is considered to be essentially insoluble (Hillier & Lumsdon, 2008) the amount of total dissolved Si from raw and calcined Ceratosil WG was increased by 10.1 mol.% due to opal-C dissolution. The total SiO_2 in Ceratosil WG was 71.1 wt.%. Ceratosil WG contained 13.3 wt.% silica polymorphs. Therefore, the silica polymorphs accounted for 18.7% of the total SiO_2 and the montmorillonite accounted for 64.3%. The remaining SiO_2 originated from the accessory silicates. 54% of the silica polymorphs was soluble opal-C, 46% was insoluble cristobalite. Accordingly, opal-C accounted for 10.1% of total SiO_2 and cristobalite for 8.6%. Even though, from studies about pozzolanic reactions, small amounts of cristobalite are believed to be dissolved due to pH increase from lime hydration after longer reaction times (>5 days; De Windt et al., 2014), the amount of dissolved crystalline cristobalite in the present study was considered to be low after 24 h reaction time. As cristobalite was still detectable by XRD of the residue after the alkaline treatment, only small amounts of cristobalite could have been dissolved even after 7 days reaction time. Further contributions to Si and Al solubility for calcined Ceratosil WG from heulandite and feldspars were neglected. Heulandite showed a solubility of 4 mol.% for Si and 6 mol.% for Al in 10 mol/L NaOH (s/l = 0.025) after 5 h (Xu & van Deventer, 2000), and the solubility for the plagioclase was <4 mol.% for Si and Al in the same study. Solubilities between 0.15% (0.07% Si) and 0.32% (0.17% Al) of the total SiO_2 and Al_2O_3 was calculated from the data of solubility experiments for feldspars by Locati et al. (2010) in 1 mol./L NaOH for 24 h at 80 °C. As only <1 wt.% heulandite was present in Ceratosil WG, the amount of this accessory dissolved was ignored; the contribution from feldspar dissolution was also ignored even though the amount of feldspar in Ceratosil WG was greater than the zeolite content.

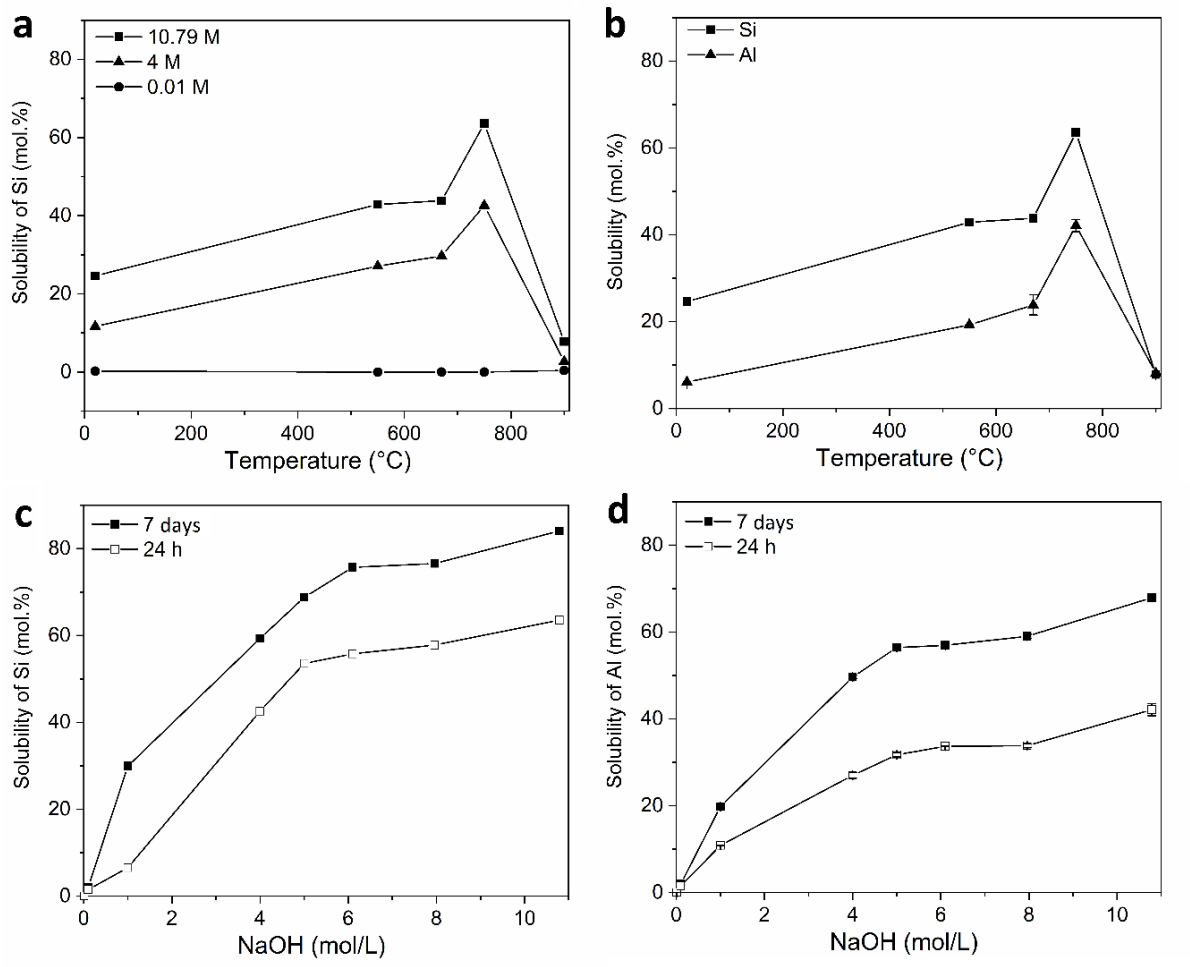

Fig. 17. a Solubility of Si of metamontmorillonite in NaOH (10.79 mol/L, 4 mol/L, 0.01 mol/L) as a function of calcination temperature (reaction time 24 h). **b** Solubility of Si and Al of metamontmorillonite (reaction time 24 h, NaOH 10.79 mol/L). **c** Solubility of Si of metamontmorillonite as a function of NaOH concentration (reaction time 24 h and 7 days, calcination temperature 750°C). **d** Solubility of Al of metamontmorillonite as a function of NaOH concentration (reaction time 24 h and 7 days, calcination temperature 750°C).

As for kaolinite, complementary solubility experiments with a second montmorillonite (Volclay – Wyoming bentonite, USA; Wolters et al., 2009) were conducted first (see Supplementary Data; bulk material was used for experiments). Montmorillonite of Volclay is completely cis-vacant, unlike Ceratosil WG. Furthermore, the particle size of montmorillonite from Volclay was significantly larger (Delavernhe et al., 2015) and, thus, the BET surface area was smaller than for the montmorillonite of Ceratosil WG described here. The first results indicated that the larger particles of Volclay showed a significantly smaller solubility due to smaller amount of edge surfaces, which matched observations for the influence of specific surface area on solubility of the metakaolinites; but, distinguishing between the influence of particle size/surface area and location of the vacancy on the dissolution was not possible. Volclay showed a maximum solubility for metamontmorillonite of 14.5 mol.% Si and 10.5 mol.% Al after 24 h (for calcination temperatures of 710 and 800 °C) in 10.79 mol/L NaOH. As for the preliminary

metamontmorillonite described, the solubility was incongruent. The solubility decreased significantly at a calcination temperature of 930 °C (max. 2 mol.% Si). After 24 h, both metamontmorillonites showed a ratio of dissolved Si and Al > 1.4 (1.4 for Volclay and 1.5 for Ceratosil WG). The ratio of dissolved Si and Al of Ceratosil WG after 7 days decreased to 1.2; a similar trend would be expected for Volclay at longer reaction times.

6.4.5 Solubility of Illite and Metaillite

As for (meta)montmorillonite, the amounts of dissolved Si and Al measured by ICP-OES were used to calculate the solubility of (meta)illite (for total dissolved values see Supplementary Data). After 24 h the lowest solubility was reached by the raw illite, e.g. 6 mol.% Si in 10.79 mol/L NaOH (*Fig. 18a*). The illite calcined at 300 °C showed a comparably low dissolution (7 mol.% Si in 10.79 mol/L NaOH), due to the fact that the DHX just started at that temperature and, therefore, the reactivity was not yet elevated. The solubility of (meta)illite increased with increasing calcination temperature (510 °C < 650 °C < 750 °C) and with increasing NaOH concentration. In 0.01 mol/L NaOH the solubility of Si did not exceed 2.5 mol.% regardless of the calcination temperature. The greatest solubility for metaillite of 44 mol.% Si was reached at a calcination temperature of 750 °C in 10.79 mol/L NaOH. The maximum amount of dissolved Al was 42 mol.% in 10.79 mol/L at a calcination temperature of 750 °C. The solubility of Al increased with calcination temperature and concentration of NaOH comparable to solubility of Si. The XRD pattern of the material calcined at 900 °C did not provide an explanation for the decreased solubility. No newly formed high-temperature phases could be detected. The reduction in solubility may have been caused by sintering of metaillite, which was observed by others previously (Buchwald et al., 2009; Dietel et al., 2017; He et al., 1995a, b). The solubility of Al and Si of metaillite (750 °C) seemed to be congruent within a deviation of max. 2 mol.% (*Fig. 18b*). Previous studies showed a strong dependence on calcination temperatures for congruency of dissolution of Si and Al from illite in 0.03 – 2.77 mol/L NaOH (He et al., 1995a, b; Köhler et al., 2003; Seiffarth et al., 2013). Uncalcined illite materials showed incongruent solubility behavior (He et al., 1995a, b; Köhler et al., 2003). For calcined illite, the method and temperature of calcination had a clear influence on solubility. For a common clay, mainly consisting of illite (37.8 wt.%) and quartz (36.8 wt.%), calcination under a reducing atmosphere led to congruent and higher solubilities, but calcination temperatures >800 °C led to incongruent dissolution independent of calcination atmosphere (Seiffarth et al., 2013). For standard illite IMt-1 the solubility was incongruent for the raw material and calcination temperatures >800 °C. Calcination between 650 and 790 °C led to a congruent dissolution (He et al., 1995a, b). As for metamontmorillonite, the reaction time was increased for metaillite from 24 h to 7 days (*Fig. 18c*). The metaillite calcined at 750 °C was chosen for these experiments due to the highest solubility after 24 h. The increase of solubility of metaillite was comparable to the observations for metamontmorillonite. The maximum solubility of Si increased up to 62 mol.% in 10.79 mol/L NaOH. The solubility of Al reached 56 mol.% (*Fig. 18d*). The phlogopite of Arginotec INX was not dehydroxylated at the calcination temperature of 750 °C. Therefore, the reactivity of the phlogopite was assumed to be low

and dissolution could be ignored, whereas the kaolinite was fully transformed into metakaolinite and, therefore, dissolved simultaneously with metaillite. The amount of Si and Al dissolved from metakaolinite contained in calcined Argiontec NX increased the total dissolved Si by a maximum of 5 mol.% and the total dissolved Al by 10 mol.% (for total dissolved values see Supplementary Data). As Arginotec NX contained <6 wt.% feldspars, the assumption was that the contribution to the total solubility could be ignored.

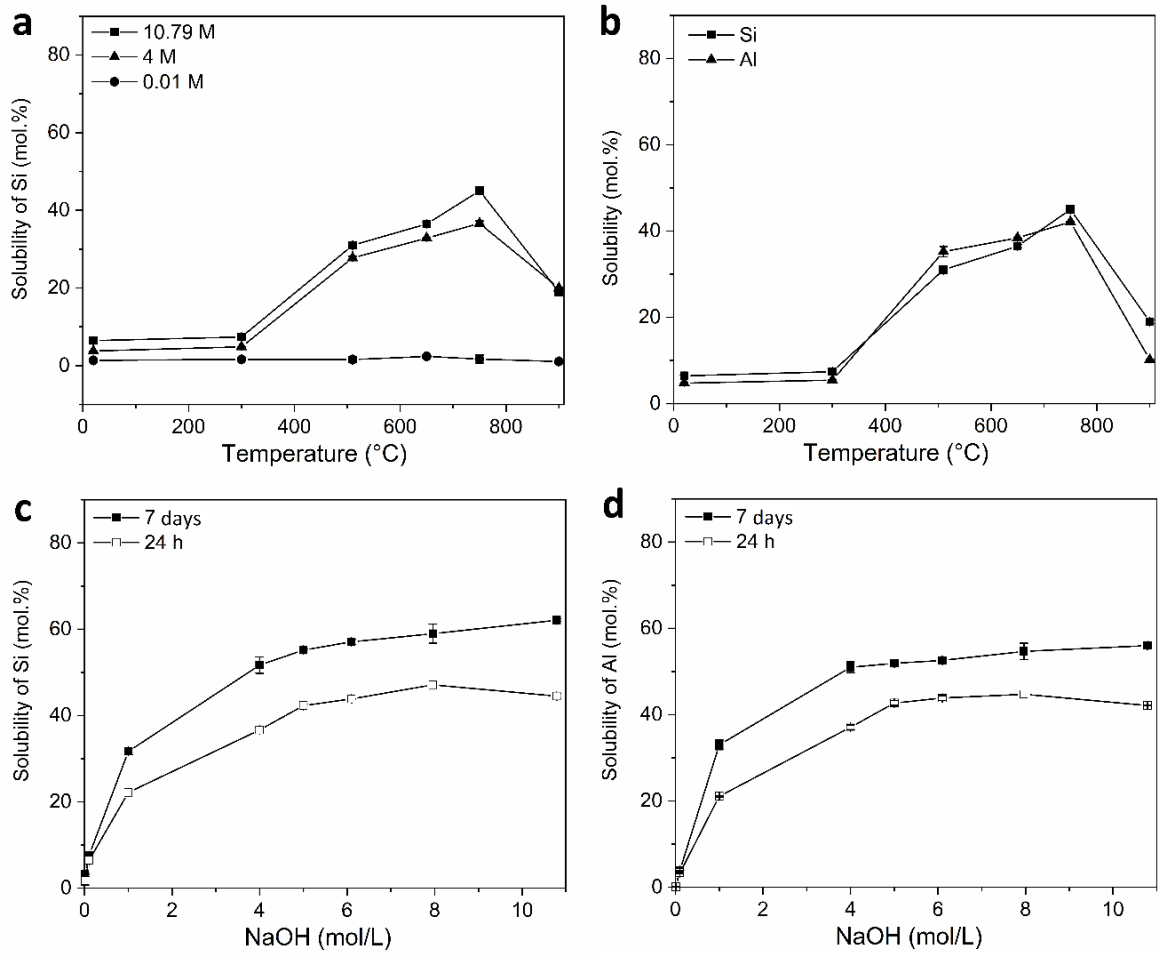

Fig. 18. a Solubility of Si of metaillite in NaOH (10.79 mol/L, 4mol/L, 0.01mol/L) as a function of calcination temperature (reaction time 24 h). **b** Solubility of Si and Al of metaillite (reaction time 24 h, NaOH 10.79 mol/L). **c** Solubility of Si of metaillite as a function of NaOH concentration (reaction time 24 h and 7 days, calcination temperature 750°C). **d** Solubility of Al of metaillite as a function of NaOH concentration (reaction time 24 h and 7 days, calcination temperature 750°C).

For investigations of the influence of the specific surface area on illite solubility, further experiments on illites with different particle sizes will be necessary. The results will almost certainly be similar to the observations made for metakaolinite and metamontmorillonite. Illite and montmorillonite showed different DHX temperatures, but anhydrous structures were still detectable by XRD after calcination. Both minerals retained some of their crystal structure after DHX. The structure of montmorillonite was lost at temperatures >750 °C, which was within the range of 700 – 800 °C observed in former studies

(McConville & Lee, 2005). Regardless of the DHX temperature, the structure of illite was not completely lost up to 900 °C, only the reflection intensity in the X-ray pattern was decreased, due to the beginning of decomposition. The trends of dissolution for all investigated clay minerals were comparable to the trends in previous studies, although the overall dissolution (in %) can scarcely be compared due to different concentrations and types of alkaline solutions (*Table 12*). The observations herein showed that the dissolution decreased in the order metakaolinite > metamontmorillonite > metaillite. As shown in previous studies, the dissolution of kaolinite was congruent. Dissolution of montmorillonite was incongruent and for illite congruency was dependent on calcination temperature. The difference in congruency could be triggered by the (5-times) higher Fe content of illite compared to montmorillonite, while Mg was (2-times) lower. A higher Fe content influences the dissolution positively, which could have led to the congruent solubility of illite compared to incongruent solubility of montmorillonite. The difference in total amount of solubility of the two 2:1 layer silicates could appear due to the turbostratic disorder of the montmorillonite. By this disorder the edge surfaces could be more accessible for the alkaline solution and, therefore, the dissolution of the montmorillonite would be increased.

6.4.6 Solubility of Aluminum Hydroxide and Amorphous SiO_2

The solubility of Hydrafil® after 24 h increased with the NaOH concentration (*Fig. 19*). In 0.01 mol/L NaOH the lowest solubility was determined (0.3 mol.%). The greatest solubility of Al after a reaction time of 24 h was reached in 10.79 mol/L NaOH with 89 mol.%. By increasing the reaction time to 7 days, the maximum solubility of 90 mol.% was reached using 6.1 and 7.96 mol/L NaOH, not only in 10.79 mol/L. Compared to the solubility of an amorphous SiO_2, which reached a solubility of 25 mol.% Si after 24 h and 55 mol.% after 7 days (Werling et al., 2020), the $Al(OH)_3$ dissolved to a greater extent. The different solubilities of SiO_2 and $Al(OH)_3$ have to be taken into account when used for adjustment of the Si:Al ratio. The results were comparable with a solubility of 30% observed by Pereira et al. (2009) in 1.2 – 2.5 mol/L NaOH after 5 days for synthetic $Al(OH)_3$ (gibbsite). Thus, any $Al(OH)_3$ source could be used to adjust the Si:Al ratio in geopolymers while the solubility of even amorphous SiO_2 varies between natural and synthetic material.

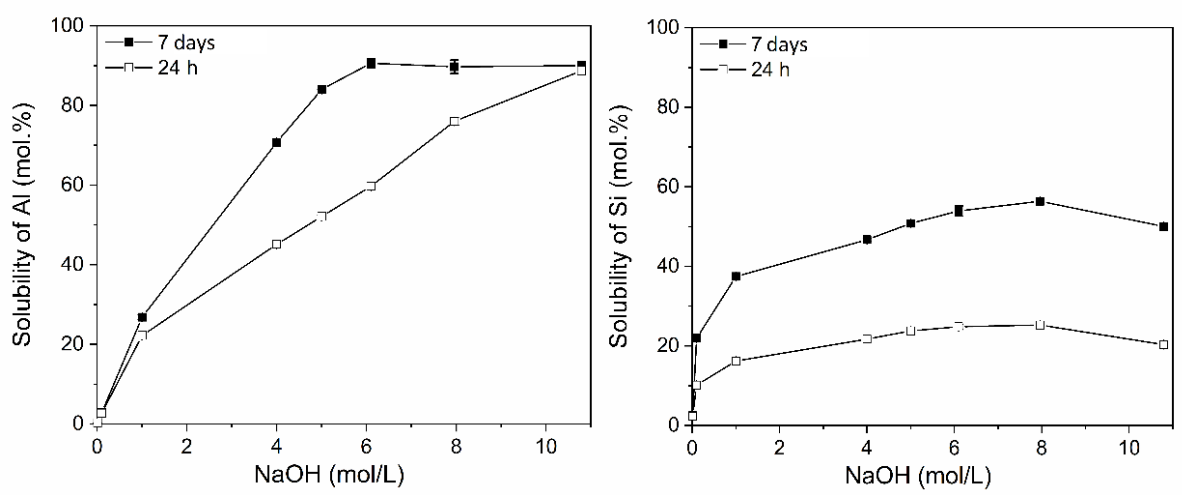

Fig. 19. Solubility of Al of Al(OH)3 (left) and Si of amorphous SiO2 (right, according to Werling et al., 2020) as a function of NaOH concentration (reaction time 24 h and 7 days).

6.4.7 Morphology, Microstructure, and Composition of Residues

Micrographs of the materials were taken before calcination, after calcination, and from the residues after the solubility experiments to show the changes in particle morphology and microstructure of the materials. The raw kaolinite displayed the structure of stacked plates (diameter 0.5 – 3 μm; height 80 – 200 nm) consisting of ~110 – 290 layers, characteristic for many kaolinites (*Fig. 20a*). After the calcination process, the plates in metakaolinite were reduced slightly in height to ~40 – 120 nm (*Fig. 20b*), but still observable. The specific surface area of the bulk material was still 10 m^2/g after calcination at 700 °C. Metakaolinite, calcined at 700 °C, was dissolved up to 80 mol.% (Al and Si) after 7 days' reaction time (Werling et al., 2020). The solid residues showed small spherical particles which were formed on the surface of larger agglomerates. At high resolution those particles appeared to have a morphology similar to hydrosodalite or nanosheets from FAU-type zeolites, but the spherical particles were X-ray amorphous (for diffraction patterns see Supplementary Data). Neither for the spherical particles nor for the agglomerates could a stacked platy structure be observed for the solid residual at lower resolution (*Fig. 20c-d*).

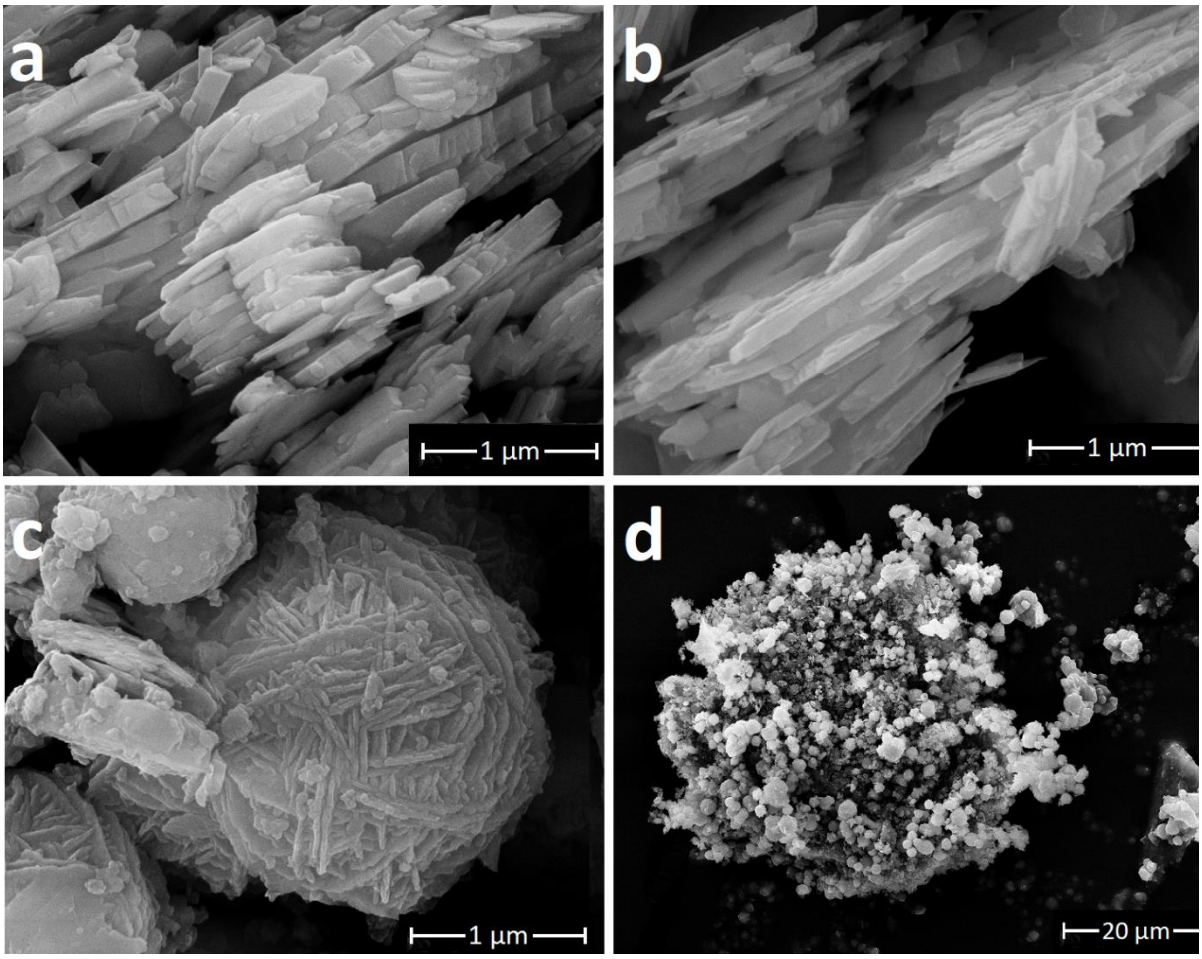

Fig. 20. a Raw kaolinite of KBE-1. **b** Metakaolinite (calcination temperature 700°C). **c** Solid residue of metakaolinite (calcination temperature 700°C) after alkaline treatment (NaOH 10.79 mol/L, reaction time 7 days). **d** Overview. Solid residue of metakaolinite (calcination temperature 700°C) after alkaline treatment (NaOH 10.79 mol/L, reaction time 7 days).

Agglomeration of particles was visible at lower resolution. The agglomerates formed showed diameters up to 50 – 60 µm. The raw montmorillonite showed aggregates (diameters between 4 and 11 µm) where single particles or stacks of layers could not be separated (*Fig. 21a*). During calcination the plates of the montmorillonite were fused together. The typical platy morphology got less obvious in the metamontmorillonite (*Fig. 21b*). The specific surface area decreased from 58 to 37 m^2/g after calcination at 750 °C. It has to be noted that the BET surface was measured for the bulk material, not pure metamontmorillonite. The size of the aggregates did not change. Metamontmorillonite, calcined at 750 °C, showed a solubility up to 84% Si and 68% Al after 7 days' reaction time. In the residue of the metamontmorillonite the platy structure was still observable for several grains (*Fig. 21c*). Agglomerates with diameters up to 75 µm existed (*Fig. 21d*).

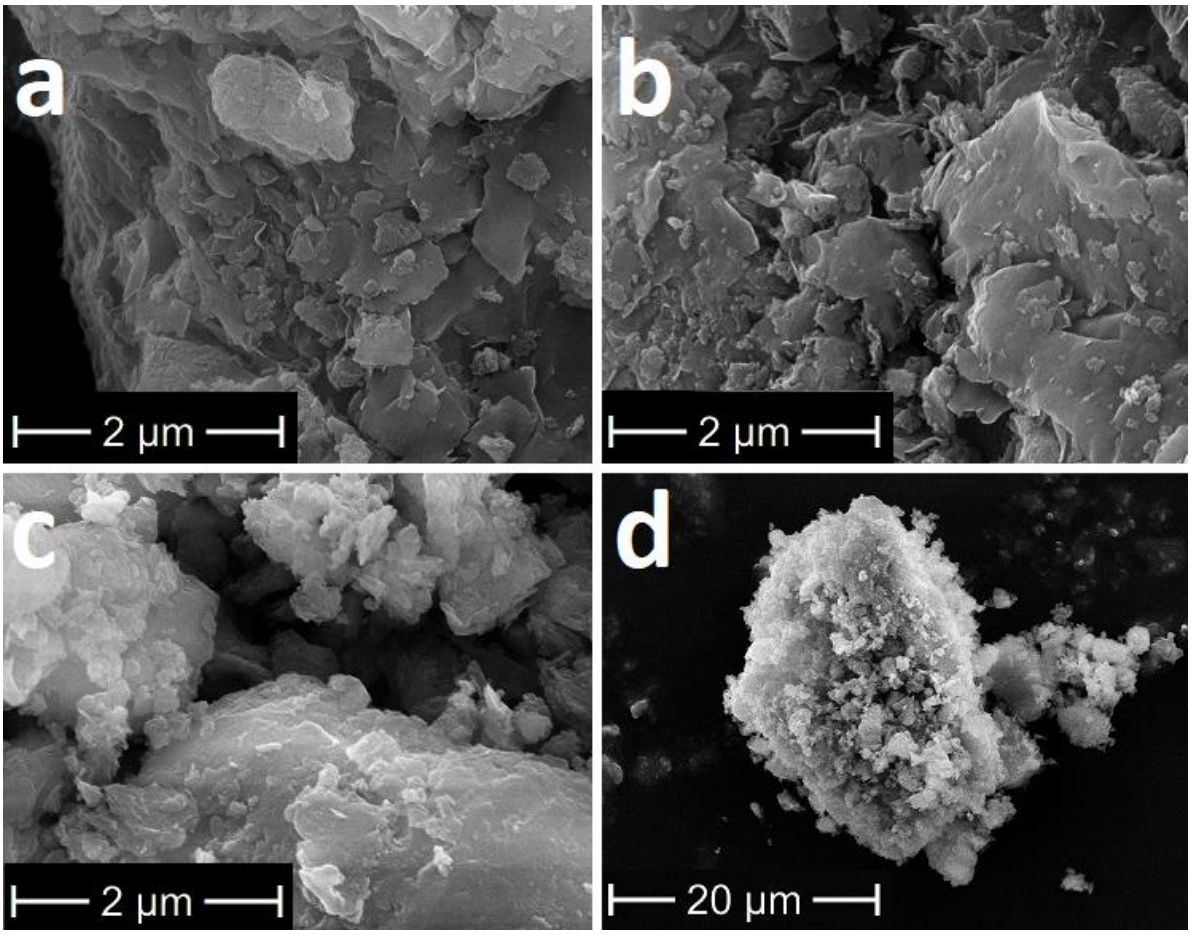

Fig. 21. a Raw montmorillonite of Ceratosil WG. **b** Metamontmorillonite (calcination temperature 750°C). **c** Solid residue of metamontmorillonite (calcination temperature 750°C) after alkaline treatment (NaOH 10.79 mol/L, reaction time 7 days). **d** Overview. Solid residue of metamontmorillonite (calcination temperature 750°C) after alkaline treatment (NaOH 10.79 mol/L, reaction time 7 days).

X-ray diffraction patterns (see Supplementary Data) showed small amounts of hydrotalcite ($Mg_6Al_2CO_3(OH)_{16}\cdot 4H_2O$), which was precipitated as a new phase. After alkaline treatment reflections of metamontmorillonite were no longer detectable. One can assume that the hydrotalcite was formed of Al and Mg, which was dissolved from the metamontmorillonite, together with either airborne CO_2 or CO_3^{2+} released due to calcite dissolution. In addition to the ESEM investigations, the raw montmorillonite and the metamontmorillonite calcined at 750 °C were analyzed by AFM. Raw montmorillonite showed particle heights of between 2.7 and 3.8 nm. Primary particle diameters up to ~40 nm were considerably smaller than indicated by the supplier (≤30 µm, aggregates, secondary particle size). Primary particles were dispersed by the ultra-sonication process before AFM measurements, which destroyed aggregates in the material. The heights of the particles showed that delamination of the layers was not reached for this material. This was already assumed because Ceratosil WG contained Ca^+ as the interlayer cation, which strongly connected the layers and was responsible for preferred formation of aggregates. For Na-saturated montmorillonites, complete delamination was

observed by others (Assemi et al., 2015; Delavernhe et al., 2015). Calcination at 750 °C caused the particle heights to decrease to ~1.5 nm. The distribution of the particle diameters was also reduced slightly by calcination (~30 nm). The raw illite (*Fig. 22a*) showed aggregates with diameters of 2 – 4 µm with particles of small diameters (40 – 250 nm). The particle size of metaillite hardly decreased during calcination (*Fig. 22b*) and the size of the aggregates was retained. The specific surface area of the bulk material decreased from 110 to 86 m^2/g after calcination at 750 °C. Metaillite, calcined at 750 °C, showed a solubility up to ~60% for Si and Al after 7 days' reaction time. The residue of the dissolution experiment showed agglomeration of smaller particles, but the platy structure was somehow retained (*Fig. 22c*). Thereby, agglomerates with diameters between 50 and 75 µm were formed (*Fig. 22d*).

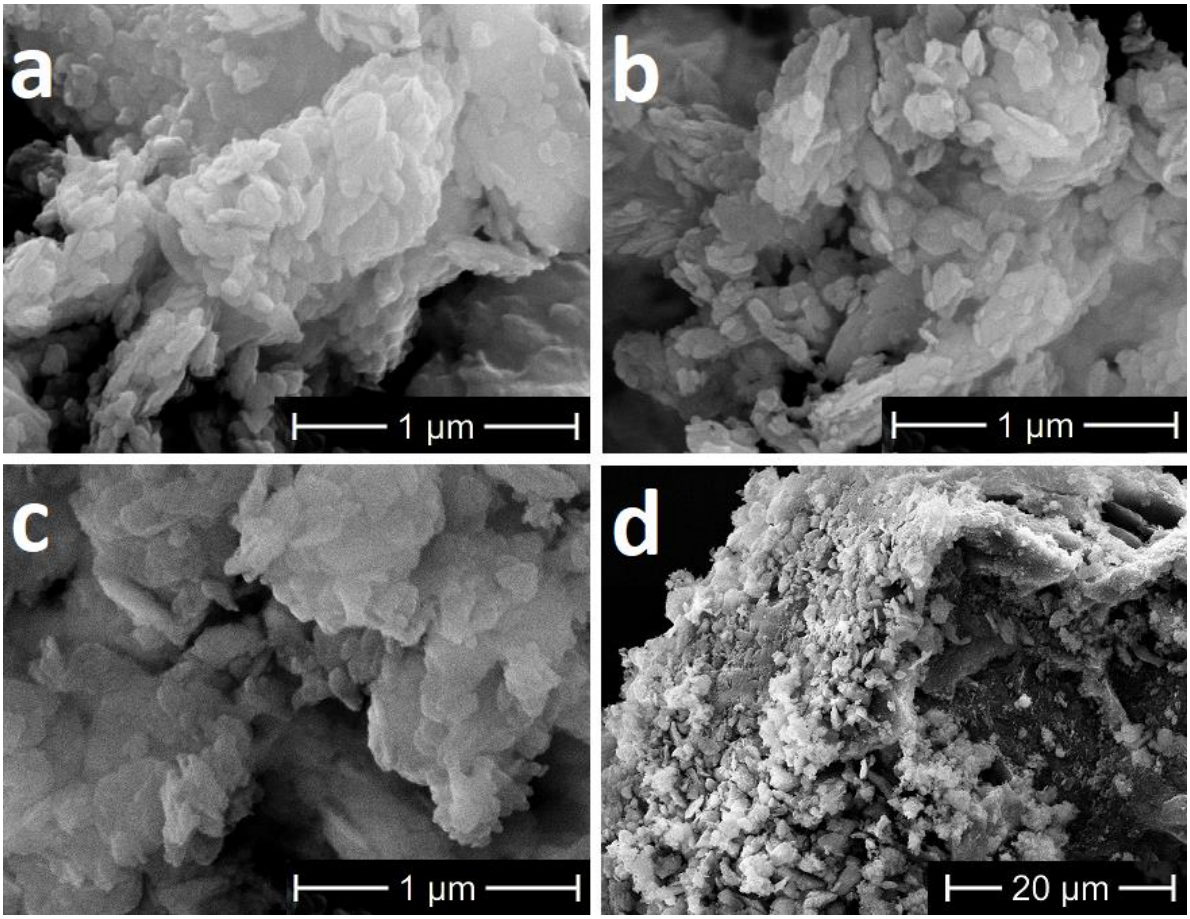

Fig. 22. a Raw illite of Arginotec NX. **b** Metaillite (calcination temperature 750°C). **c** Solid residue of metaillite (calcination temperature 750°C) after alkaline treatment (NaOH 10.79 mol/L, reaction time 7 days). **d** Overview. Solid residue of metaillite (calcination temperature 750°C) after alkaline treatment (NaOH 10.79 mol/L, reaction time = 7 days).

The reflections in the X-ray patterns similar to raw illite (see Supplementary Data) were still present. The phases contained in the residue were equivalent to the phases in the calcined material. As for montmorillonite, AFM investigations were executed for the raw illite and metaillite (calcined at 750 °C). Raw illite showed heights up to 2.9 nm, which was lower on average than the particles of the raw

montmorillonite. The particle diameters were between 20 and 40 nm, while the D50 was determined with <150 nm by conventional particle size measurements. Metaillite contained few larger aggregates (8.9 – 9.5 nm); but, except from those aggregates, the particle height was comparable to that of raw illite. A sample height of 0.9 nm would correspond to a single layer of illite. The morphology of clay minerals has a significant influence on their solubility properties. A progressive decrease of the specific surface area at calcination temperatures (775 – 925 °C) higher than the DHX temperature was observed for Friedland clay due to partial sintering of grains (Dietel et al., 2017). Friedland clay contains kaolinite as well as an interstratified illite-smectite. The decrease of the specific surface area (by one fifth) and, therefore, increase of particle size led to a decrease in the solubility (by about half) of Friedland clay in 5 mol/L KOH (Dietel et al., 2017). The same observations were made for samples of the same clay mineral type (e.g. kaolinite group) described in this work. The calcined samples with a larger specific surface area showed an increased solubility. Still, metaillite solubility was considerably lower than the solubility for the other metaclay minerals, although the material showed the largest specific surface area. Therefore, the specific surface area can only be used to predict the solubility for the same type of clay mineral. Furthermore, this trend can only be observed for dehydroxylated clay minerals. The raw materials with larger specific surface areas showed considerably lower solubilities because of the reduced reactivity without preliminary DHX.

6.4.8 Suitability as Precursors for Geopolymers

The materials studied differed in the purity of the clay minerals. The chosen kaolin was relatively pure (93 wt.% kaolinite). The bentonite as source of montmorillonite (67.1 wt.% montmorillonite) showed larger amounts of impurities, such as 13.3 wt.% silica polymorphs, >10 wt.% feldspars, and 1.9 wt.% calcite. The studied illite (76.4 wt.%) had slightly smaller amounts of impurities compared to the montmorillonite but was not as pure as the kaolin. Therefore, the amounts of phases not contributing to the evolving geopolymer matrix would be different. The impurities with low solubility could function as fillers but the formation of different phases simultaneously with geopolymer formation could not be excluded. The phases formed during geopolymer production with the studied materials need to be investigated further. For the metaillite studied, as with metamontmorillonite, the highest solubility for Si and Al was reached with a calcination temperature of 750 °C in 10.79 mol/L NaOH although the dehydroxylation temperature (TDHX) at 504 °C of the trans-vacant illite in Arginotec INX was much lower than TDHX at 663 °C for the cis-vacant montmorillonite of Ceratosil WG. Thus, 750 °C was considered as the optimal calcination temperature for the thermal activation of these materials prior to the production of geopolymers. Earlier studies of Garg and Skibsted (2015) and Seiffarth et al. (2013) found optimal calcination temperatures of 800 °C for two montmorillonites and between 750 and 800 °C for an illite and an interstratified illite-smectite. The optimal calcination temperature for the well ordered kaolinite was slightly lower at 700 °C. The optimal calcination temperature determined in this study applies only for the clay minerals investigated here. General statements about the optimal calcination for kaolinites cannot be derived directly from these findings. For dioctahedral 2:1 layer

silicates, e.g. montmorillonites and illites, taking into account the influence of octahedral vacancies on the dehydroxylation behavior will be necessary. As trans-vacant varieties dehydroxylate at much lower temperatures than cis-vacant varieties, the optimal calcination for cis-vacant might differ from that of trans-vacant varieties, although the present results indicate that the optimal calcination temperature was in the same range for both varieties. With an increasing number of studies about calcination, setting up general rules about optimal calcination temperatures for clay mineral groups may be possible in the future. Thermal activation of all three clay minerals was regarded as successful, as >50% of the metaclay minerals was dissolved with the optimal thermal pretreatment. The production of geopolymers with those materials in waterglass ($Na_{2x}Si_yO_{2y+x}$) free systems by sole activation with NaOH would be possible. The first tests producing geopolymers with varying Si:Al ratios, NaOH concentrations, and solid/liquid ratios, showed that geopolymers with a metakaolinite (Werling et al., 2020), metaillite, or metamontmorillonite precursor hardened. Further experiments on mechanical properties and phase content will follow. In the case of an adjustment of the Si:Al ratio with respect to Al, the solubility of Hydrafil® indicated that a pre-solution in NaOH would be useful if the geopolymers were produced with lower NaOH concentrations. For geopolymers produced with 10.79 mol/L NaOH, pre-solution would not yield any advantage. The influence of adjusting the Si:Al ratio needs to be studied further. Incomplete dissolution (<100%) for all studied clay minerals and $Al(OH)_3$ must be considered for the stoichiometric composition of the resulting geopolymers. By using more $Al(OH)_3$, the desired Si:Al could be reached, but simultaneously the amount of unreacted powder in the sample would increase. Depending on the material properties (e.g. particle size), unreacted $Al(OH)_3$ could act as a filler without negative impacts on the evolving geopolymers. Fillers can have a positive influence on the mechanical properties of the resulting geopolymer, e.g. by increasing compressive strength (Duxson et al., 2005; Xu & Van Deventer, 2000). Incomplete dissolution of the metaclay minerals can lead to excess Na^+ which does not react. Due to free Na^+, carbonation of the geopolymers can appear and affect the mechanical properties of the binder (Fletcher et al., 2005; Nikolov et al., 2017; Werling et al., 2020). Furthermore, for metamontmorillonite the incongruent dissolution led to smaller amounts of dissolved Al than expected. It has to be considered that the Si:Al ratio of a geopolymer produced with this metamontmorillonite will be lower than the stoichiometric ratio of the montmorillonite. The dissolved Si from both the metamontmorillonite and opal-C could form CSH phases together with Ca from the metamontmorillonite and the decomposed calcite during geopolymer production (De Windt et al., 2014) or the Si:Al ratio of the emerged geopolymers would increase. CSH phases could coexist with the geopolymer matrix. Instead of the evolution of CSH phases, the formation of CASH or N(C)ASH may also be possible. Coexistence of NASH phases with calcium containing phases is possible. Generally, emphasis is necessary that the findings from solubility experiments are limited, given that the liquid:solid ratio differs from that used for geopolymer production; but, even during solubility experiments, reaching 100% solubility was not possible. Therefore, further studies will be necessary to answer satisfactorily whether this happens due to thermodynamic or kinetic effects.

6.5 Summary and Conclusions

The montmorillonite studied showed DHX at the highest temperature (663 °C), kaolinite was intermediate (583 °C), and illite was the lowest (504 °C). Optimal thermal activation due to maximum dissolution was obtained at 700 °C for the studied kaolinite and 750 °C for both studied cis-vacant montmorillonite and trans-vacant illite. During calcination, kaolinite was transformed into X-ray amorphous metakaolinite. Metamontmorillonite and metaillite were not X-ray amorphous after calcination. Dissolution was incomplete for all metaclay minerals. Metakaolinite showed the highest solubility after 24 h compared to both calcined materials containing 2:1 layer silicates. The solubility of the metaclay minerals decreased in the order metakaolinite > metamontmorillonite > metaillite. While metakaolinite (700 °C) and metaillite (750 °C) showed congruent dissolution, metamontmorillonite (750 °C) showed incongruent dissolution. While the distribution of octahedral vacancies in 2:1 layer minerals strongly influenced the dehydroxylation temperature, optimal activation temperature was similar and solubility was influenced by chemical composition and turbostratic disorder. Dissolution characteristics of the raw materials with respect to Si:Al were similar to the materials calcined at 900 °C and higher. The uncalcined samples showed very low solubilities (<30 mol.% Si) independent of the type of clay mineral. Calcination at temperatures significantly higher than 750 °C led to decreased solubility for the metamontmorillonite as well as for the metaillite, while metakaolinite still showed high dissolution after calcination at 900 °C. $Al(OH)_3$ showed almost complete solubility up to 89 mol.% Al in 10.79 mol/L NaOH after 24 h and would be suitable to adjust the Si:Al ratio for geopolymer production. To optimize the dissolution in lower NaOH concentrations, a longer reaction time up to 7 days, i.e. pre-solution prior to mixing the precursors, should be considered for $Al(OH)_3$. Furthermore, the lateral dimension of the layers of the clay minerals (e.g. the specific surface area and accessible edge surface) influenced the solubility. The comparison of the solubility of two different metakaolinites showed that the metakaolinite with the larger specific surface area was dissolved to a greater extent. The same trend was observed for the solubility of two different metamontmorillonites. The results of the solubility experiments and first tests on geopolymer production in waterglass ($Na_{2x}Si_yO_{2y+x}$) free systems led to the assumption that all three clay minerals are suitable as precursors. Different amounts of unreacted metaclay minerals in the hardened binders are expected, which supposedly will influence the mechanical properties of the resulting geopolymers.

Acknowledgments

This project was funded by Deutsche Forschungsgemeinschaft under EM79/8-1. The ICP-OES measurements were performed with the help of Chantalle Kotschenreuther (Institute of Applied Geoscience, Karlsruhe Institute of Technology (KIT), Karlsruhe, Germany) and Silke Berberich (Competence Center for Material Moisture (CMM), Karlsruhe Institute of Technology (KIT), Karlsruhe, Germany). XRF measurements were performed by Nora Groschopf (Johannes Gutenberg-Universität, Mainz, Germany). The authors thank Yi-Yu Liu (CMM) for preparation of AFM samples by spin coating. AFM measurements were performed by Peter Krolla (Institute of Functional Interfaces,

Karlsruhe Institute of Technology (KIT), Karlsruhe, Germany). The authors would like to express their sincere thanks to the reviewers for their very helpful comments and suggestions.

References

Amram, K., & Ganor, J. (2005). The combined effect of pH and temperature on smectite dissolution rate under acidic conditions. *Geochimica et Cosmochimica Acta, 69(10),* 2535–2546.

Assemi, S., Sharma, S., Tadjiki, S., Prisbrey, K., Ranville, J., & Miller, J. D. (2015). Effect of surface charge and elemental composition on the swelling and delamination of montmorillonite nanoclays using sedimentation field–flow fractionation and mass spectroscopy. *Clays and Clay Minerals, 63(6),* 457–468.

Badogiannis, E., Kakali, G., & Tsivilis, S. (2005). Metakaolin as supplementary cementitious material: Optimization of kaolin to metakaolin conversion. *Journal of Thermal Analysis and Calorimetry, 81(2),* 457–462.

Bauer, A., & Berger, G. (1998). Kaolinite and smectite dissolution rate in high molar KOH solutions at 35 and 80 C. *Applied Geochemistry, 13(7),* 905–916.

Bauer, A., & Velde, B. (1999). Smectite transformation in high molar KOH solutions. *Clay Minerals, 34(2),* 259–273.

Bauer, A., Velde, B., & Berger, G. (1998). Kaolinite transformation in high molar KOH solutions. *Applied Geochemistry, 13(5),* 619–629.

Brunauer, S., Emmett, P. H., & Teller, E. (1938). Adsorption of gases in multimolecular layers. *Journal of the American Chemical Society, 60(2),* 309–319.

Buchwald, A., Hohmann, M., Posern, K., & Brendler, E. (2009). The suitability of thermally activated illite/smectite clay as raw material for geopolymer binders. *Applied Clay Science, 46(3),* 300–304.

Carroll-Webb, S. A., & Walther, J. V. (1988). A surface complex reaction model for the pH–dependence of corundum and kaolinite dissolution rates. *Geochimica et Cosmochimica Acta, 52(11),* 2609–2623.

Charlet, L., Alt-Epping, P., Wersin, P., & Gilbert, B. (2017). Diffusive transport and reaction in clay rocks: A storage (nuclear waste, CO2, H2), energy (shale gas) and water quality issue. *Advances in Water Resources, 106,* 39–59.

Chermak, J. (1992). Low temperature experimental investigation of the effect of high pH NaOH solutions on the Opalinus Shale, Switzerland. *Clays and Clay Minerals, 40,* 650–650.

Cuevas, J., De La Villa, R. V., Ramírez, S., Sánchez, L., Fernández, R., & Leguey, S. (2006). The alkaline reaction of FEBEX bentonite: A contribution to the study of the performance of bentonite/concrete engineered barrier systems. *Journal of Iberian Geology, 32(2),* 151–174.

De Windt, L., Deneele, D., & Maubec, N. (2014). Kinetics of lime/bentonite pozzolanic reactions at 20 and 50 °C: Batch tests and modeling. *Cement and Concrete Research, 59,* 34–42.

Delavernhe, L., Steudel, A., Darbha, G., Schäfer, T., Schuhmann, R.,Wöll, C., Geckeis, H., & Emmerich, K. (2015). Influence of mineralogical and morphological properties on the cation exchange behavior of dioctahedral smectites. *Colloids and Surfaces A: Physicochemical and Engineering Aspects, 481,* 591–599.

Dietel, J., Warr, L.N., Bertmer, M., Steudel, A., Grathoff, G.H., & Emmerich, K. (2017). The importance of specific surface area in the geopolymerization of heated illitic clay. *Applied Clay Science, 139,* 99–107.

Doebelin, N., & Kleeberg, R. (2015). Profex: A graphical user interface for the Rietveld refinement program BGMN. *Journal of Applied Crystallography, 48(5),* 1573–1580.

Dohrmann, R., Kaufhold, S., & Lundqvist, B. (2013). The role of clays for safe storage of nuclear waste. In F. Bergaya & G. Lagaly (Eds.). *Developments in Clay Science, 5,* 677–710.

Drits, V., Besson, G.,&Muller, F. (1995). An improved model for structural transformation of heat–treated aluminous dioctahedral 2: 1 layer silicates. *Clays and Clay Minerals, 43(6),* 718–731.

Duxson, P., Provis, J. L., Lukey, G. C., Mallicoat, S. W., Kriven, W. M., & Van Deventer, J. S. (2005). Understanding the relationship between geopolymer composition, microstructure and mechanical properties. *Colloids and Surfaces A: Physicochemical and Engineering Aspects, 269(1–3),* 47–58.

Elert, K., Pardo, E. S., & Rodriguez–Navarro, C. (2015). Mineralogical evolution of di–and trioctahedral smectites in highly alkaline environments. *Clays and Clay Minerals, 63(6),* 414–431.

Elzea, J., Odom, I., & Miles, W. (1994). Distinguishing well ordered opal-CT and opal-C from high temperature cristobalite by X-ray diffraction. *Analytica Chimica Acta, 286(1),* 107–116.

Emmerich, K., Wolters, F., Kahr, G., & Lagaly, G. (2009). Clay profiling: The classification of montmorillonites. *Clays and Clay Minerals, 57(1),* 104–114.

Fernández, R., Cuevas, J., Sánchez, L., de la Villa, R. V., & Leguey, S. (2006). Reactivity of the cement–bentonite interface with alkaline solutions using transport cells. *Applied Geochemistry, 21(6),* 977–992.

Fletcher, R.A., MacKenzie, K. J., Nicholson, C. L., & Shimada, S. (2005). The composition range of aluminosilicate geopolymers. *Journal of the European Ceramic Society, 25(9),* 1471–1477.

Garg, N., & Skibsted, J. (2015). Heated montmorillonite: Structure, reactivity, and dissolution. *Calcined clays for sustainable concrete,* 117–124.

Garg, N., & Skibsted, J. (2019). Dissolution kinetics of calcined kaolinite and montmorillonite in alkaline conditions: Evidence for reactive Al (V) sites. *Journal of the American Ceramic Society, 102(12),* 7720–7734.

Glass, H. D. (1954). High–temperature phases from kaolinite and halloysite. *American Mineralogist: Journal of Earth and Planetary Materials, 39(3–4),* 193–207.

Grathoff, G. H., &Moore, D. (1996). Illite polytype quantification using WILDFIRE [C] calculated X–ray diffraction patterns. *Clays and Clay Minerals, 44(6),* 835–842.

Grim, R. E., & Kulbicki, G. (1961). Montmorillonite: High temperature reactions and classification. American Mineralogist: *Journal of Earth and Planetary Materials, 46(11–12),* 1329–1369.

Güven, N. (1990). Longevity of bentonite as buffer material in a nuclear–waste repository. *Engineering Geology, 28(3–4),* 233–247.

He, C., Makovicky, E., & Øsbæck, B. (1995a). Thermal stability and pozzolanic activity of calcined illite. *Applied Clay Science, 9(5),* 337–354.

He, C., Osbaeck, B., & Makovicky, E. (1995b). Pozzolanic reactions of six principal clay minerals: Activation, reactivity assessments and technological effects. *Cement and Concrete Research, 25(8),* 1691–1702.

Hillier, S., & Lumsdon, D. (2008). Distinguishing opaline silica from cristobalite in bentonites: A practical procedure and perspective based on NaOH dissolution. *Clay Minerals, 43(3),* 477–486.

Honty, M., De Craen, M., Wang, L., Madejová, J., Czímerová, A., Pentrák, M., Striček, I., & Van Geet, M. (2010). The effect of high pH alkaline solutions on the mineral stability of the Boom Clay – Batch experiments at 60 °C. *Applied Geochemistry, 25(6),* 825–840.

Hu, N., Bernsmeier, D., Grathoff, G. H., & Warr, L. N. (2017). The influence of alkali activator type, curing temperature and gibbsite on the geopolymerization of an interstratified illite–smectite rich clay from Friedland. *Applied Clay Science, 135,* 386–393.

Huertas, F. J., Chou, L., & Wollast, R. (1999). Mechanism of kaolinite dissolution at room temperature and pressure. Part II: Kinetic study. *Geochimica et Cosmochimica Acta, 63(19–20),* 3261–3275.

Izadifar, M., Thissen, P., Steudel, A., Kleeberg, R., Kaufhold, S., Kaltenbach, J., Schuhmann, R., Dehn, F., & Emmerich, K. (2020). Comprehensive examination of dehydroxylation of kaolinite, disordered kaolinite, and dickite: Experimental studies and Density Functional Theory. *Clays and Clay Minerals, 68(4),* 319–333.

Janek, M., Komadel, P., & Lagaly, G. (1997). Effect of autotransformation on the layer charge of smectites determined by the alkylammonium method. *Clay Minerals, 32(4),* 623–632.

Karnland, O., Olsson, S., Nilsson, U., & Sellin, P. (2007). Experimentally determined swelling pressures and geochemical interactions of compacted Wyoming bentonite with highly alkaline solutions. *Physics and Chemistry of the Earth, Parts A/B/C, 32(1–7),* 275–286.

Kayabali, K. (1997). Engineering aspects of a novel landfill liner material: Bentonite–amended natural zeolite. *Engineering Geology, 46(2),* 105–114.

Khalifa, A. Z., Pontikes, Y., Elsen, J., & Cizer, Ö. (2019). Comparing the reactivity of different natural clays under thermal and alkali activation. *RILEM Technical Letters, 4,* 74–80.

Khalifa, A. Z., Cizer, Ö., Pontikes, Y., Heath, A., Patureau, P., Bernal, S. A., & Marsh, A. T. (2020). Advances in alkali–activation of clay minerals. *Cement and Concrete Research, 132,* 106050.

Köhler, S. J., Dufaud, F., & Oelkers, E. H. (2003). An experimental study of illite dissolution kinetics as a function of pH from 1.4 to 12.4 and temperature from 5 to 50 °C. *Geochimica et Cosmochimica Acta, 67(19),* 3583–3594.

Kuwahara, Y. (2006). In-situ AFM study of smectite dissolution under alkaline conditions at room temperature. *American Mineralogist, 91(7),* 1142–1149.

Locati, F., Marfil, S., Baldo, E., & Maiza, P. (2010). Na2O, K2O, SiO2 and Al2O3 release from potassic and calcic–sodic feldspars into alkaline solutions. Cement and Concrete Research, 40(8), 1189–1196.

Madsen, F. T. (1998). Clay mineralogical investigations related to nuclear waste disposal. *Clay Minerals, 33(1),* 109–129.

McConville, C. J., & Lee, W. E. (2005). Microstructural development on firing illite and smectite clays compared with that in kaolinite. *Journal of the American Ceramic Society, 88(8),* 2267–2276.

Metz, V., Amram, K., & Ganor, J. (2005). Stoichiometry of smectite dissolution reaction. *Geochimica et Cosmochimica Acta, 69(7),* 1755–1772.

Mosser-Ruck, R., & Cathelineau, M. (2004). Experimental transformation of Na, Ca-smectite under basic conditions at 150 °C. *Applied Clay Science, 26(1–4),* 259–273.

Nagy, K. L. (2018). Chemical weathering rates of silicate minerals. *In F. W. Arthur & L. B. Susan (Eds.), Chapter 5.* Dissolution and precipitation kinetics of sheet silicates, 173–234.

Nakayama, S., Sakamoto, Y., Yamaguchi, T., Akai, M., Tanaka, T., Sato, T., & Iida, Y. (2004). Dissolution of montmorillonite in compacted bentonite by highly alkaline aqueous solutions and diffusivity of hydroxide ions. *Applied Clay Science, 27(1),* 53–65.

Nikolov, A., Rostovsky, I., & Nugteren, H. (2017). Geopolymer materials based on natural zeolite. *Case Studies in Construction Materials, 6,* 198–205.

Pabalan, R. T., & Pitzer, K. S. (1987). Thermodynamics of NaOH (aq) in hydrothermal solutions. *Geochimica et Cosmochimica Acta, 51(4),* 829–837.

Pereira, J. A., Schwaab, M., Dell'Oro, E., Pinto, J. C., Monteiro, J.L., & Henriques, C. A. (2009). The kinetics of gibbsite dissolution in NaOH. *Hydrometallurgy, 96(1–2),* 6–13.

Rozalén, M. L., Huertas, F. J., Brady, P. V., Cama, J., García-Palma, S., & Linares, J. (2008). Experimental study of the effect of pH on the kinetics of montmorillonite dissolution at 25 °C. *Geochimica et Cosmochimica Acta, 72(17),* 4224–4253.

Rozalen, M., Huertas, F. J., & Brady, P. V. (2009). Experimental study of the effect of pH and temperature on the kinetics of montmorillonite dissolution. *Geochimica et Cosmochimica Acta, 73(13),* 3752–3766.

Sato, T., Kuroda, M., Yokoyama, S., Fukushi, K., Tanaka, T., & Nakayama, S. (2003). Mechanism and kinetics of smectite dissolution under alkaline conditions. *Geochimica et Cosmochimica Acta, 67(18),* A415.

Sato, T., Kuroda, M., Yokoyama, S., Tsutsui, M., Pacau, C., Ringor, C., Fukushi, K., Tanaka, T., & Nakayama, S. (2005). Dissolution kinetics of smectite under alkaline conditions. *Clays in Natural and Engineered Barriers for Radioactive Waste Confinement.* Int. Meeting, March, 14–18, Tours, France.

Seiffarth, T., Hohmann, M., Posern, K., & Kaps, C. (2013). Effect of thermal pre-treatment conditions of common clays on the performance of clay-based geopolymeric binders. *Applied Clay Science, 73*, 35–41.

Shubbar, A. A., Sadique, M., Kot, P., & Atherton, W. (2019). Future of clay–based construction materials – A review. *Construction and Building Materials, 210*, 172–187.

Sonuparlak, B., Sarikaya, M., & Aksay, I. A. (1987). Spinel phase formation during the 980 °C exothermic reaction in the kaolinite-to-mullite reaction series. *Journal of the American Ceramic Society, 70(11)*, 837–842.

Steudel, A., Batenburg, L. F., Fischer, H. R., Weidler, P. G., & Emmerich, K. (2009a). Alteration of non–swelling clay minerals and magadiite by acid activation. *Applied Clay Science, 44(1)*, 95–104.

Steudel, A., Batenburg, L. F., Fischer, H. R., Weidler, P. G., & Emmerich, K. (2009b). Alteration of swelling clay minerals by acid activation. *Applied Clay Science, 44(1)*, 105–115.

Stevens, R. (1946). A system for calculating analyses of micas and related minerals to end members. *U.S. Geological Survey Bulletin, 950*, 101–119.

Tregger, N. A., Pakula, M. E., & Shah, S. P. (2010). Influence of clays on the rheology of cement pastes. *Cement and Concrete Research, 40(3)*, 384–391.

Valenzuela Díaz, F. R., & Santos, P. d. S. (2001). Studies on the acid activation of Brazilian smectitic clays. *Química Nova, 24*, 345–353.

Werling, N., Dehn, F., Krause, F., Steudel, A., Schuhmann, R., & Emmerich, K. (2020). Solubility of precursors and carbonation of waterglass-free geopolymers. *Clays and Clay Minerals, 68(5)*, 524–531.

Wolters, F., & Emmerich, K. (2007). Thermal reactions of smectites—Relation of dehydroxylation temperature to octahedral structure. *Thermochimica Acta, 462(1–2)*, 80–88.

Wolters, F., Lagaly, G., Kahr, G., Nueesch, R., & Emmerich, K. (2009). A comprehensive characterization of dioctahedral smectites. *Clays and Clay Minerals, 57(1)*, 115–133.

Xu, H., & Van Deventer, J. (2000). The geopolymerisation of alumino–silicate minerals. *International Journal of Mineral Processing, 59(3)*, 247–266.

Zysset, M., & Schindler, P. W. (1996). The proton promoted dissolution kinetics of K–montmorillonite. *Geochimica et Cosmochimica Acta, 60(6)*, 921–931.

7. Rehydroxylation of calcined swellable clay minerals at ambient conditions

The following study was submitted for publishing in Applied Clay Science and is a reprint of:

Werling, N., Kuligiewicz, A., Steudel, A., Schuhmann, R., Dehn, F., Emmerich, K. (2022). Rehydroxylation of calcined swellable clay minerals at ambient conditions. Applied Clay Science, (under review).

Sequences which were edited are marked in italics.

Abstract - Four typical reactions occur during thermal treatment of clay minerals, namely dehydration, dehydroxylation, breakdown of structure, and recrystallization of high temperature phases. After dehydration and/or dehydroxylation are completed, rehydration and rehydroxylation of the clay minerals are possible. The uptake of H_2O after dehydroxylation was observed in different atmospheres with varying temperature, pressure, and humidity. Rehydroxylation of non-swellable clay minerals occurred in bricks and ancient pottery. Swellable clay mineral rehydroxylation could enable the reuse of molding forms for foundry. As swellable clay minerals or mixtures of different clay minerals come into focus as precursors for geopolymers, it is important to pay attention to rehydroxylation in this context as well. Due to H_2O uptake after dehydroxylation, the reactivity of the calcined clay precursor and the properties of the geopolymer itself could be influenced. Therefore, the extent of rehydroxylation under ambient conditions, in which geopolymer precursors are stored until processing, has to be investigated. This work studied the rehydration and rehydroxylation of three different homoionic (Na^+, Ca^{2+}, Mg^{2+}) exchanged trans- and cis-vacant dioctahedral smectites at equal relative humidity (75% r.H.) at different temperatures (22, 40, and 60 °C) after calcination at 700 °C. Simultaneous thermal analysis was used to determine the amount of H_2O uptake (after 4, 24, 48, 72, and 168 h) due to rehydroxylation. The experimental data for mass gain during rehydroxylation was used for kinetic calculations of the activation energy (E_a). The experiments showed that rehydroxylation between 8.7% for a Na^+ saturated sample and up to 37.3% for a predominantly Mg^{2+}saturated sample took place within 7 d, depending on the material and interlayer cation. The α-free isoconvertional approach resulted in E_a of rehydroxylation in the range 32-90 kJ/mol for Ca-exchanged samples.

Keywords – dehydroxylation, rehydroxylation, 2:1 layer silicates, clay minerals, geopolymer precursor

7.1 Introduction

During thermal treatment clay minerals are subject to different reactions, including dehydration, dehydroxylation, structure decomposition and recrystallization to high temperature phases (Emmerich, 2013). Under certain conditions, if clay minerals are exposed to humidity after dehydroxylation, they will rehydrate and rehydroxylate. Rehydroxylation of clay minerals was documented in steam at high pressures up to 140 MPa (Roy and Brindley, 1956; Rocha et al., 1990; Emmerich et al., 1999; Muller et al., 2000; Wilson et al., 2003; Yusiharni and Gilkes, 2012), in the presence of water vapor or in liquid water at ambient pressure (Heller et al., 1962; Emmerich, 2000; Wilson et al., 2003; Perez-Rodriguez et al., 2010; Derkowski and Kuligiewicz, 2017), as well as at ambient conditions (Kawano and Tomita, 1991; Derkowski et al. 2012a, b).

Rehydroxylation of non-swellable clay minerals, like kaolinite polytypes (Hamilton and Hall, 2012) and pyrophyllite (Perez-Rodriguez et al., 2010), was studied due to the impact on ceramic and brick properties. Furthermore, the determination of rehydroxylation was used in dating of ancient pottery (Wilson et al., 2009; Hall et al., 2013; Clelland et al., 2015). Studies on rehydroxylation of non-swellable clay minerals remain scarce. Mass-gain of fired kaolinite was demonstrated to positively correlate with the amount of metakaolinite remaining in the sample after dehydroxylation, i.e. inversely proportional to the temperature of firing (dehydroxylation) (Mesbah et al. 2010). Similar behavior was observed for pyrophyllite (Perez-Rodriguez et al., 2010). Swellable clay minerals, like smectites, find application in molding forms in foundry (Siddique et al., 2010) and are partially dehydroxylated during molding process. Rehydration and rehydroxylation of the partially dehydroxylated smectites influence the recycling and reuse of the molding forms (Emmerich et al., 2011). Another potential application for dehydroxylated smectites is as a precursor for geopolymers. Dehydroxylation during the calcination process increases the reactivity (Garg and Skibsted, 2015) of the material to a maximum. The impact of rehydroxylation on the final geopolymer is not yet known, but supposedly unfavorable.

In nature pure smectites are the most commonly found as a component of bentonites. Smectites are 2:1 layer silicates with a layer charge of 0.2 to 0.6 per formula unit (pfu) and hydrated interlayer cations (Guggenheim et al., 2006). De- and rehydroxylation of smectites depend on the composition and structure of the 2:1 layers and the type of interlayer cations (Mackenzie and Bishui, 1958; Drits, et al., 1995; Muller et al., 2000; Wolters and Emmerich, 2007; Derkowski and Kuligiewicz, 2017). Bentonites usually contain dioctahedral smectites in which two out of three octahedral positions are occupied and octahedral cations are distributed over *trans*- and *cis*-sites. In *trans*-vacant (*tv*) smectites the two adjacent OH groups of the occupied M2 positions release a H_2O molecule during the dehydroxylation. A residual O atom (O_r) is retained (Drits et al. 1995). Dehydroxylation of *cis*-vacant (*cv*) smectites occurs in two stages. Firstly, the development of the O_r and, secondly, the migration of cations from the occupied *trans*-position (M1) onto a vacant *cis*- (M2) position, which requires additional energy. Due to these properties *tv* smectites dehydroxylate at lower temperatures than the *cv* smectites (Wolters and

Emmerich, 2007). Dehydroxylation temperature can be used to distinguish between *cv* and *tv* smectites, with the line between *tv* and *cv* usually defined at about 600 °C. However, dehydroxylation behavior of smectite depends also on exchangeable cation, sample amount, heating rate and further experimental conditions (Drits et al., 1995; Wolters and Emmerich, 2007). The structure of dehydroxylated *tv* and *cv* smectite layers is *trans*-vacant and rehydroxylated dioctahedral smectites with low iron content remain *tv* (Muller et al., 2000; Drits et al., 2012). The interlayer cations influence dehydroxylation temperature up to 50 K. The structure and hydration of the interlayer cations control the ability to reopen the interlayer for rehydration and rehydroxylation (Derkowski et al., 2012b; Derkowski and Kuligiewicz 2017). For reopening the collapsed interlayer additional energy is needed because of the strong interaction of interlayer cations with the 2:1 layers (Derkowski et al., 2012a). The reexpansion of the interlayer depends on the size of the interlayer cation ($K^+ > Na^+ \approx Ca^{2+} > Mg^{2+}$) (Kawano and Tomita, 1991). For rehydroxylation the water molecules need to enter the interlayer and must pass through the ditrigonal cavities to reach the octahedral sheet and the residual O_r atoms. It may occur that the interlayer cations are bound close to the plane of basal O atoms and are located directly above the ditrigonal cavity. Therefore, they can block the reentry of water molecules into the octahedral sheet (Derkowski et al. 2012b). Experimental conditions like temperature, time, water availability and pressure, are further influencing factors for rehydration and rehydroxylation.

The aim of this study was to investigate the amount of rehydration and rehydroxylation of three different homoionic smectites (at equal relative humidity) depending on the temperature. The experimental data for mass gain during rehydroxylation was used for kinetic calculations of the activation energy (E_a).

7.2 Materials & Methods

7.2.1 Homoionic materials

Pure montmorillonite samples were obtained by enriching the < 2 µm fraction from three different bentonites: BV, BC and BP, obtained from Clariant (Clariant Produkte GmbH, Germany). Detailed description of samples can be found in Steudel et al. (2015) and Delavernhe et al (2015). The < 2 µm fraction was obtained by sedimentation. Subsequently, the suspension of the < 2 µm fraction was divided into two parts. Batch 1 was not treated further. Batch 2 was saturated with Ca^{2+}. For homoionic exchange the corresponding chloride solution ($CaCl_2$; Merck KGaA, Germany) was used until homoionic saturation was reached (Steudel & Emmerich, 2013). After homoionic saturation batch 1 and 2 were dialyzed until the conductivity was below 5 µS/cm, to remove chloride and excess cations. After dialysis the samples were dried at 60 °C and manually ground. Batches will be denoted as B*X*_Y with X = C, V or P and Y standing for the predominant exchangeable cation.

Following the classification of Emmerich et al. (2009), the studied smectites could be classified as low-charged cv beidellitic montmorillonite (BV), low-charged cv/tv montmorillonite (BP), and low-charged cv/tv ferrian beidellitic montmorillonite (BC). Tetrahedral and octahedral cations per formula unit

$[O_{10}(OH)_2]$ and distribution of cis- and trans-vacant layers were obtained from Steudel et al. (2015) and Delavernhe et al. (2015) (*Table 13*). Molar weight and maximum mass loss due to dehydroxylation were calculated from the structural formulae related to the final mass of the ignited solid.

7.2.2 Dehydroxylation and rehydroxylation of homoionic samples

Samples were stored under ambient conditions (21 °C, 50 – 60% r.H.) before dehydration and dehydroxylation.

Samples were dehydrated (DHD) and dehydroxylated (DHX) in in a L9/12/B180 furnace (Nabertherm, Germany). 700 mg of a sample were placed in an unglazed ceramic saggar and ramp heated to 10 K/min to 700 °C. Samples for each rehydroxylation temperature (22, 40, and 60 °C) were prepared separately. The samples were transferred immediately without cooling into a desiccator with an atmosphere of 75 (±0.4)% r.H. and prescribed rehydroxylation temperature. Small portions of samples were taken for measurements after RHX times of 4, 24, 48, 72 and 168 h.

7.2.3 Analytical Techniques

CEC was determined according to the procedure described in Chapter 3.2.

The completeness of homoionic cation exchange was studied on the supernatant of the CEC measurements by inductively coupled plasma optic emission spectrometry (ICP-OES) with an Optima 8300DV (PerkinElmer, Massachusetts, USA). The calibration for Na, K, Mg and Ca concentrations in solution was performed up to 30 mg/L. 5 ml of the liquid supernatants were acidified with 0.2 ml 1 mol/L HNO_3 and diluted with 4.8 ml deionized water (dilution factor 2).

At first, a series *of STA* measurements was performed on the homoionic samples without previous dehydroxylation. Those samples were stored under ambient conditions (21 °C, 50 – 60% r.H.) before measurements. The samples after rehydroxylation were taken directly from the storage desiccators (75% ±0.4 r.H. above saturated NaCl solution) before measurements. *STA measurements were carried out as described in Chapter 3.4.* To check the completeness of DHX and potential remaining OH^- groups, a STA measurement for each dehydroxylated sample was performed without RHX. After DHX in the furnace was finished, the samples for these measurements were transferred to a desiccator, with P_2O_5 as desiccant to prevent RHX, and were measured by STA immediately.

Table 13. Tetrahedral and octahedral cations per formula unit [$O_{10}(OH)_2$] (from Steudel et al., 2015 & Delavernhe et al., 2015), molar weight (M), ratio of tv and cv 2:1 layers.

		Inter-layer	tetrahedral occupation		octahedral occupation				M	octahedral structure	
sample	Inter-layer cation	M^+	Si	Al	Al	Fe^{3+}	Fe^{2+}	Mg		tv	cv
									[g/mol]	[%]	[%]
BV_Na	Na^+	0.262	3.926	0.074	1.595	0.189	0.009	0.221	371.8	0	100
BP_Na	Na^+	0.342	3.964	0.036	1.379	0.157	0.021	0.522	374.1	39	61
BC_Na	Na^+	0.310	3.891	0.109	1.334	0.337	0.020	0.373	377.9	44	56

7.2.4 Kinetic Calculations

Three kinetic models were used to study kinetics of rehydroxylation in the present study: the time to the quarter model (TTTQ), the power-law model, and the α-free isoconvertional approach.

Mass gain of the dehydroxylated clay minerals and ceramics is usually described with the time to the quarter model (Hall et al., 2013), applicable to the isothermal conditions:

$$\Delta m = k_{RHX}(T)t^{0.25} \quad \text{(Eq. 1)}$$

with Δm = fractional mass gain, $k_{RHX}(T)$ = rehydroxylation rate constant (temperature dependent), and t is elapsed time since dehydroxylation.

Values of k_{RHX} obtained from microbalance experiments with ceramic materials at 10-20 °C were in the $1 - 5 \cdot 10^{-3}$ $yr^{-1/4}$ range, indicating that long-term rehydroxylation is slow (Hall et al., 2013). The temperature dependence of k_{RHX} can be described by the Arrhenius-like equation (Hall et a. 2013):

$$\frac{\mathrm{dln}k_{RHX}}{\mathrm{d}(\frac{1}{T})} = \frac{\mathrm{Ea}}{4\mathrm{R}} \quad \text{(Eq. 2)}$$

where $\alpha = \alpha_0$ at a reference temperature T_0. Ea is the activation energy of rehydroxylation and R is the gas constant (Hall et al., 2013). The activation energy describes the height of the activation barrier that controls the rate-limiting step, although the concept of Ea is strictly applicable to a single-step process only. Rehydroxlyation is a multi-step process of at least three steps: adsorption, diffusion, and the reaction with O_r and thus Ea is Ea of the rate limiting process.

The TTTQ model can be thought of as a special case of a generalized power-law (Bangham) model (Dalal, 1974; Largitte and Pasquier, 2016), that is used in the adsorption kinetic studies. For the isothermal rehydroxylation, power-law model takes the following form (symbols as in Eq. 1):

$$\Delta m = k_{RHX}t^n \quad \text{(Eq. 3)}$$

The exponent n in Eq. 3 is an adjustable parameter. Power-low model belongs to the class of diffusional models, in which kinetics of adsorption are controlled by the internal diffusion of adsorbed species in the adsorbent.

As a third approach used, was α-free isoconvertional approach of Kuligiewicz and Derkowski (2021), which uses the equation:

$$\ln\left(\frac{d\Delta m}{dt}\right) = LnA + Ln\big(f(\alpha)\big) + Ln(\Delta m_{MAX}) - \frac{E_a}{RT} \quad \text{(Eq. 4)}$$

Eq. 4 is equivalent of the isoconvertional approach for isothermal conditions (Vyazovkin et al., 2011), however, it enables to use only mass change (Δm) instead of the reaction progress (α) in the calculations. Effectively, this means that the knowledge of the end point of the reaction is not required. The end point would be the maximum mass gain when RHX is completed. The α-free isoconvertional calculations can

bypass this problem. As in all isoconvertional approaches, however, the α-free approach requires comparison of dΔm/dt values for the same dm value at all temperatures. This was not always possible due to the limited time resolution of experimental data. In order to solve this issue, power law was used to model mass gain curves and, subsequently, dΔm/dt values corresponding to the predefined Δm values were calculated, which allowed for E_a calculation.

7.3 Results & Discussion

7.3.1 Cation exchange capacity and exchangeable cations

CEC was between 69 and 127 cmol(+)/kg. The BP samples showed the highest, those of BC the lowest CEC. For all samples, the difference between the calcium and the sodium exchanged batches was in a range of maximum 5 cmol(+)/kg (*Table 14*). The calcium exchanged samples (B*X*_Ca) were almost completely exchanged and showed amounts of > 90% Ca^{2+} as main cation (*Table 14*). The sodium exchanged samples (B*X*_Na) still contained up to 21% Ca^{2+}, but the main exchangeable cation was Na^{+} with amounts > 70%. Only the homoionic exchange of BC_Na seemed to have failed. The exchanged cations for this sample were mainly Ca^{2+} and Mg^{2+}. Therefore, BC_Na will be referred to as BC_Ca/Mg hereafter.

Table 14. CEC and percentage of exchangeable cations.

	BV_Na	BV_Ca	BP_Na	BP_Ca	BC_Ca/Mg	BC_Ca
CEC [cmol(+)/kg]	88	89	127	123	74	69
Exchanged cation [%]						
Ca	21	93.1	19.3	94.1	74.4	92
Na	70.3	0.5	72	0.4	4.6	0.3
Mg	8	6.1	7.9	4.9	19.4	6
K	0.7	0.3	0.9	0.5	1.6	1.7

CEC decreased significantly after dehydroxylation at 700 °C. Independently from the main exchanged cation, the CEC decreased by 93 – 99% to a maximum of 5 cmol(+)/kg (*Table 15*). BC_Ca showed a complete loss of CEC. The loss of CEC after heating could be attributed to the collapse of the interlayers. The collapsed interlayers could not be penetrated by the Cu-trien anymore, therefore, an exchange of cations was not possible. Only small amounts of cations from the edges were still exchangeable (Steudel et al. 2015), as was confirmed by the ICP-OES measurements (*Table 15*).

Table 15. CEC and reduction of exchangeable cations after heating up to 700 °C.

	BV_Na	BV_Ca	BP_Na	BP_Ca	BC_Ca/Mg	BC_Ca
CEC [cmol(+)/kg]	1	3	2	2	5	0
Reduction of exchanged cation [cmol(+)/kg]						
Ca	- 19	- 84	- 23	- 120	- 65	- 80
Na	- 62	- 1	- 86	- 1	+ 1	- 0
Mg	- 6	- 5	- 9	- 5	- 15.5	- 5
K	- 1	- 0	- 1	- 1	- 0	- 2

7.3.2 Dehydration and dehydroxylation behavior

For the differentiation between *cis*- and *trans*-vacant sites the STA data of the, undehydroxylated materials were used. As mentioned before, *cis*-vacant montmorillonites dehydroxylate at higher temperatures (> 600 °C) compared to *trans*-vacant ones. The interlayer cations influenced the DHX temperatures only slightly (within a range of 6 K). Both samples of BV showed temperatures of DHX > 700 °C (observed in the DSC signal and in the mass spectrometer m/z = 18 signal) (*Fig. 23a+b*). This verified that the material had 100% *cis*-vacant sites (*Table 13*). The second DHX peak observed for BV_Na is related to sudden release of entrapped water (Emmerich, 2013). Traces of CO_2 (m/z = 44) could be observed by mass spectrometer. The decomposition of CO_2 containing phases (carbonates) contributed to about 0.13% (BV_Na) and 0.15% (BV_Ca) of the mass loss > 300 °C. For the samples of BP, the mass spectrometer (m/z = 18) peak started below and ended above 600 °C. The starting temperature of the reaction showed that water release already started < 600 °C and continued to about 640 °C (*Fig. 24a+b*). These results confirmed a mixture of *cis*- and *trans*-vacant sites in the BP samples. For the samples of BC a mixture of *cis*- and *trans*-vacant sites was detected because two peaks (at about 520 and 665 °C) were well separated from each other (*Fig. 25a+b*). As for BV samples before, traces of CO_2 were detected by mass spectrometer (m/z = 44). About 0.27% (BC_Na) and 0.29% (BC_Ca) of the mass loss > 300 °C could be attributed to decomposition of carbonates.

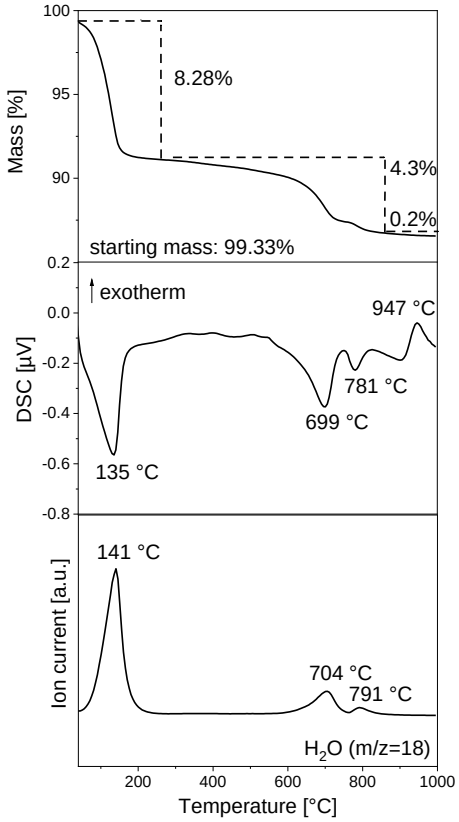

Fig. 23a. Thermal reactions of the homoionic material of BV_Na

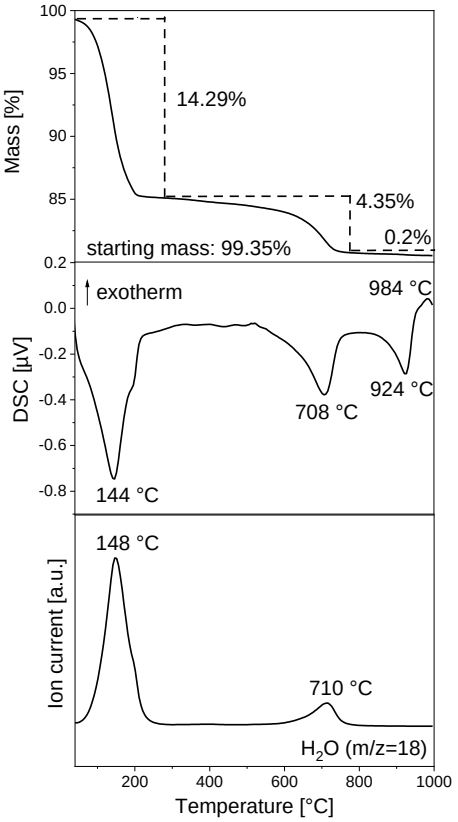

Fig. 23b. Thermal reactions of the homoionic material of BV_Ca

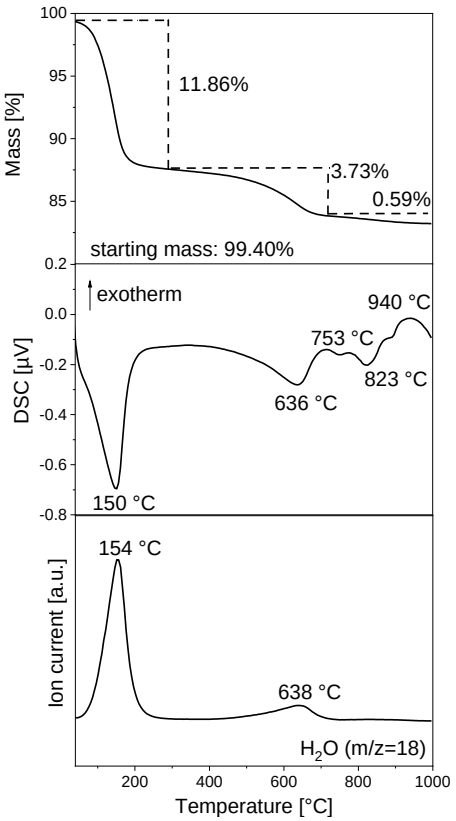

Fig. 24a. Thermal reactions of the homoionic material of BP_Na

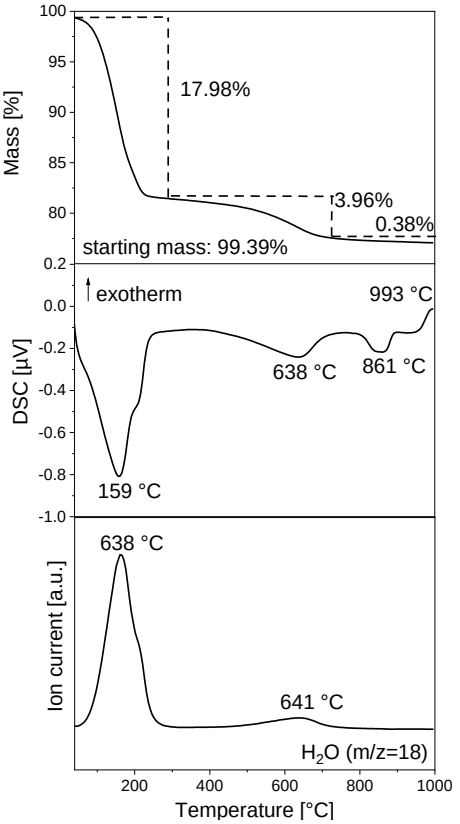

Fig. 24b. Thermal reactions of the homoionic material of BP_Ca

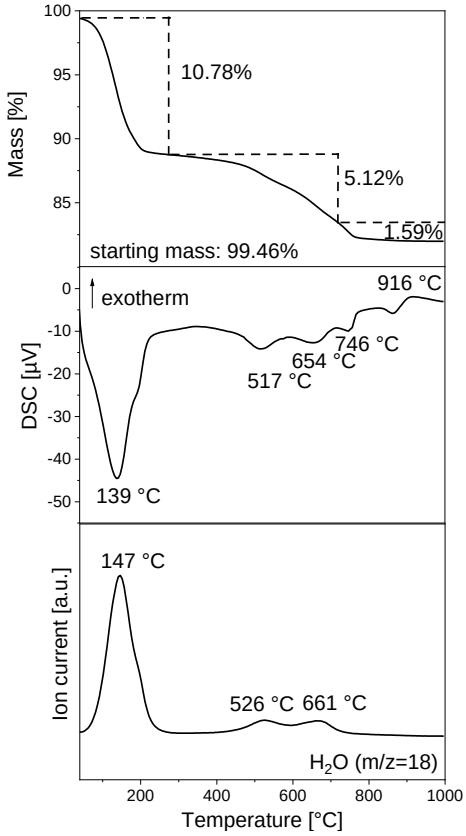

Fig. 25a. Thermal reactions of the homoionic material of BC_Ca/Mg

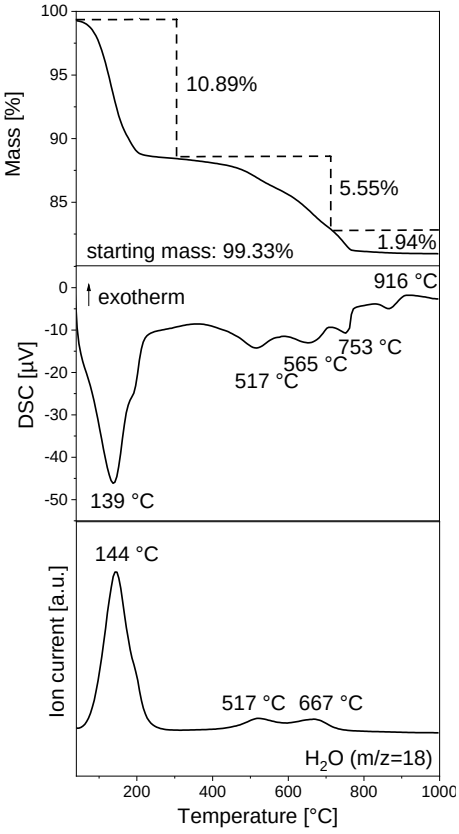

Fig. 25b. Thermal reactions of the homoionic material of BC_Ca

The moisture of the initial homoionic smectites was calculated from the mass loss during the isothermal segment of the STA at 35 °C and the mass loss during the dynamic segment up to 300 °C and was related to the initial mass of the sample. Accordingly, the water content was calculated in relation to the dry mass at 300 °C (*Table 16*).

The calcium exchanged samples of BV and BP showed larger water contents than their sodium exchanged counterparts. Both samples of BC showed nearly the same water content because of similar interlayer saturation by divalent cations. Divalent cations like Ca^{2+} and Mg^{2+} show a significantly larger hydration energy compared to Na^{+} (or other monovalent cations). The samples of BP showed the largest water content. The samples of BV had an intermediate water content. The lowest water content was detected for BV_Na because none of the samples of BC had a monovalent cation in the interlayer. For divalent interlayer cations, the samples of BC showed the lowest water content.

Table 16. Moisture and water content values calculated from mass loss during DHD, mass loss during DHX, and calculated degree of DHX (heating rate 10 K/min; starting temperature for DHD 35 °C and for DHX 300 °C).

	Dehydration			Dehydroxylation		
	$T_{end,DHD}$ [°C]	moisture [%]	Water content [%]	$T_{end,DHX}$ [°C]	Δm_{DHX} [%]*	Degree of DHX [%]
BV_Na	300	8.9	9.1	850	3.9	68
BV_Ca	300	14.9	16.8	800	4.9	79
BP_Na	300	12.5	13.6	730	4.2	72
BP_Ca	300	18.6	22.1	750	4.6	73
BC_Ca/Mg	300	11.3	12.2	715	5.4	90
BC_Ca	300	11.6	12.3	715	5.9	99

*normalized to mass at 300 °C

Mass loss during DHX (Δm_{DHX}) was normalized to the dry weight of the sample at 300 °C to be comparable to stochiometric release of water during DHX. By comparing Δm_{DHX} obtained from STA measurements with the theoretical mass loss due to DHX (calculated from the structural formulae) the degree of DHX of the samples was determined (*Table 16*).

Further mass loss after DHX was detectable for the samples by additional STA measurements and attributed to remaining OH^- groups, which were not removed during DHX in the furnace. By normalization to dry weight $\Delta m_{remainingOH^-}$ was obtained (*Table 17*). It was necessary to use $\Delta m_{remainingOH^-}$ for subsequent corrections of the uptake of H_2O by RHX.

Table 17. Mass loss due to remaining OH^- groups after DHX.

sample	Heating rate [°C/min]	Remaining OH^-		
		T_{start} [°C]	T_{end} [°C]	$\Delta m_{remainingOH^-}$ [%]
BV_Na	10	300	1000	0.8
BV_Ca	10	300	1000	0.6
BP_Na	10	300	1000	0.8
BP_Ca	10	300	1000	0.8
BC_Ca/Mg	10	300	1000	1.0
BC_Ca	10	300	1000	0.8

7.3.3 Rehydration and rehydroxylation behavior

To obtain the degree of RHX (in %) the mass loss (Δm_{RHX}) during repeated (2^{nd}) DHX after RHX in the desiccator was related to the dry weight of the sample ($m_{300\ °C}$). Subsequently, $\Delta m_{remainingOH}$- was subtracted from Δm_{RHX} to correct the mass loss values ($\Delta m_{corrected}$). To determine RHX (in %), $\Delta m_{corrected}$ was divided by the calculated maximum Δm_{DHX} (from structural formula).

After 7 d of RHX at 60 °C BV_Na showed a mass loss of 0.55% up to 300 °C (*Fig. 26a*) which was attributed to rehydrated water. Between 300 and 650 °C a second mass loss (0.5%) of rehydroxylated water was detected. The third mass loss with a peak temperature of 797 °C was already detected during STA (up to 1000 °C) of the starting material (*Fig. 23a*). As DHX before RHX took place at 700 °C in the oven, this mass loss was attributed to OH groups not removed during the initial dehydroxylation. For BV_Ca mass loss due to rehdydrated water until 300 °C was 1.53% (*Fig. 26b*). From 300 to 650 °C mass loss was 1.1% due to rehydroxylated water.

BP_Na showed a mass loss of 1.75% up to 300 °C and of 0.4% between 300 and 650 °C due to rehydrated and rehydroxylated water (*Fig. 27a*). For BP_Ca mass loss due to rehydrated water was 2.56%, and due to rehydroxylated water 0.8% (*Fig. 27b*). Both samples of BP showed further release of water at about 850 – 880 °C which was not attributed to RHX.

BC_Ca/Mg showed a mass loss of 3.28% up to 300 °C due to rehydrated water. The mass loss (300 – 650 °C) due to rehydroxylated water was 1.7% (*Fig. 28a*). Mass loss due to rehydrated water in BC_Ca was 2.97% and 1.1% for rehydroxylated water (*Fig. 28b*).

All of the samples showed peak temperatures for the release of rehydroxylated OH groups between 463 and 511 °C. These observations showed that all samples were *trans*-vacant after RHX, which is characteristic for rehydroxylated smectites, regardless of the initial octahedral vacancies (Emmerich, 2000; Muller et al., 2000; Derkowski et al., 2012a; Hall et al., 2013; Derkowski and Kuligiewicz, 2017).

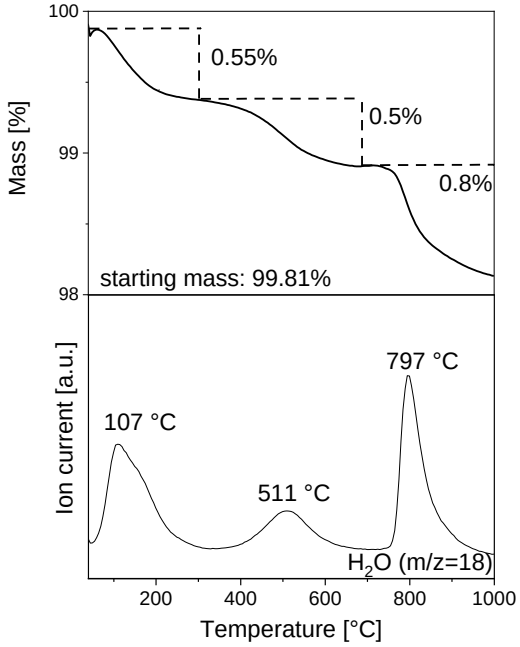

Fig. 26a. Thermal reactions of BV_Na after RHX (7 d at 60 °C).

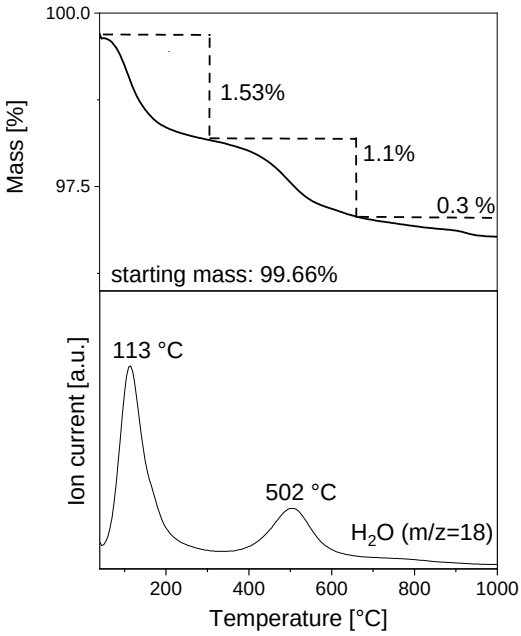

Fig. 26b. Thermal reactions of BV_Ca after RHX (7 d at 60 °C).

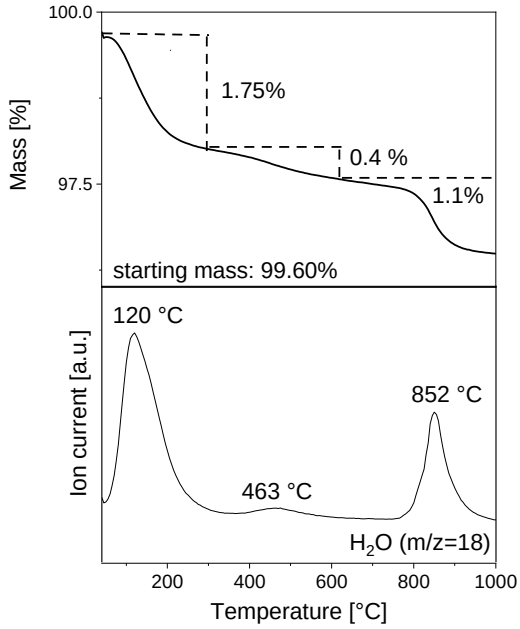

Fig. 27a. Thermal reactions of BP_Na after RHX (7 d at 60 °C).

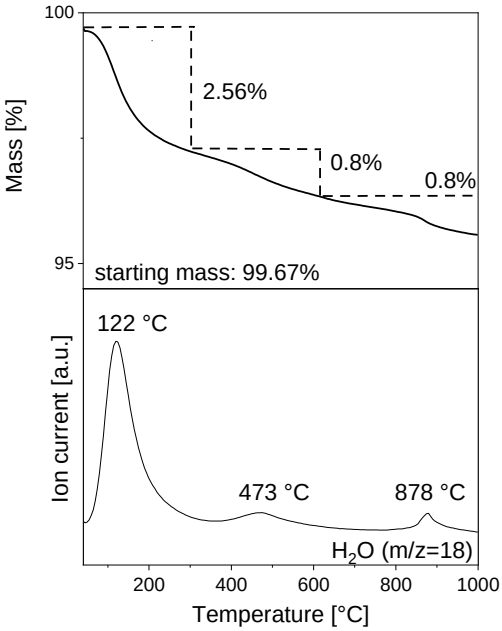

Fig. 27b. Thermal reactions of BP_Ca after RHX (7 d at 60 °C).

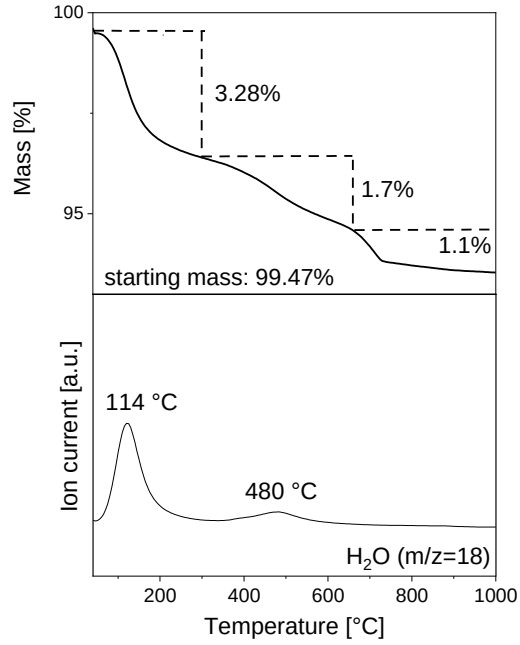

Fig. 28a. Thermal reactions of BC_Ca/Mg after RHX (7 d at 60 °C).

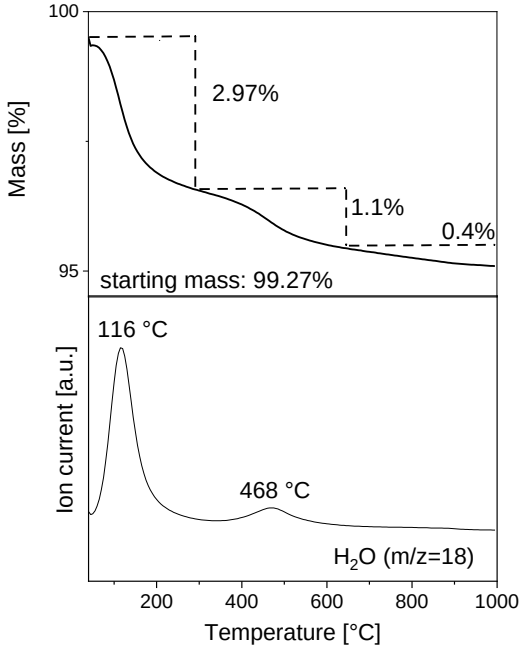

Fig. 28b. Thermal reactions of BC_Ca after RHX (7 d at 60 °C).

The adsorbed water content of the rehydrated-rehydroxylated (RHD) samples was small compared to the adsorbed water content of the initial samples (*Table 18*). The largest RHD was observed for the samples of BC both with mainly divalent interlayer cations. BP samples showed intermediate RHD and BV samples the lowest recovered water content. The RHD correlated to the particle size of the respective material. BV had the largest particle diameters (⌀ about 200 nm; Delavernhe et al., 2015) and the lowest recovered water content of all materials. BP had intermediate particle diameters (⌀ about 100 nm) and showed an intermediate recovered water content. BC had the smallest particles (⌀ about 75 nm) and showed the largest recovered water content. For larger particles the diffusion pathways are longer, therefore, the transport of water for RHD takes longer and inhibits the restoration.

Table 18. Recovered water content after 7 days of RHD (calculated by mass loss of 2nd DHD) at 75% r.H..

sample	Recovered water content [%]		
	22 °C	40 °C	60 °C
BV_Na	0.3	0.6	0.8
BV_Ca	1.6	1.6	1.9
BP_Na	1.9	1.7	2.2
BP_Ca	3.4	3.8	3.0
BC_Ca/Mg	4.0	4.0	4.0
BC_Ca	3.8	4.0	3.8

Smectites generally tend to adsorb less water at higher temperatures for constant RHX. BV samples adsorbed more water with increased temperature which was compensated for by kinetics; i.e., the increase in adsorption rate caused by increase in temperature offset the decrease in adsorption capacity. For BP and BC samples the "maximum" of adsorption was shifted towards lower temperatures. At 40 °C increased reaction rate compensated the decrease in adsorption capacity, but at 60 °C the decrease in adsorption capacity cannot be compensated by the increase in adsorption rate.

The RHX increased with increasing storage temperature for every sample, independent from the interlayer cation. BV_Na showed RHX of 0.2% at 22 °C, 5.3% at 40 °C, and 8.7% at 60 °C after 7 days in the desiccators (*Fig. 29a*). BV_Ca showed a larger degree of RHX than the Na^+ saturated batch (*Fig. 29b*). After 4 h at 40 °C RHX was 4.5% and 5.5% at 60 °C. Only at 22 °C BV_Ca did not show RHX after 4 h, similar to BV_Na. The maximum after 7 d at 22 °C was 4.4%, at 40 °C it was 11.4%, and at 60 °C the maximum degree of RHX was 16%.

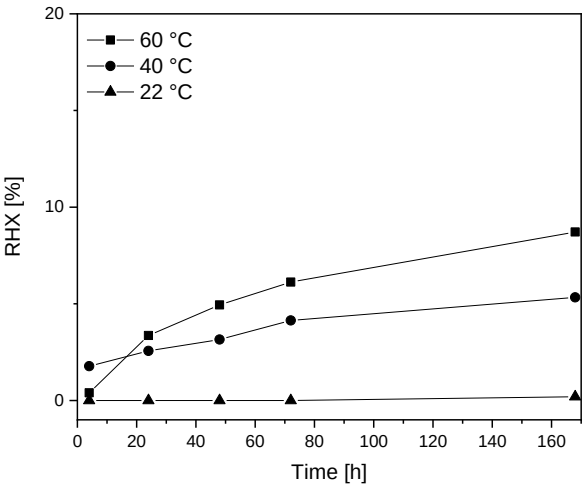

Fig. 29a. Degree of RHX (in %) of BV_Na at 22, 40, and 60 °C after reaction times between 4 and 168 h.

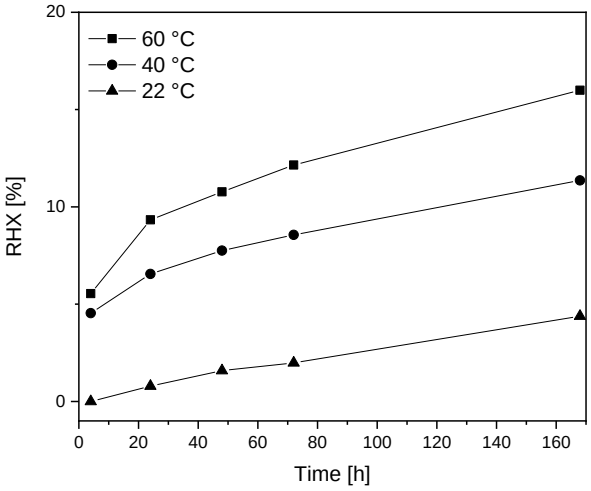

Fig. 29b. Degree of RHX (in %) of BV_Ca at 22, 40, and 60 °C after reaction times between 4 and 168 h.

For BP_Na the degree of RHX after 4 h was the lowest (*Fig. 30a*). At 22 °C no RHX was detected. At 40 °C RHX of 0.6% was reached after 4 h and at 60 °C RHX was 4.4%. As for BV samples before, RHX increased with time. At 22 °C the maximum of 6.5% was reached after 7 d, as well as 8.7% at 40 °C, and 13.8% at 60 °C. BP_Ca showed a larger degree of RHX (*Fig. 30b*), as observed for BV before. After 4 h the maximum RHX at 22 °C was 1.4%, about 6% at 40 and 60 °C. After 7 d BP_Ca reached a maximum RHX of 9.8% at 22 °C, 15.7% at 40 °C, and 15.9% at 60 °C.

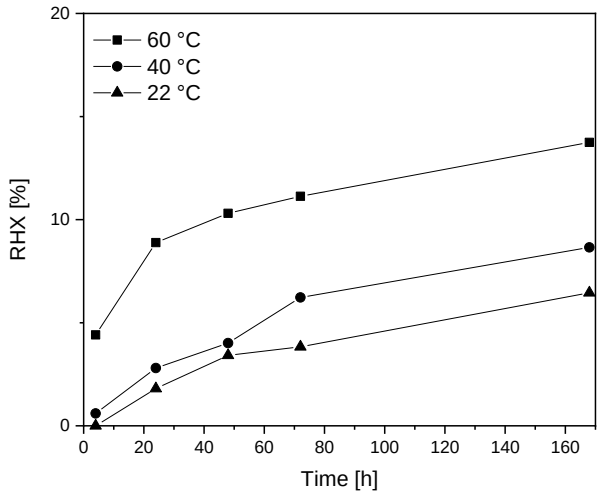

Fig. 30a. Degree of RHX (in %) of BP_Na at 22, 40, and 60 °C after reaction times between 4 and 168 h.

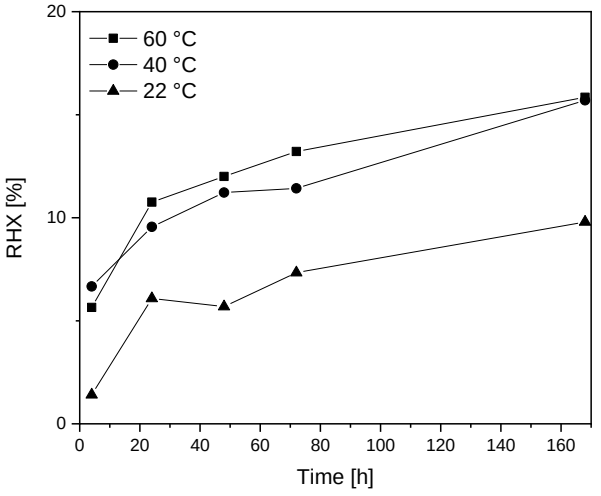

Fig. 30b. Degree of RHX (in %) of BP_Ca at 22, 40, and 60 °C after reaction times between 4 and 168 h.

BC_Ca/Mg showed the largest degree of RHX of all samples (*Fig. 31a*). After 4 h RHX at 22 °C reached 5.3%, 11.4% at 40 °C and, 17.6% at 60 °C. The RHX increased significantly up to 7 d to 24.1% at 22 °C, 34% at 40 °C, and 37.3% at 60 °C. BC_Ca showed RHX of < 4% after 4 h for each temperature (*Fig. 31b*). After 7 d RHX reached a maximum of 5.4% at 22 °C, 10.3% at 40 °C, and 13.6% at 60 °C, comparable to the RHX of the other Ca-saturated smectites. The largest RHX was reached for BC_Ca/Mg, which could be explained by the two different divalent interlayer cations. Due to the amount of Mg^{2+} with a higher hydration energy compared to Ca^{2+}, the sample showed a larger RHX compared to BC_Ca.

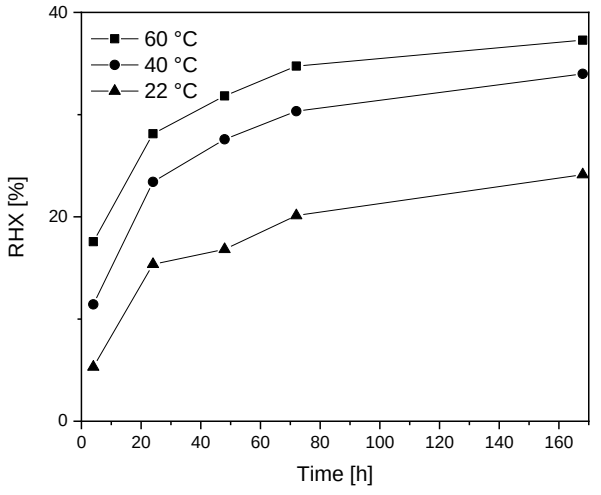

Fig. 31a. Degree of RHX (in %) of BC_Ca/Mg at 22, 40, and 60 °C after reaction times between 4 and 168 h.

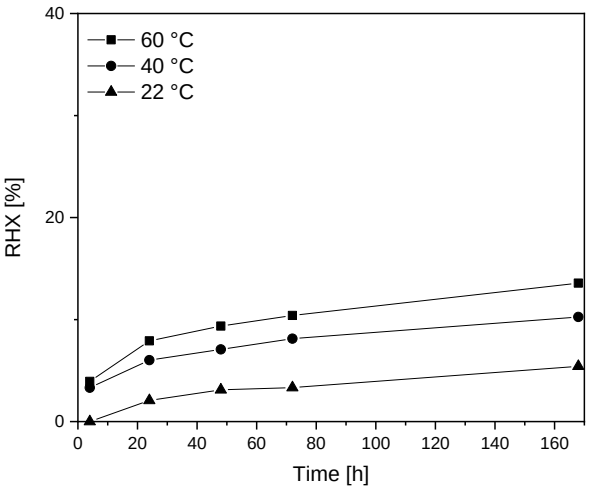

Fig. 31b. Degree of RHX (in %) of BC_Ca at 22, 40, and 60 °C after reaction times between 4 and 168 h.

The temperature during DHX influences the ability for RHX and has to be well below the thermal decomposition of the dehydroxylated 2:1 layers (Derkowski and Kuligiewicz, 2017). The same applies for the reactivity of calcined smectites to be used as precursors of geopolymers (He et al., 1995; Garg & Skibsted, 2015; Werling et al., 2022). The temperature for DHX in this study was fixed at 700 °C to ensure a high degree of DHX but also to enable RHX. DHX of rehydroxylated samples took place in a maximum temperature range between 450 – 550 °C for all samples, which is characteristic for restored tv octahedral sheets, regardless of the initial octahedral vacancies, which is in the agreement with earlier studies (Emmerich, 2000; Muller et al., 2000; Derkowski et al., 2012a; Hall et al., 2013; Derkowski and Kuligiewicz, 2017). The degree of RHX was dependent on initial 2:1 layer characteristics and interlayer occupation. All of the montmorillonites analyzed in this study showed tetrahedral charge (0.036 – 0.109 corresponding to 11 – 35% of the total layer charge), which favored spontaneous RHX of Al-rich dioctahedral smectites under ambient conditions (Emmerich, 2000), while ideal montmorillonites (no tetrahedral charge) showed almost no RHX (Derkowski and Kuligiewicz, 2017). However, for the Ca-saturated samples dehydroxylated at 700 °C and rehydroxylated at 75% r.H. and 60 °C for 7 d the degree of RHX varied only slightly between 13.6 and 16.0%. The lowest value was observed for BC_Ca with the highest amount of tetrahedral charge (*Table 13*) but lowest CEC (*Table 14*). BP_Ca had the lowest amount of tetrahedral charge but the highest CEC (*Tables 13 & 14*) and reached about the same degree of RHX as BV_Ca. RHX depends on the ability to reopen the interlayer space, starting at the edges of the 2:1 layers with migration of H_2O through the interlayer and subsequently through the ditrigonal cavity of the tetrahedral sheet. As larger interlayer cations (e.g. K^+) have a lower probability to migrate into the 2:1 layer during DHX, they increase the ability for RHX, because the interlayer stays partly open for following migration of H_2O back into interlayers and subsequently the 2:1 layers (Derkowski and Kuligiewicz, 2017). With smaller cations (e.g. Li^+, Na^+, Ca^{2+}) it is more likely that they migrate through the ditrigonal cavity and bind to residual oxygen atoms after DHX (Emmerich et al., 1999). But RHX is still possible if the smaller cations migrate back to the interlayer by rehydration, which opens up the pathway for water molecules to reach the residual oxygen for RHX. While Na^+ and Ca^{2+} are similar in their ionic radius (154 and 174 pm, respectively), the hydration energy of Ca^{2+} is more than four times the hydration energy of Na^+. And even though the ionic radius of Mg^{2+} (130 pm) is lower than the ionic radius of Li^+ (134 pm), its hydration energy is more than six times the hydration energy of Na^+. The high hydration energies of Ca^{2+} and Mg^{2+} favor the water uptake in the interlayer of the dehydroxylated smectites and thus finally also the RHX of Ca^{2+} or Ca^{2+}/Mg^{2+} saturated dehydroxylated smectites over the same materials saturated by mainly Na^+.

7.3.4 Kinetic calculations

Kinetic calculations of RHD were not possible due to the evident changes in kinetic regime in some samples, the calculations were only executed for RHX data.

The kinetic model for RHX of ceramics and ancient pottery is based on the $(time)^{1/4}$ power law (Derkowski and Kuligiewicz, 2017). This approach is by default used to determine ceramic RHX (Wilson et al, 2009). For ceramics, RHX activation energy values in the range of 60 – 90 kJ/mol were found by Hall and Hoff (2012). Clelland et al. (2015) calculated activation energies between 60 – 120 kJ/mol for RHX of an ancient brick. The kinetics of RHX for swellable clay minerals can act as a proxy of ceramics RHX (Derkowski and Kuligiewicz, 2017), therefore, models for ceramics RHX at near ambient conditions were well suited for the calculations in this study. Calculations for activation energy were executed using three different approaches (TTTQ, power law, and α-free isoconvertional). E_a of rehydroxylation for sample BV_Na could not be calculated, because this sample showed almost no rehydroxylation at 22°C (RHX < 0.2% after 7 d), thus effectively only two points were available in Arrhenius plots for this sample.

TTTQ model was able to accurately fit the experimental data (*Figure 32*). The obtained E_a values were, however, scattered between 49-141 kJ/mol (*Table 19*). Such a huge variability of activation energy calculated by the same kinetic model for systems supposedly controlled by the same mechanism is inexplainable. Sample BP_Ca had lower Ea than BP_Na, and sample BC_Ca/Mg lower than BC_Ca, which on the qualitative level agrees with the observed differences in the degree of rehydroxylation observed for these samples. No clear relationship between crystallite size or 2:1 layer structure and E_a value was observed.

Coefficients (k and n) in power law model were optimized so to obtain the best fit of experimental data, using the results of TTTQ model as starting values. Initial tests showed that data points coming from 4 h of rehydroxylation do not follow the relationship for the remaining rehydroxylation times (*Figure 33*). This was interpreted as experimental artifact coming from the fact that the samples were not in thermal equilibrium with the environment during initial stages of rehydroxylation. These points were therefore excluded from the fitting procedure. E_a values obtained with the power law model were 23 – 46 kJ/mol higher than corresponding E_a values obtained with the TTTQ model, with the exception of sample BC_Ca/Mg, for which the difference was 62 kJ/mol. Qualitative trends between interlayer cation type and E_a value were preserved. Power law model was able to better fit experimental data than TTTQ model, likely due to the larger number of adjustable parameters (*Figure 32*). Power law model was therefore used to calculate "isoconvertional" $d\Delta m/dt$ values required for calculation of E_a with the α-free isoconvertional approach.

E_a of rehydroxylation obtained with α-free isoconvertional approach was in 32 – 90 kJ/mol range for Ca-exchanged samples. E_a was calculated for 0.05 (%) Δm increments. Only data covering mass gains

observed in RHX experiments at all three temperatures studied were considered as reliable. In practice this interval was between the lowest mass gain noted for 60 °C and the highest mass gain noted at 22 °C. E_a values decreased systematically with reaction progress, which cannot be easily reconciled with the clear decrease of the reaction rate with time for all samples (*Figure 33*).

Table 19. Activation energies obtained with TTTQ and power law.

sample	TTTQ model[1]		Power law[2]	
	E_a (kJ/mol)	R2	E_a (kJ/mol)	R2
BV_Na	n.a.*	n.a.*	n.a.*	n.a.*
BV_Ca	141	0.9997	187	0.8180
BP_Na	90	0.9610	121	0.8748
BP_Ca	52	0.8254	75	0.9815
BC_Ca/Mg	49	0.9299	111	0.9593
BC_Ca	95	0.9204	121	0.8468

*not applicable

[1]according to Hall et al. (2013)

[2]according to Largitte and Pasquier (2016)

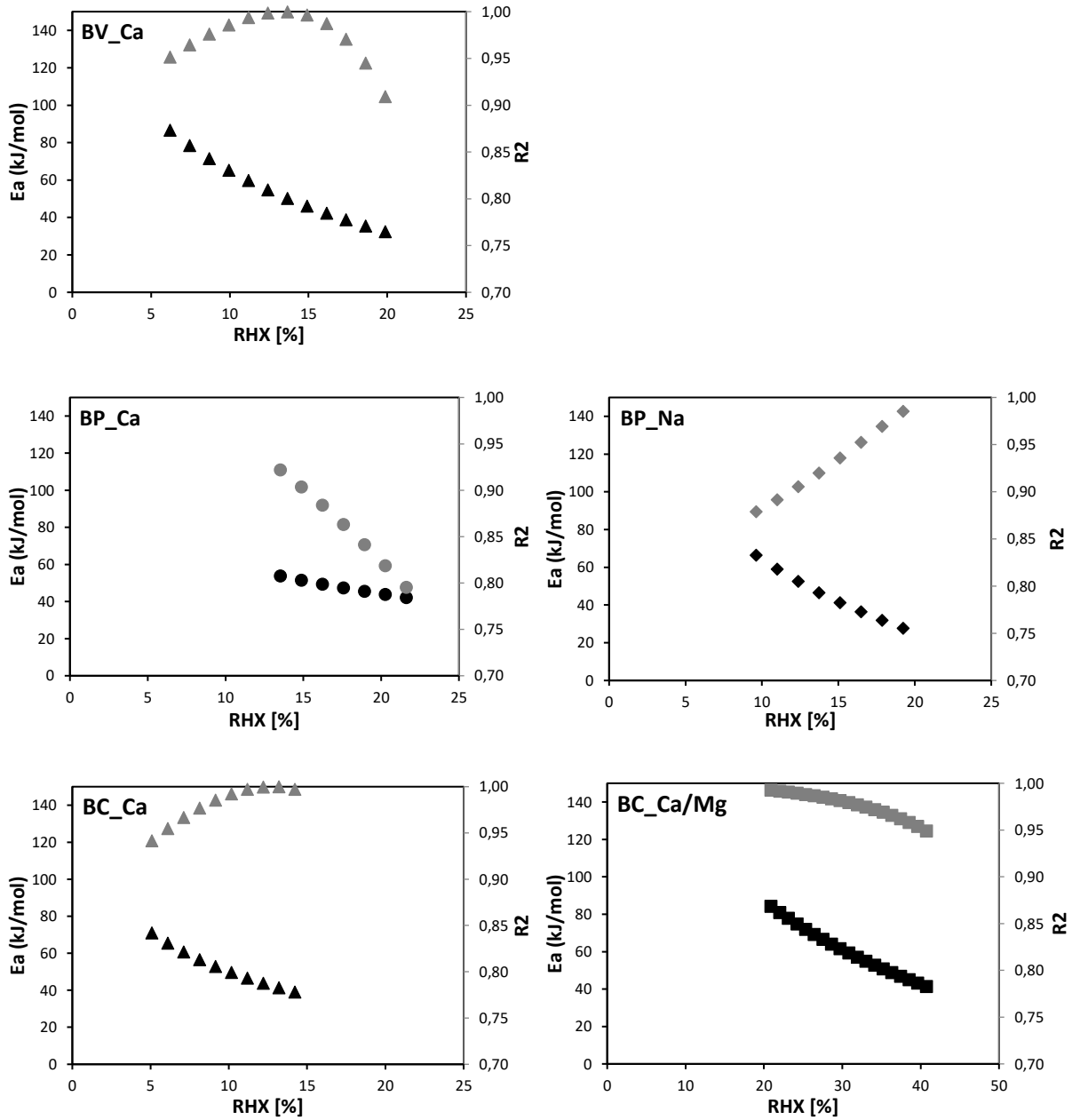

Fig. 32. Changes of E_a and R^2 of the Arrhenius plots with the reaction progress.

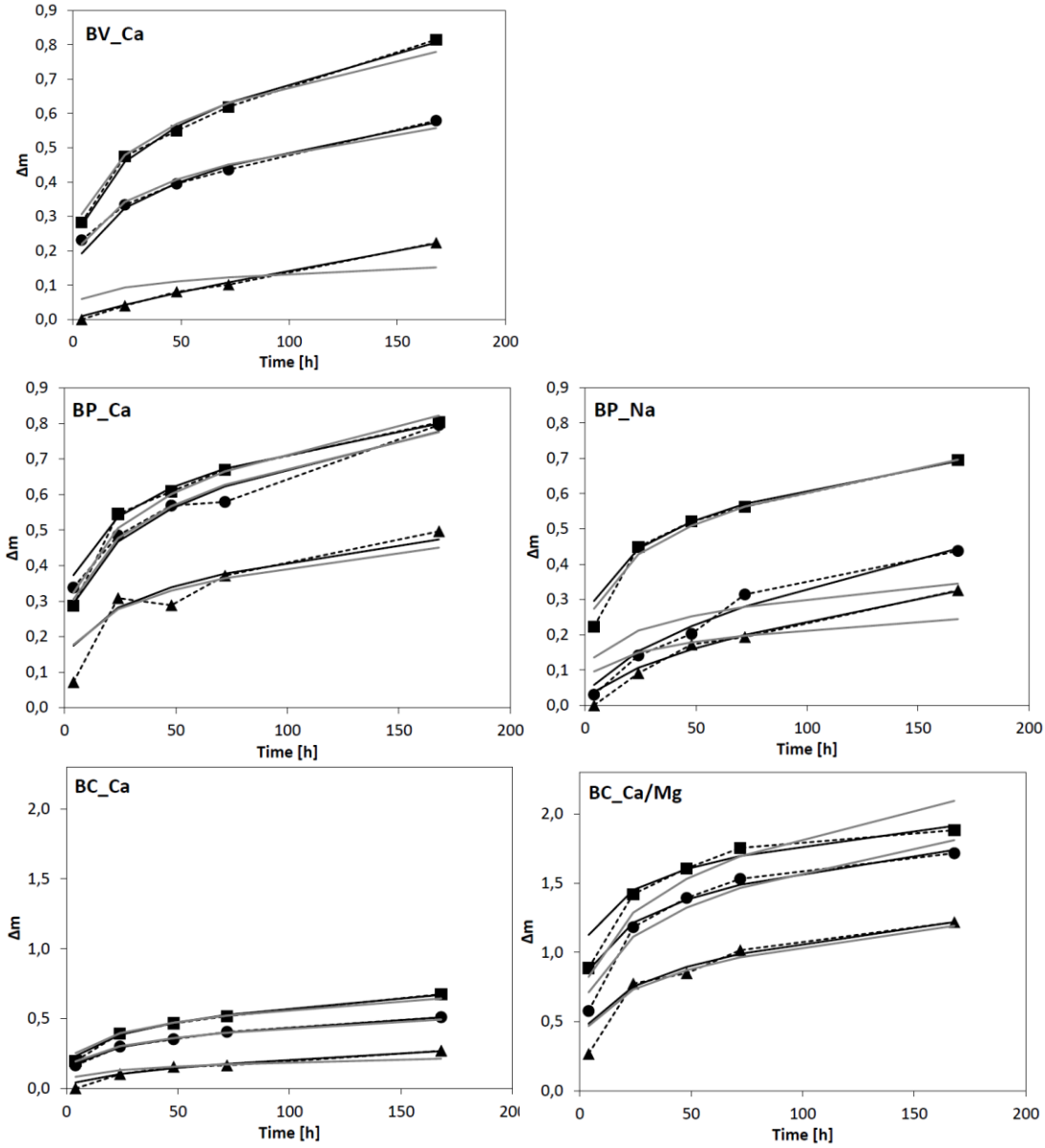

Fig. 33. Mass gain data (Δm) for RHX (▲ 22 °C; ● 40 °C; ■ 60 °C) along with fits with the TTTQ model (solid grey lines) and the power law model (solid black lines).

7.4 Summary

The samples showed a CEC between 69 (BC_Ca) and 127 (BP_Na) cmol(+)/kg. CEC was similar for the same montmorillonite with different interlayer cations (within 5 cmol(+)/kg). By heating up to 700 °C, CEC decreased. A maximum CEC of 5 cmol(+)/kg was reached. The decrease in CEC lay between 93 and 99% for all samples. As the ability to exchange cations was significantly lower after heating, the number of exchanged cations decreased as well.

The water content of the samples stored at ambient conditions before thermal treatment was between 9.1% (BV_Na) and 22.1% (BP_Ca). The Ca^{2+} exchanged samples showed larger water contents compared to the Na^{+} exchanged ones. The studied montmorillonites showed different degrees of DHX after heating up to 700 °C. The degrees lay between 77 (BV_Na) and 100% (BC). A larger degree of

DHX for the Ca^{2+} exchanged samples compared to the Na^{+} exchanged counterparts was observed. After DHX some OH^{-} groups remained in the heated materials, due to incomplete DHX.

The degree of RHX increased with time and temperature. All samples showed the largest amount of water uptake after 7 d at 60 °C. BV_Na showed the lowest RHX (8.7%). The degree of RHX for BV_Ca (16%), BP_Na (13.8%), BP_Ca (15.9%), and BC_Ca (13.6%) was in the same range. Only BC_Ca/Mg showed a significantly larger RHX of 37.3%. The Ca^{2+} exchanged samples showed larger values for RHX than the Na^{+} exchanged ones. It was shown that RHX of swellable clay minerals depended on temperature, time, and interlayer cation. After RHX the montmorillonites had a trans-vacant octahedral arrangement independently from the octahedral vacancies of the starting material (temperature of 2^{nd} DHX < 600 °C). All samples showed the ability to reopen interlayer for RHD and RHX.

E_a values obtained by TTTW model scattered between 49 – 141 kJ/mol. To obtain the best fit of experimental data the coefficients (k and n) in the power law model were optimized using the results of TTTQ model as starting values. The power law model fitted the experimental data better than the TTTQ model and, therefore, was used to calculate "isoconvertional" $d\Delta m/dt$ values required for calculation of E_a with the α-free isoconvertional approach. This approach resulted in E_a of rehydroxylation in the range 32 – 90 kJ/mol for Ca-exchanged samples.

Acknowledgement

This project is funded by Deutsche Forschungsgemeinschaft under EM79/8-1. The ICP-OES measurements were performed with the help of Dr. Eleanor Bakker and Silke Berberich (Competence Center for Material Moisture (IMB-CMM), Karlsruhe Institute of Technology (KIT), Karlsruhe).

References

Delavernhe, L., Steudel, A., Darbha, G., Schäfer, T., Schuhmann, R., Wöll, C., Geckeis, H., & Emmerich, K. (2015). Influence of mineralogical and morphological properties on the cation exchange behavior of dioctahedral smectites. *Colloids and Surfaces A: Physicochemical and Engineering Aspects, 481*, 591-599.

Clelland, S. J., Wilson, M., Carter, M., & Batt, C. M. (2015). RHX dating: measurement of the activation energy of rehydroxylation for fired-clay ceramics. *Archaeometry, 57(2), 392-404.*

Derkowski, A., Drits, V. A., & McCarty, D. K. (2012). Nature of rehydroxylation in dioctahedral 2: 1 layer clay minerals. *American Mineralogist, 97(4), 610-629.*

Derkowski, A., Drits, V. A., & McCarty, D. K. (2012). Rehydration of dehydrated-dehydroxylated smectite in a low water vapor environment. *American Mineralogist, 97(1), 110-127.*

Derkowski, A., & Kuligiewicz, A. (2017). Rehydroxylation in smectites and other clay minerals observed in-situ with a modified thermogravimetric system. *Applied Clay Science, 136, 219-229.*

Drits, V., Besson, G., & Muller, F. (1995). An improved model for structural transformation of heat-treated aluminous dioctahedral 2: 1 layer silicates. *Clays and Clay Minerals, 43(6), 718-731.*

Drits, V. A., Derkowski, A., & McCarty, D. K. (2012). Kinetics of partial dehydroxylation in dioctahedral 2: 1 layer clay minerals. *American Mineralogist, 97(5-6), 930-950.*

Emmerich, K. (2000). Spontaneous rehydroxylation of a dehydroxylated cis-vacant montmorillonite. *Clays andnClay Minerals, 48(3), 405-408.*

Emmerich, K. (2013). Full characterization of smectites. *Developments in clay science, Vol. 5, 381-404.*

Emmerich, K., Madsen, F. T., & Kahr, G. (1999). Dehydroxylation behavior of heat-treated and steam-treated homoionic cis-vacant montmorillonites. *Clays and Clay Minerals, 47(5), 591-604.*

Emmerich, K., Schuhmann, R. and Steudel, A. (2011) Rehydroxylierung von Smectiten nach partieller Dehydroxylation: Erkenntnisse für den Einsatz von Bentoniten in Gießereiformsanden. Schuhmann, R. (ed), Karlsruhe, Germany.

Emmerich, K., Wolters, F., Kahr, G., & Lagaly, G. (2009). Clay profiling: the classification of montmorillonites. *Clays and Clay Minerals, 57(1), 104-114.*

Garg, N., & Skibsted, J. (2015). Heated montmorillonite: structure, reactivity, and dissolution. *Calcined Clays for Sustainable Concrete, 117-124.*

Guggenheim, S., Adams, J. M., Bain, D., Bergaya, F., Brigatti, M. F., Drits, V.A., Formoso, M.L.L., Galán, E., Kogure, T., & Stanjek, H. (2006). Summary of recommendations of nomenclature committees relevant to clay mineralogy: report of the Association Internationale pour l'Etude des Argiles (AIPEA) Nomenclature Committee for 2006. *Clays and Clay Minerals, 54(6), 761-772.*

Hall, C., Hamilton, A., & Wilson, M. A. (2013). The influence of temperature on rehydroxylation [RHX] kinetics in archaeological pottery. *Journal of archaeological science, 40(1), 305-312.*

Hall, C., & Hoff, W. D. (2012). Moisture expansivity of fired-clay ceramics. *Journal of the American Ceramic Society, 95(4), 1204-1207.*

Hall, C., Wilson, M. A., & Hoff, W. D. (2011). Kinetics of Long-Term Moisture Expansion in Fired-Clay Brick. *Journal of the American Ceramic Society, 94(11), 3651-3654.*

Hamilton, A., & Hall, C. (2012). A review of rehydroxylation in fired-clay ceramics. *Journal of the American Ceramic Society, 95(9), 2673-2678.*

He, C., Osbaeck, B., & Makovicky, E. (1995). Pozzolanic reactions of six principal clay minerals: Activation, reactivity assessments and technological effects. *Cement and Concrete Research, 25*(8), 1691-1702.

Heller, L., Farmer, V., Mackenzie, R., Mitchell, B., & Taylor, H. (1962). The dehydroxylation and rehydroxylation of triphormic dioctahedral clay minerals. *Clay Minerals Bulletin, 5(28), 56-72.*

Kawano, M., & Tomita, K. (1991). Dehydration and rehydration of saponite and vermiculite. *Clays and Clay Minerals, 39(2), 174-183.*

Kuligiewicz, A., & Derkowski, A. (2021). Rehydroxylation of fired clays: Is the time to the quarter (TTTQ) model correct? *Journal of archaeological science, 125, 105301*.

Mackenzie, R., & Bishui, B. (1958). The montmorillonite differential thermal curve. II. Effect of exchangeable cations on the dehydroxylation of normal montmorillonite. *Clay Minerals Bulletin, 3(20), 276-286*.

Muller, F., Drits, V., Plançon, A., & Robert, J.-L. (2000). Structural transformation of 2: 1 dioctahedral layer silicates during dehydroxylation-rehydroxylation reactions. *Clays and Clay Minerals, 48(5), 572-585.*

Perez-Rodriguez, J. L., Duran, A., Sanchez Jimenez, P. E., Franquelo, M. L., Perejón, A., Pascual-Cosp, J., & Pérez-Maqueda, L. A. (2010). Study of the dehydroxylation–rehydroxylation of pyrophyllite. *Journal of the American Ceramic Society, 93(8), 2392-2398.*

Rocha, J., Adams, J. M., & Klinowski, J. (1990). The rehydration of metakaolinite to kaolinite: evidence from solid-state NMR and cognate techniques. *Journal of Solid-State Chemistry, 89(2), 260-274*.

Roy, R., & Brindley, G. (1956). Hydrothermal reconstitution of the kaolin minerals. *Clays and Clay Minerals, 4, 125-132.*

Siddique, R., Kaur, G., & Rajor, A. (2010). Waste foundry sand and its leachate characteristics. *Resources, Conservation and Recycling, 54(12), 1027-1036*.

Steudel, A., & Emmerich, K. (2013). Strategies for the successful preparation of homoionic smectites. *Applied Clay Science, 75, 13-21*.

Steudel, A., Heinzmann, R., Indris, S., & Emmerich, K. (2015). CEC and 7Li MAS NMR Study of Interlayer Li+ in the Montmorillonite–Beidellite Series at Room Temperature and After Heating. *Clays and Clay Minerals, 63(5), 337-350*.

Tributh, H., & Lagaly, G. (1986). Aufbereitung und Identifizierung von Boden- und Lagerstättentonen. II. Korngrößenanalyse und Gewinnung von Tonsubfraktionen. *GIT-Fachzeitschrift für das Laboratorium, 30, 771-776.*

Werling, N., Kaltenbach, J., Weidler, P. G., Schuhmann, R., Dehn, F., & Emmerich, K. (2022). Solubility of Calcined Kaolinite, Montmorillonite, and Illite in High Molar NaOH and Suitability as Precursors for Geopolymers. *Clays and Clay Minerals, 70,* 270-289.

Wilson, M. A., Carter, M. A., Hall, C., Hoff, W. D., Ince, C., Savage, S. D., Mckay, B., & Betts, I. M. (2009). Dating fired-clay ceramics using long-term power law rehydroxylation kinetics. *Proceedings of the Royal Society A: Mathematical, Physical and Engineering Sciences, 465(2108), 2407-2415*.

Wilson, M. A., Hoff, W. D., Hall, C., McKay, B., & Hiley, A. (2003). Kinetics of moisture expansion in fired clay ceramics: a (time) 1/4 law. *Physical review letters, 90(12), 125503*.

Wolters, F., & Emmerich, K. (2007). Thermal reactions of smectites—Relation of dehydroxylation temperature to octahedral structure. *Thermochimica Acta, 462(1-2), 80-88*.

Wolters, F., Lagaly, G., Kahr, G., Nueeshch, R., & Emmerich, K. (2009). A comprehensive characterization of dioctahedral smectites. *Clays and Clay Minerals, 57(1), 115-133*.

Yusiharni, E., & Gilkes, R. (2012). Rehydration of heated gibbsite, kaolinite and goethite: An assessment of properties and environmental significance. *Applied Clay Science, 64, 61-74.*

8. Micromechanical properties of geopolymers with different calcined clay precursors

The following study was submitted for publishing in Applied Clay Science and is a reprint of:

Werling, N., Schwaiger, R., Dathe, F., Dehn, F., Emmerich, K. (2022). Micromechanical properties of geopolymers with different calcined clay precursors. Applied Clay Science, (under review).

Sequences which were edited are marked in italics.

Abstract - Geopolymers and supplementary cementitious materials (SCM) are potential substitutes for ordinary Portland cement (OPC). Calcined common clays appear to be well suited as raw materials for the production of geopolymers. Due to the multiphase composition of common clays, it is necessary to study geopolymers first, which are prepared of individual calcined clay minerals. Nanoindentation was used to investigate the mechanical properties of geopolymers produced of a metakaolinite, a metasmectite, and a metaillite, as precursors. For geopolymer production Si:Al ratios between 1:1 – 3:1 and NaOH concentrations ranging from 4 – 10.79 mol/L were used. All geopolymers were prepared without the use of commercial waterglass. All three clay minerals could be constituents of a natural common clay. Additionally, mercury porosimetry was used to determine the porosity and average pore radius of the samples. The porosity of the studied geopolymers (20.3 – 31.6%) was in the range found for cement pastes. The average pore radius decreased with increasing concentration of NaOH or increasing Si:Al ratio. Hardness and average pore radius of the geopolymers with the same precursor showed a negative correlation. The highest hardness (1.09 GPa) of all geopolymers was reached by one produced with the metasmectite precursor. On average, the metakaolinite geopolymers reached a hardness of 0.19 GPa and a Young's modulus of 4.72 GPa. For the metasmectite geopolymers the average hardness was 0.60 GPa and average Young's modulus was 18.88 GPa. The metaillite geopolymers showed an average hardness of 0.26 GPa and an average Young's modulus of 8.43 GPa. A positive correlation of the Si:Al ratio and the hardness was determined. The hardness values found in this study were comparable to hardness values of cement pastes.

Keywords – Geopolymers, nanoindentation, calcined clay minerals, metakaolinite, metasmectite, metaillite

8.1 Introduction

The cement industry is responsible for 5 – 8% of the annual worldwide CO_2 emissions (McLellan et al. 2011). A large proportion of the emissions originates from the combustion of limestone ($CaCO_3$) during the production of the cement clinker. Geopolymers and supplementary cementitious materials (SCM) are potential substitutes for ordinary Portland cement (OPC). Natural clays to be calcined for geopolymer production or to be used as SCM contain no or low amounts of carbonates and calcination takes place at temperatures below the thermal decomposition of the carbonates. Thus, applying SCM or using geopolymers as a binder in construction can reduce the CO_2 emissions between 40 and 80% (McLellan et al., 2011; Davidovits 2013). While SCM substitute only a certain amount of OPC, geopolymers are OPC-free binders. Unlike OPC which is a hydraulic binder and SCM which show either hydraulic or pozzolanic activity, geopolymers are alkaline activated binders. Alkaline activated binders are subdivided in high Ca and low Ca/Ca-free types (Dehn et al., 2017). Geopolymers belong to the low Ca/Ca-free alkaline activated binders.

Geopolymers are inorganic polymers with a 3-dimensional structure which are produced of aluminosilicate precursors under highly alkaline conditions. Calcined clay minerals can be used as precursors. The precursors are activated with a highly alkaline solution like NaOH/KOH or waterglass, which leads to a polycondensation and the formation of geopolymer binders. During the first step of polycondensation the calcined clay minerals are dissolved. The second step includes the reorganization and diffusion of monomers and forming of oligomers due to association of the Si- and Al-tetrahedra. The consolidation of the 3-dimensional geopolymer network takes place in a third step.

Many studies on geopolymers use metakaolinite as a precursor, because it was already shown that adequate compressive strengths (up to 80 MPa for paste) can be reached (Pouhet & Cyr, 2016; Lahoti et al. 2017). To reduce the costs of geopolymers and make them more competitive to OPC in construction industry, it would be beneficial to use calcined common clays as precursors. Common clays are a mixture of different clay minerals and calcined common clays appear to be well suited as precursors for geopolymers. Due to their multiphase composition, it is necessary to study geopolymers produced of individual clay minerals first. While there are many studies on macroscopic compressive strength of geopolymers (Pouhet and Cyr, 2016; Lahoti et al. 2017), less information about micromechanical properties are available especially for geopolymers produced with different calcined clay mineral precursors. Nanoindentation can be used to investigate the micromechanical properties of geopolymers (Škvára et al., 2006; Němeček et al., 2011; Pelisser et al., 2013; Das et al., 2015).

This study investigates the micromechanical properties and microstructure of geopolymers produced with three different calcined clay mineral precursors (metakaolinite, metasmectite, and metaillite). Nanoindentation measurements were conducted to evaluate the hardness dependent on the used calcined clay mineral precursor. Additionally, mercury porosimetry was used to investigate the porosities of the

geopolymers. By comparing the properties of the hardened geopolymers, the suitability of the different calcined clay minerals as a precursor was evaluated.

For the production of the geopolymers in this study, no commercial waterglass was used. Waterglass in geopolymer production is commonly used for the adjustment of the Si:Al ratio. But, first by the use of commercial waterglass the environmental benefits compared to OPC are reduced, because of the CO_2 emissions due to the raw materials used for waterglass production. Second, waterglass itself polymerizes and this polymerization would disguise the properties of the geopolymers produced of the calcined clay minerals. In this study solid amorphous SiO_2 or crystalline $Al(OH)_3$ were used to in-/decrease the Si:Al ratio of the natural clay mineral precursors.

8.2 Materials & Methods

8.2.1 Solid precursors

The used Bavarian kaolin KBE-1, Bavarian bentonite Ceratosil®WG, and illitic clay Arginotec INX were described in chapter 2. The amorphous SiO_2 and the crystalline aluminum hydroxide powders were described in chapter 2, as well.

In the subsequent manuscript the terms metakaolinite, metasmectite, and metaillite will be used when referred to the calcined bulk material of KBE-1, Ceratosil WG, and Arginotec INX.

8.2.2 Alkaline activator

For alkaline activation ultra-pure NaOH solutions (Carl Roth GmbH & Co.KG, Karlsruhe, Germany) with concentrations of 10.70 mol/L (32%), 7.96 mol/L (25%), 6.1 mol/L (20%), 5 mol/L, and 4 mol/L were used.

8.2.3 Methods

Nanoindentation was carried out as described in Chapter 3.9.

Mercury porosimetry was performed according to Chapter 3.7.

8.3 Experimental Procedure

8.3.1 Calcination of the clay minerals

The materials were calcined according to the procedure described in chapter 4.1. The bulk materials were heated to the final temperature and placed in a desiccator for cooling down to room temperature. For metakaolinite 700 °C, for metasmectite and metaillite 750 °C were chosen as final temperature.

8.3.2 Geopolymer production

Geopolymers were produced according to the process explained in Chapter 4.3.

8.3.3 Sample preparation for nanoindentation

The geopolymer samples for nanoindentation were prepared as described in Chapter 4.4.

8.3.4 Sample preparation for mercury porosimetry

The samples for mercury porosimetry were prepared according to the process explained in Chapter 4.5.

8.4 Results & Discussion

8.4.1 Micromechanical properties

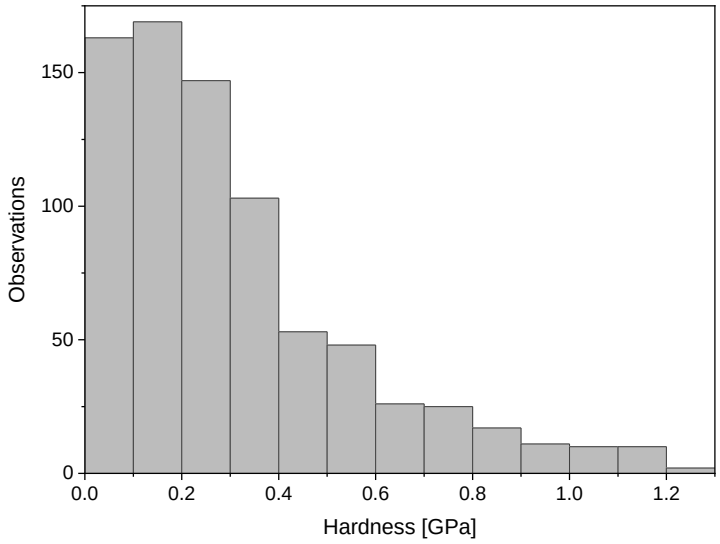

Fig. 34. Histogram for distribution of hardness over the surface of geopolymer K7.

The hardness of the metakaolinite geopolymers varied across the sample surface (*Fig. 34*). Some areas showed very low hardness values after hardening which could indicate incorporated particles of unreacted material. On average, all geopolymers with the metakaolinite precursor showed evolved hardness, except geopolymer K4 (*Fig. 35*). K4 was prepared with the lowest used concentration of NaOH (4 mol/L) and it could be assumed that metakaolinite was not activated sufficiently using this NaOH concentration. In earlier research it was already shown that the concentration of the activator solution influences the solubility of the precursor (Werling et al., 2022) and strength development of geopolymers (Heah et al., 2013).

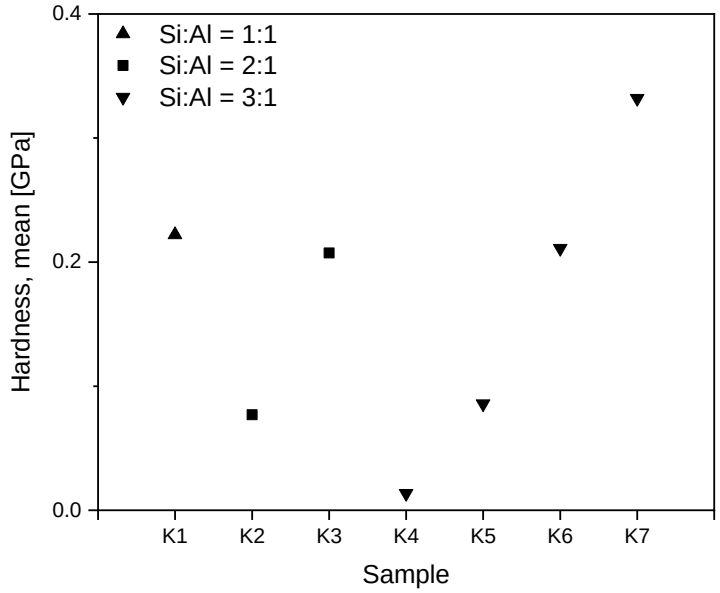

Fig. 35. Mean values for hardness of metakaolinite geopolymers.

The geopolymers with the metakaolinite precursor developed a hardness between 0.01 GPa for K4 and 0.33 GPa for K7. K1, with a Si:Al ratio of 1:1, showed a hardness of 0.22 GPa. K2 and K3 were prepared with a higher Si:Al ratio of 2:1. K3 was prepared with a higher NaOH concentration (7.96 mol/L) compared to K2 and developed a higher value of hardness (0.21 GPa compared to 0.08 GPa for K2). K4 – K 7 were produced with the highest Si:Al ratio of 3:1. As mentioned before, K4 did not develop significant hardness (0.01 GPa). The hardness of K5 – K7 increased with the concentration of NaOH. K5, prepared with 5 mol/L NaOH, showed a hardness of 0.09 GPa. K6 was produced with 6.1 mol/L NaOH and had a hardness of 0.21 GPa. As previously indicated, K7 developed the highest hardness of the metakaolinite geopolymers (0.33 GPa). The hardness showed a positive correlation with the concentration of NaOH. The same trend was observed for Si:Al ratio and hardness.

The values obtained for the metakaolinite geopolymers were in the range of values determined in previous studies (Pelisser et al., 2013; Zhang et al., 2017). According to Zhang et al. (2017) partially developed geopolymer gels develop a hardness in the range of $0.1\ \text{GPa} \leq H \leq 0.35\ \text{GPa}$. Completely reacted and hardened geopolymers reach a hardness between $0.35\ \text{GPa} \leq H \leq 1.5\ \text{GPa}$ (Zhang et al., 2017). These values were obtained for geopolymers produced with a commercial waterglass (sodium silicate solution). Waterglass itself has a hardness development, additional to the hardness of metakaolinite geopolymer. This could explain the lower values of "partially developed geopolymer gels" for geopolymers produced without commercial waterglass like the ones investigated here.

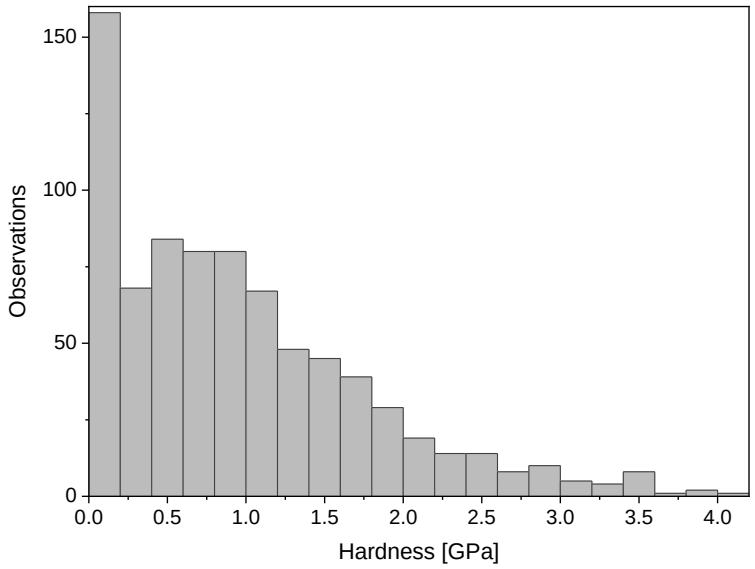

Fig. 36. Histogram for distribution of hardness over the surface of geopolymer C5.

The hardness of geopolymers produced with the metasmectite precursor varied across the sample surface (*Fig. 36*), as observed for metakaolinite geopolymers before. Four different geopolymers were produced from the metasmectite which showed a hardness between 0.29 – 1.09 GPa (*Fig. 37*).

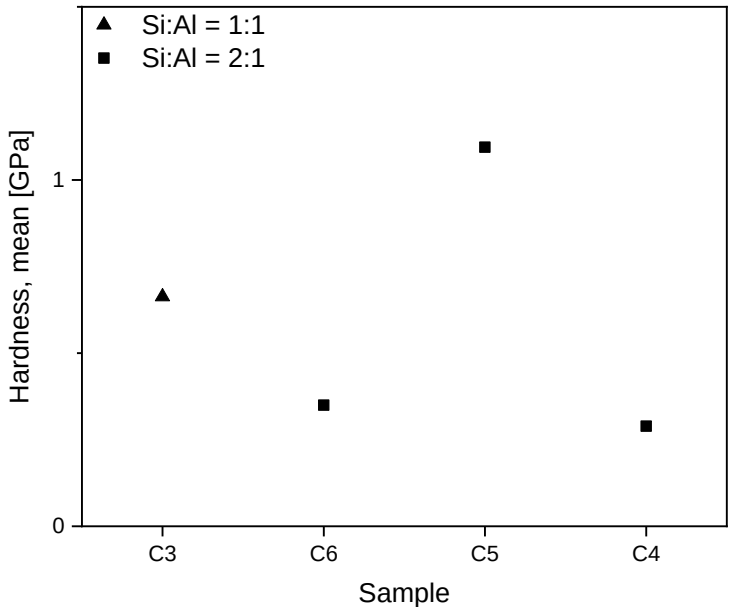

Fig. 37. Mean values for hardness of metasmectite geopolymers.

C3, which was the only metasmectite geopolymer prepared with a Si:Al ratio of 1:1, developed a hardness of 0.66 GPa. For the samples prepared with a Si:Al ratio of 2:1, C5 showed a higher hardness (1.09 GPa) compared to C4 (0.29 GPa), although C4 was prepared with a higher concentration of NaOH (6.1 mol/L). Comparing the hardness of C5 and C6 (0.35 GPa), the same positive correlation with NaOH concentration as for metakaolinite geopolymers could be observed. C6 with a lower concentration of

NaOH showed a lower hardness than C5. C4 seemed to be out of line, because it even developed less hardness compared to C3 with the same NaOH concentration but a lower Si:Al ratio. It is noteworthy, that metasmectite geopolymers showed higher values for hardness compared to metakaolinite ones.

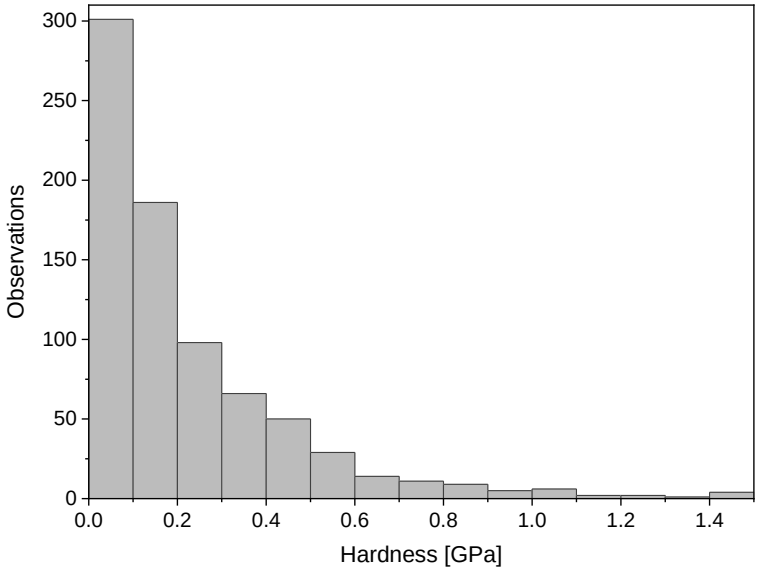

Fig. 38. Histogram for distribution of hardness over the surface of geopolymer I2.

Only two geopolymers were producible for the metaillite precursor. The water demand of the precursor was very high and not all of the mixtures could be mixed homogeneously. A variation of the hardness across the sample surface was observed (*Fig. 38*) as for all geopolymers before. The mean values for hardness of the geopolymers with metaillite precursor was in a range of 0.24 – 0.28 GPa (I2 – I3; *Fig. 39*), which was lower than for the geopolymers with metasmectite precursor. The lower values for hardness could be explained by the mixture properties. I2 and I3 were producible, but the mixtures were difficult to homogenize and very viscous. Furthermore, the geopolymers with metaillite were only producible with the lowest concentrations of NaOH (4 and 5 mol/L) and a Si:Al ratio equal to natural kaolinite (1:1). For higher NaOH concentrations and Si:Al ratios, higher values for hardness could be expected. Therefore, it would be important to enhance the production process so that metaillite geopolymers with higher NaOH concentrations could be produced. As the metaillite geopolymers still developed hardness values in the range of the metakaolinite geopolymers, it could be assumed that metaillite is suitable as a precursor for geopolymer production, too.

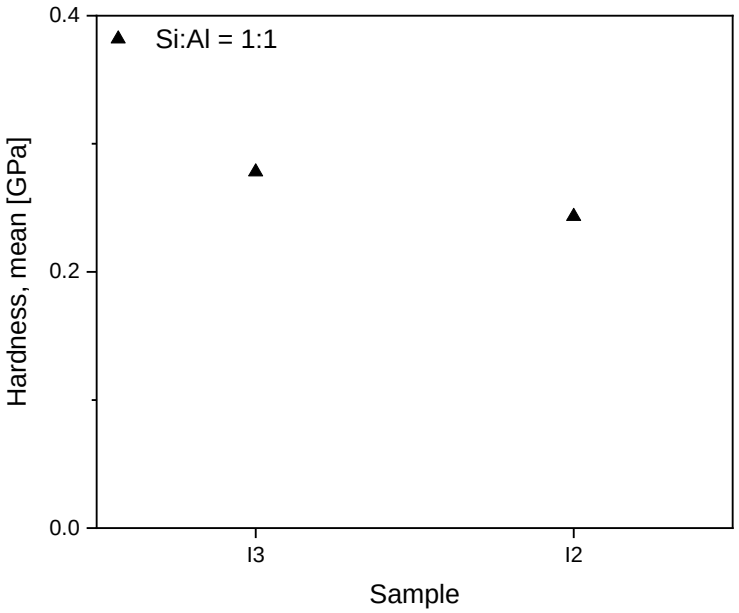

Fig. 39. Mean values for hardness of metaillite geopolymers.

Besides hardness, Young's modulus was determined by nanoindentation (*Table 20*). The values for Young's modulus were mainly in the range found in preliminary research for metakaolinite based geopolymers (Pelisser et al., 2013; Zhang et al., 2017). According to Zhang et al. (2017) partially developed geopolymer gels showed Young's moduli of 2 GPa ≤ E ≤ 5.5 GPa and geopolymer gels after completed reaction 5.5 GPa ≤ E ≤ 25 GPa. Only geopolymer K4 was significantly out of this range. As explained before K4 most likely contained large amounts of unreacted material.

Table 20. Average of Young's modulus (E) of geopolymers.

Sample	E average [GPa]	Standard deviation [GPa]
K1	5.98	4.09
K2	2.91	2.25
K3	5.70	3.28
K4	0.42	0.18
K5	2.04	2.58
K6	3.57	1.86
K7	8.09	3.93
C3	13.42	9.60
C6	17.30	10.68
C5	30.22	12.32
C4	14.57	9.17
I3	6.72	4.38
I2	10.13	5.14

Hardness and Young's modulus of cement pastes were already studied by nanoindentation measurements and model calculations. Model calculations yielded values in the range of 0.73 (low density CSH) – 1.27 GPa (high density CSH) for hardness of cement paste and values for Young's modulus from 23.4 (low density CSH) – 31.4 GPa (high density CSH) (Zhu et al., 2007). By nanoindentation measurements of cement pastes a maximum hardness of 1.1 GPa and Young's modulus

of 26.6 GPa were determined by Pelisser et al. (2010). Vandamme & Ulm (2010) measured a maximum hardness of 0.812 GPa and Young's modulus of 31.35 GPa, which was in the same order of magnitude. The Young's moduli of the herein studied geopolymers were below the values for cement paste. Only C5 showed a modulus close to the value determined by Vandamme & Ulm (2010). The Young's moduli followed the trends determined for hardness, e.g. for metakaolinite geopolymers K4 showed the lowest and K7 the highest modulus. Comparing the moduli of the different geopolymers, the metasmectite geopolymers showed the highest values and the metakaolinite geopolymers the lowest. The maximum hardness reached by C5 (1.09 GPa) was as high as the maximum hardness for cement paste of 1.1 GPa determined by Pelisser et al. (2010) and even higher as 0.812 GPa of Vandamme & Ulm (2010). Based on these results, it could be stated that the micromechanical properties of the prepared geopolymers were comparable to those of cement pastes. As an average hardness for OPC pastes 0.5 GPa is given in literature (Skvara et al., 2006). The average hardness of the herein studied geopolymers was 0.35 GPa (excluding K4 with no significant development of hardness). Therefore, the geopolymers with metakaolinite, metasmectite, and metaillite precursors could be a possible replacement for cement concerning hardness and Young's modulus.

As it was possible to produce geopolymers with all three calcined clay minerals, it could be assumed that geopolymer production should be possible with a mixture of calcined clay minerals, like calcined common clays, as well.

8.4.2 Porosity

In addition to the micromechanical properties, the porosity of the samples was studied by mercury porosimetry measurements. The geopolymers with metakaolinite precursor showed porosities between 20.3 and 31.6% (*Table 21*). The average pore radii varied significantly between the samples, a decrease with increasing concentration of NaOH was observed. Furthermore, geopolymers with a lower Si:Al ratio showed a higher average pore radius for the same concentration of NaOH. The pore radii were in a range of 231 – 854 nm. K4 with no significant development of hardness showed the biggest average pore radius. The sample with the highest hardness of the metakaolinite geopolymers (K7) had the lowest average pore radius of 231 nm.

Table 21. Porosity (%) and average pore radius (nm) of metakaolinite geopolymers.

Sample	K1	K2	K3	K4	K5	K6	K7
Porosity [%]	29.2	22.5	28.4	20.3	23.6	21.5	31.6
Average pore radius [nm]	301	779	368	854	495	414	231

The porosities of the geopolymers with metasmectite and metaillite precursors were in the same dimension as for the metakaolinite geopolymers. For metasmectite geopolymers porosities between 27.2 and 31.6% were determined (*Table 22*). The porosity of the metaillite geopolymers was slightly lower (23.4 – 25.8%; *Table 22*). The average pore radii of the metasmectite geopolymers (274 – 490 nm) were

in the range of the metakaolinite geopolymers, except C4. The metaillite geopolymers had an average pore radius between 98 and 130 nm which was comparable to the geopolymers with the other precursors.

Table 22. Porosity (%) and average pore radius (nm) of metasmectite and metaillite geopolymers.

Sample	C3	C6	C5	C4	I3	I2
Porosity	27.2	28.8	30.6	31.6	23.4	25.8
Average pore radius [nm]	490	320	274	14	130	98

K4 showed the lowest porosity (20.3%) of all geopolymers, but the largest average pore radius (854 nm) by far. This observation correlated with the absence of hardness in this sample. K7, which showed the highest hardness of the metakaolinite geopolymers, developed the highest porosity (31.6%). The porosity values of the metakaolinite geopolymers in this study were within the range shown in former research for porosity of metakaolin based geopolymers between 28.5 – 30.9% (Aredes et al., 2015). The average pore radius of K7 (231 nm) was among the lower values of the herein studied geopolymers. Sample C4 developed a significantly lower average pore radius (14 nm) than all other geopolymers. This can only be interpreted to a limited extent as C4 was outside of any trend for hardness before. Therefore, it has to be assumed that the pore radii values are out of the range as well. C5 and C6 followed the same trend as the metakaolinite geopolymers. C6 developed a lower porosity than C5, already indicated by the lower hardness shown before. The average pore radius (320 nm) was higher compared to C5 (274 nm). I2 and I3 showed comparable values for porosity and average pore radius. Due to the comparable hardness of these samples this result was expected.

According to literature the porosity measured by mercury intrusion equals the open porosity of a material (Aredes et al., 2015). In preliminary research unblended cement pastes (with no addition of supplementary materials) showed values of 20 – 49% for open porosity. Blended cement pastes with addition of fly ash or silica fume showed open porosities in the same range (Day & Marsh, 1988). All of the produced geopolymers in this study were within that range.

A negative correlation between hardness and average pore radius of the geopolymers with the same precursor was observed. A higher average pore radius indicates more, bigger macropores in the geopolymer which will lead to a pore network with lower strength. It is more likely to hit a pore with the indenter during nanoindentation which will lead to measuring more areas without significant hardness. The addition of silica (e.g. silica fume) to fly ash geopolymers led to an increase in porosity of geopolymer pastes, but to a decrease in geopolymer mortars due to filler properties (Dutta et al., 2010). With the amorphous silica used in this study no such effect was observed. It was shown before that the Si:Al ratio has no significant influence on the porosity of metakaolinite geopolymers (Aredes et al., 2015).

8.5 Summary

All of the studied geopolymers showed a development of hardness, except one metakaolinite geopolymer produced with the lowest concentration of NaOH (4 mol/L). For the geopolymers produced with metakaolinite precursor a geopolymer sample produced with 7.96 mol/L NaOH and a Si:Al ratio of 3:1 developed the highest hardness. For geopolymer samples which had an equal Si:Al ratio, an increase in hardness with concentration of NaOH could be observed. Metakaolinite geopolymers prepared with the same concentration of NaOH showed that the hardness increased in positive correlation with the Si:Al ratio. This trend was observable for two of the metasmectite geopolymers as well. The metasmectite geopolymer produced with 5 mol/L NaOH and a Si:Al ratio of 2:1 developed the highest hardness of all samples. The metaillite geopolymers were prepared with only slightly different concentrations of NaOH (5 mol/L and 4 mol/L) and showed similar values for hardness. A negative correlation of average pore radius and hardness was observed for geopolymers produced with the same precursor. The suitability as a geopolymer precursor was determined for all three calcined clay minerals, conditional of the improvement of production for some mixtures. The observations led to the assumption that a mixture of the herein studied clay minerals, e.g. in form of natural common clays, could be suitable for the production of geopolymers after determining the optimal production parameters.

Acknowledgement

The authors acknowledge the help of Stephan Gehlsen (Institute for Concrete Structures and Building Materials (IMB), Karlsruhe Institute of Technology (KIT), Karlsruhe, Germany) with the mercury porosimetry measurements. The project was funded by Deutsche Forschungsgemeinschaft (DFG) under EM79/8-1.

References

Aredes, F., Campos, T., Machado, J., Sakane, K., Thim, G., & Brunelli, D. (2015). Effect of cure temperature on the formation of metakaolinite-based geopolymer. *Ceramics International, 41(6)*, 7302-7311.

Das, S., Yang, P., Singh, S. S., Mertens, J. C. E., Xiao, X., Chawla, N., & Neithalath, N. (2015). Effective properties of a fly ash geopolymer: Synergistic application of X-ray synchrotron tomography, nanoindentation, and homogenization models. *Cement and Concrete Research, 78*, 252-262.

Davidovits, J. (2013). Geopolymer cement. A review. *Geopolymer Institute, Technical papers, 21*, 1-11.

Day, R. L., & Marsh, B. K. (1988). Measurement of porosity in blended cement pastes. *Cement and Concrete Research, 18(1)*, 63-73.

Dehn, F., Koenig, A., & Herrmann, A. (2017). Alkalisch-aktivierte Bindemittel und Geopolymer-Bindemittel als Alternative zu Zement. *Neue Herausforderungen im Betonbau*, 155-170.

Dutta, D., Thokchom, S., Ghosh, P., & Ghosh, S. (2010). Effect of silica fume additions on porosity of fly ash geopolymers. *J. Eng. Appl. Sci, 5(10),* 74-79.

Heah, C. Y., Kamarudin, H., Mustafa Al Bakri, A. M., Bnhussain, M., Luqman, M., Khairul Nizar, I., Ruzaidi, C.M., & Liew, Y. M. (2013). Kaolin-based geopolymers with various NaOH concentrations. *International Journal of Minerals, Metallurgy, and Materials, 20(3),* 313-322.

Izadifar, M., Thissen, P., Steudel, A., Kleeberg, R., Kaufhold, S., Kaltenbach, J., Schuhmann, R., Dehn, F., & Emmerich, K. (2020). Comprehensive examination of dehydroxylation of kaolinite, disordered kaolinite, and dickite: Experimental studies and density functional theory. *Clays and Clay Minerals, 68(4),* 319-333.

Lahoti, M., Narang, P., Tan, K. H., & Yang, E.-H. (2017). Mix design factors and strength prediction of metakaolin-based geopolymer. *Ceramics International, 43(14),* 11433-11441.

McLellan, B. C., Williams, R. P., Lay, J., van Riessen, A., & Corder, G. D. (2011). Costs and carbon emissions for geopolymer pastes in comparison to ordinary portland cement. *Journal of Cleaner Production, 19(9),* 1080-1090.

Němeček, J., Šmilauer, V., & Kopecký, L. (2011). Nanoindentation characteristics of alkali-activated aluminosilicate materials. *Cement and Concrete Composites, 33(2),* 163-170.

Oliver, W. C., & Pharr, G. M. (1992). An improved technique for determining hardness and elastic modulus using load and displacement sensing indentation experiments. *Journal of materials research, 7(6),* 1564-1583.

Pelisser, F., Guerrino, E. L., Menger, M., Michel, M. D., & Labrincha, J. A. (2013). Micromechanical characterization of metakaolin-based geopolymers. *Construction and Building Materials, 49,* 547-553.

Pouhet, R., & Cyr, M. (2016). Formulation and performance of flash metakaolin geopolymer concretes. *Construction and Building Materials, 120,* 150-160.

Škvára, F., Kopecký, L., Nemecek, J., & Bittnar, Z. (2006). Microstructure of geopolymer materials based on fly ash. *Ceramics-Silikaty, 50(4),* 208-215.

Vandamme, M., Ulm, F.-J., & Fonollosa, P. (2010). Nanogranular packing of C–S–H at substochiometric conditions. *Cement and Concrete Research, 40(1),* 14-26.

Werling, N., Dehn, F., Krause, F., Steudel, A., Schuhmann, R., & Emmerich, K. (2020). Solubility of precursors and carbonation of waterglass-free geopolymers. *Clays and Clay Minerals, 68(5),* 524-531.

Werling, N., Kaltenbach, J., Weidler, P. G., Schuhmann, R., Dehn, F., & Emmerich, K. (2022). Solubility of Calcined Kaolinite, Montmorillonite, and Illite in High Molar NaOH and Suitability as Precursors for Geopolymers. *Clays and Clay Minerals, 70,* 270-289.

Zhang, M., Zhao, M., Zhang, G., El-Korchi, T., & Tao, M. (2017). A multiscale investigation of reaction kinetics, phase formation, and mechanical properties of metakaolin geopolymers. *Cement and Concrete Composites, 78,* 21-32.

Zhu, W., Hughes, J. J., Bicanic, N., & Pearce, C. J. (2007). Nanoindentation mapping of mechanical properties of cement paste and natural rocks. *Materials characterization, 58(11-12),* 1189-1198.

9. Conclusions and Outlook

Investigations on further modifications concerning mixing ratios, premixing, hardening process, etc. will be necessary to reach the most favorable properties depending on the requested application. Further research will be needed in the field of additives. Additives are needed especially for improving the workability, which is the major issue concerning calcined clay precursors.

It was shown that geopolymers have comparable properties to OPC concerning hardness and porosity. The production of geopolymers without the use of waterglass was possible, which showed that the supplementary strength development of waterglass is not needed for geopolymer production. Additional investigations will be necessary to evaluate mechanical properties, like compressive strength, to compare the results with the properties determined by the nanomechanical investigations. By this comparison it will be possible to predict the compressive strength by the results from nanoindentation measurement in the future. But, before geopolymers can replace OPC in construction industry more research on technical and industrial scale will be equally necessary.

Concerning the costs for geopolymer production the best option to keep it at a minimum is to use cement plants for the production. Cement plants are already available in many locations, which means no additional costs will occur to build new production facilities.

While there is more research needed before geopolymers can be used commercially, LC^3 and oxyfuel technology could be bridging technologies. LC^3 is ready to use and can help reduce the emissions immediately, but as the CO_2 reduction is limited to 50% the use of other options, like geopolymers, should be the overriding goal. To compensate for the remaining 50% of CO_2 emissions during the production of LC^3, CCS is propagated. But, for CCS it will be necessary to find suitable locations for storage. The costs for exploration of storage locations will increase with higher demand for storage, as there are limited options which are suitable.

Acknowledgements

Writing a dissertation would not be possible without all kinds of support.
First of all, I would like to thank Prof. Dr. Katja Emmerich for supervising the thesis and for helping me to improve my scientific skills. I would also like to thank her for her help in solving problems and overcoming barriers. The support in applying for grants and the bureaucratic requirements was very important for me.
I want to acknowledge Prof. Dr. Frank Dehn for reviewing and editing the jointly published research papers.
Thanks to PD Dr. Peter Thissen for co-reviewing my work and the doctoral committee for their time and handling of the doctoral process.
I would also like to thank Dr. Annett Steudel, who supported me a lot, especially at the beginning of my thesis. Thanks to her help, it was very easy to get to know the laboratories, measurement methods and scientific working methods. Furthermore, she was a great help to integrate me into the whole research group and to establish further important contacts in the KIT environment.
A special thanks goes to Dr. Eleanor Bakker, who made my daily work life very pleasant. She was always available for discussions and new impulses when they were needed. Working together on scientific competitions was very educational and a nice addition to the daily science routine. In addition, she always had an open ear for problems and many reassuring words.
I would like to thank Silke Schönauer very much for the good cooperation and answering all my questions, especially regarding administrative issues. Thank you for the nice conversations and lunches together.
I would like to thank all my colleagues at the Competence Center for Material Moisture (CMM). Anke Ehbrecht, Dr.-Ing. Rainer Schuhmann, Frank Königer, Dr. Peter Boháč, Rebekka Oberle and Rosemarie Bender made me feel very welcome in the working group right from the beginning.
A special thanks goes to my friends. Especially to Valentin Goldberg and Alexander Sternagel, who always willingly and patiently listened to my problems and helped me with good advice. A joint quiz group, with other members, has also provided relaxation and fun on many Wednesday evenings.
Finally, I would like to thank my family, who have always had my back. In the most important moments, they have provided the appropriate distraction and relaxation. This support made it possible for me to fully concentrate on the challenges of a doctorate and to successfully master the task.

Declaration of Authorship

Chapter 5

Clays and Clay Minerals

SOLUBILITY OF PRECURSORS AND CARBONATION OF WATERGLASS-FREE GEOPOLYMERS

Check for updates

N. Werling[1] *, F. Dehn[2], F. Krause[3], A. Steudel[1], R. Schuhmann[1], and K. Emmerich[1]

[1]Competence Center for Material Moisture (CMM), Karlsruhe Institute of Technology (KIT), Hermann-von-Helmholtz-Platz 1, 76344 Eggenstein-Leopoldshafen, Germany
[2]Institute for Concrete Structure and Building Materials (IMB), Karlsruhe Institute of Technology (KIT), Gotthard-Franz-Str. 3, 76131 Karlsruhe, Germany
[3]Institute of Functional Interfaces (IFG), Karlsruhe Institute of Technology (KIT), Hermann-von-Helmholtz-Platz 1, 76344 Eggenstein-Leopoldshafen, Germany

Abstract—Geopolymers have the potential to function as an environmentally friendly substitute for ordinary Portland cement, with up to 80% less CO_2 emission during production. The effect is best utilized for geopolymers prepared with amorphous silica instead of waterglass ($Na_2Si_2O_{5+x}$) to adjust the Si:Al ratio. The reactivity of the precursors with the alkaline activator affects the final mineralogical properties of the binder. The purpose of the present study was to investigate the amount of different phases formed during geopolymerization and to understand the quantitative evolution of carbonation during geopolymer synthesis by determining the solubility of metakaolinite and amorphous SiO_2 in NaOH at various concentrations. The solubility was studied by ICP-OES measurements. X-ray diffraction was used for qualitative and quantitative phase analysis of the geopolymers. The solubility of the precursors increased with calcination temperature of metakaolinite, reaction time for amorphous SiO_2, and at higher NaOH concentrations. Partial dissolution resulted in free Na^+, which is a source for the formation of carbonates in the geopolymers. Thermonatrite occurred prior to trona formation in all samples.

Keywords—Amorphous silica · Carbonation · Geopolymers · Metakaolinite

INTRODUCTION

Geopolymer binders are inorganic polymers with a 3-dimensional framework structure of oligomers with various ratios of Si, Al, O, and OH−. The negative charge created by Si/Al substitutions is balanced by the cation of the alkaline activator solution. As well as supplementary cementitious materials (SCM), geopolymer binders are potential substitutes for ordinary Portland cement (OPC), and emit up to 40–80% less CO_2 than OPC during their production (McLellan et al. 2011; Davidovits 2013). The lower emissions are mainly due to the fact that the raw materials contain no structural CO_2. In contrast to SCM, which replace only a certain amount of OPC, geopolymers are ideally OPC-free binders. OPC is a hydraulic binder, while geopolymers are alkaline-activated binders. High-Ca and low-Ca/Ca-free types of alkaline-activated binders differ from one another (Herrmann et al. 2018): in that geopolymers contain little or no Ca. Aluminosilicates (fly ash, furnace slag, silica fume, or calcined clays) function as precursors and are activated with a highly alkaline solution (waterglass and/or highly concentrated alkali brines), which leads to a geopolymerization reaction (Davidovits 1991). The polymerization takes place in three successive reactions: the dissolution of the precursors in the alkaline activator solution; the reorganization and diffusion of monomers; and, afterwards, the formation of the 3-dimensional network and hardening of the binder (Haah et al. 2013; Ibañez et al. 2015).

The mechanical properties of geopolymers are comparable to those of binders prepared with OPC (Oh et al. 2010; Guo et al. 2014; Djobo et al. 2016; Yaseri et al. 2017; Hájková 2018). When calcined clay minerals such as metakaolinite (Si/Al = 1:1) are used as a precursor, adjusting the Si/Al ratio may be necessary to optimize the mechanical performance of the geopolymers (Duxson et al. 2005; Ozer and Soyer-Uzun 2015; Yaseri et al. 2017). A Si/Al ratio of 2:1 is given as a suitable ratio (Davidovits 1982; Yaseri et al. 2017). For this purpose, commercial waterglass solutions are mostly used for the production of geopolymers. The term waterglass describes aqueous solutions of the glassy frozen melts of alkali silicates, mostly sodium silicates, with varying SiO_2:M_2O (M: Na, K, or Li) ratios (e.g. Na_2SiO_3). In the production of geopolymers, however, waterglass accounts for most of the CO_2 emissions. The environmental benefit is reduced by commercial waterglass, therefore, in comparison with OPC cements. The usage of alkaline brines (e.g. NaOH) can lead to a reduction in CO_2 emissions of up to 50% and the Si/Al ratio can be adjusted by alternative SiO_2 sources (Mellaikali et al. 2016). Microcrystalline or amorphous SiO_2 can be obtained by combustion of organic materials or by technical manufacturing (e.g. silica fume). Rice husk ash appeared to be suitable for producing an alkaline-activator solution in combination with NaOH (He et al. 2013; Tchakouté et al. 2016). Furthermore, waste glass and sugar cane bagasse ash performed well in terms of geopolymer production (Tchakouté et al. 2016, 2017). The solubility of any other alternative SiO_2 sources in NaOH was not considered here. The

* E-mail address of corresponding author: nadja.werling@kit.edu
DOI: 10.1007/s42860-020-00096-4
© The Author(s) 2020

Published online: 10 November 2020

Electronic supplementary material The online version of this article (https://doi.org/10.1007/s42860-020-00096-4) contains supplementary material, which is available to authorized users.

Werling, N., Dehn, F., Krause, F., Steudel, A., Schuhmann, R., & Emmerich, K. (2020). Solubility of precursors and carbonation of waterglass-free geopolymers. *Clays and Clay Minerals*, *68*(5), 524-531. https://doi.org/10.1007/s42860-020-00096-4

Declaration of authorship:

Nadja Werling (NW) prepared the samples and gathered the data. Felix Krause supported the electron microscopy measurements. Katja Emmerich (KE) helped evaluate the data. NW wrote the manuscript, which was reviewed and edited by all authors.

Chapter 6

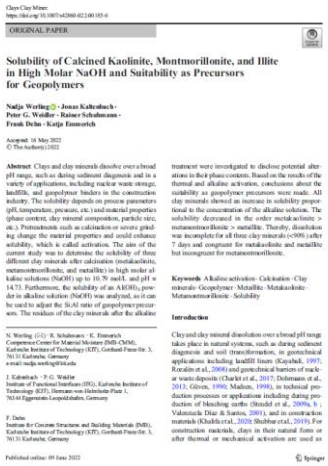

Clays Clay Miner.
https://doi.org/10.1007/s42860-022-00185-6

ORIGINAL PAPER

Solubility of Calcined Kaolinite, Montmorillonite, and Illite in High Molar NaOH and Suitability as Precursors for Geopolymers

Nadja Werling · Jonas Kaltenbach · Peter G. Weidler · Rainer Schuhmann · Frank Dehn · Katja Emmerich

Accepted: 16 May 2022
© The Author(s) 2022

Abstract Clays and clay minerals dissolve over a broad pH range, such as during sediment diagenesis and in a variety of applications, including nuclear waste storage, landfills, and geopolymer binders in the construction industry. The solubility depends on process parameters (pH, temperature, pressure, etc.) and material properties (phase content, clay mineral composition, particle size, etc.). Pretreatments such as calcination or severe grinding change the material properties and could enhance solubility, which is called activation. The aim of the current study was to determine the solubility of three different clay minerals after calcination (metakaolinite, metamontmorillonite, and metaillite) in high molar alkaline solutions (NaOH) up to 10.79 mol/L and pH ≈ 14.73. Furthermore, the solubility of an $Al(OH)_3$ powder in alkaline solution (NaOH) was analyzed, as it can be used to adjust the Si:Al ratio of geopolymer precursors. The residues of the clay minerals after the alkaline treatment were investigated to disclose potential alterations in their phase contents. Based on the results of the thermal and alkaline activation, conclusions about the suitability as geopolymer precursors were made. All clay minerals showed an increase in solubility proportional to the concentration of the alkaline solution. The solubility decreased in the order metakaolinite > metamontmorillonite > metaillite. Thereby, dissolution was incomplete for all three clay minerals (<90%) after 7 days and congruent for metakaolinite and metaillite but incongruent for metamontmorillonite.

Keywords Alkaline activation · Calcination · Clay minerals · Geopolymer · Metaillite · Metakaolinite · Metamontmorillonite · Solubility

Introduction

Clay and clay mineral dissolution over a broad pH range takes place in natural systems, such as during sediment diagenesis and soil (transformation, in geotechnical applications including landfill liners (Kayabali, 1997; Rozalén et al., 2008) and geotechnical barriers of nuclear waste deposits (Charlet et al., 2017; Dohrmann et al., 2011; Gilson, 1990; Madsen, 1998), in technical production processes or applications including during production of bleaching earths (Steudel et al., 2009a, b; Valenzuela Díaz & Santos, 2001), and in construction materials (Khalifa et al., 2020; Shubbar et al., 2019). For construction materials, clays in their natural form or after thermal or mechanical activation are used as

N. Werling (✉) · R. Schuhmann · K. Emmerich
Competence Center for Material Moisture (MM), Karlsruhe Institute of Technology (KIT), Gotthard-Franz-Str. 3, 76131 Karlsruhe, Germany
e-mail: nadja.werling@kit.edu

J. Kaltenbach · P. G. Weidler
Institute of Functional Interfaces (IFG), Karlsruhe Institute of Technology (KIT), Hermann-von-Helmholtz-Platz 1, 76344 Eggenstein-Leopoldshafen, Germany

F. Dehn
Institute for Concrete Structure and Building Materials (IMB), Karlsruhe Institute of Technology (KIT), Gotthard-Franz-Str. 3, 76131 Karlsruhe, Germany

Published online: 09 June 2022

Springer

Werling, N., Kaltenbach, J., Weidler, P. G., Schuhmann, R., Dehn, F., & Emmerich, K. (2022). Solubility of Calcined Kaolinite, Montmorillonite, and Illite in High Molar NaOH and Suitability as Precursors for Geopolymers. *Clays and Clay Minerals 70*, 270–289. https://doi.org/10.1007/s42860-022-00185-6

Declaration of authorship:

NW prepared the samples and gathered the data. Jonas Kaltenbach supported the electron microscopy measurements. Peter G. Weidler determined the specific surface areas. KE helped evaluate the data. NW wrote the manuscript, which was reviewed and edited by all authors.

Chapter 7

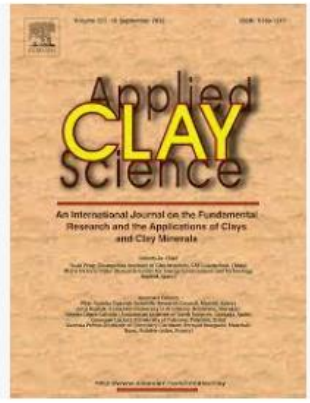

N. Werling, A. Kuligiewicz, A. Steudel, R. Schuhmann, F. Dehn, K. Emmerich (2022). Rehydroxylation of calcined swellable clay minerals at ambient conditions. *Applied Clay Science,* (under review).

Declaration of authorship:

NW prepared run the measurements and gathered the data. Artur Kuligiewicz executed the kinetic calculations to determine the activation energies. Annett Steudel did the homoionic exchange of the samples. KE helped evaluate the data. NW wrote the manuscript, which was reviewed and edited by all authors.

Chapter 8

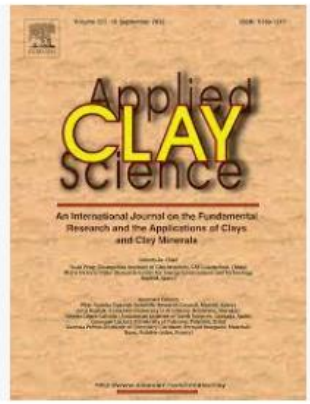

N. Werling, R. Schwaiger, F. Dathe, F. Dehn, K. Emmerich (2022). Micromechanical properties of geopolymers with different calcined clay precursors. *Applied Clay Science*, (under review).

Declaration of authorship:

NW prepared the samples and gathered the data. Ruth Schwaiger executed the nanoindentaion measurements and helped evaluate the results. Felix Dathe supported the mercury porosimetry. KE helped evaluate the data. NW wrote the manuscript, which was reviewed and edited by all authors.

Author's Publications

Peer-reviewed Publications

Werling, N., Dehn, F., Krause, F., Steudel, A., Schuhmann, R., & Emmerich, K. (2020). Solubility of precursors and carbonation of waterglass-free geopolymers. *Clays and Clay Minerals, 68(5),* 524-531.

Dathe, F., Strelnikova, V., Werling, N., Emmerich, K., & Dehn, F. (2021). Influence of lime, calcium silicate and portlandite on alkali activation of calcined common clays. *Open Ceramics, 7,* 100152.

Werling, N., Kaltenbach, J., Weidler, P. G., Schuhmann, R., Dehn, F., & Emmerich, K. (2022). Solubility of Calcined Kaolinite, Montmorillonite, and Illite in High Molar NaOH and Suitability as Precursors for Geopolymers. *Clays and Clay Minerals, 70,* 270-289.

Werling, N., Kuligiewicz, A., Steudel, A., Schuhmann, R., Dehn, F., Emmerich, K. Rehydroxylation of calcined swellable clay minerals at ambient conditions. *Applied Clay Science* (submitted 8/2022).

Werling, N., Schwaiger, R., Dehn, F., Schuhmann, R. and Emmerich, K. (2019) Nanoindentation and related mechanical properties of geopolymers prepared from different calcined clay precursors. *Applied Clay Science* (submitted 8/2022).

Conference Contributions

Werling, N., Schwaiger, R., Dehn, F., Schuhmann, R. and Emmerich, K. (2019) Nanoindentation to evaluate the mechanical properties of geopolymers: first steps., GeoMünster, poster presentation.

Werling, N., Schwaiger, R., Hirsch, A., Dehn, F., Schuhmann, R. and Emmerich, K. (2021) Comparison of micromechanical and macromechanical properties of geopolymers, International Conference on the Chemistry of Construction Materials" (ICCCM) 2020, poster presentation.

Werling, N., Dehn, F., Krause, F., Schuhmann, R. and Emmerich, K. (2021) Solubility of calcined clay minerals and suitability as precursors for geopolymers, 3rd European Mineralogical Conference, Cracow, Poland, oral presentation.

Werling, N., Kaltenbach, J., Schuhmann, R., Dehn, F., Emmerich, K. (2022) Solubility of calcined clay minerals and suitability as precursors for geopolymers, International Conference on Calcined Clay for Sustainable Concrete (CCSC 2022), Lausanne, Switzerland, oral presentation.

Werling, N., Kuligiewicz, A., Steudel, A., Schuhmann, R., Dehn, F., Emmerich, K. (2022) Rehydroxylation of calcined swellable clay minerals at ambient conditions, International Conference on Calcined Clay for Sustainable Concrete (CCSC 2022), Lausanne, Switzerland, poster presentation.

Supplementary Material to Chapter 5

The following electronic supplementary data was published online in addition to:

Werling, N., Dehn, F., Krause, F., Steudel, A., Schuhmann, R., & Emmerich, K. (2020). Solubility of precursors and carbonation of waterglass-free geopolymers. *Clays and Clay Minerals*, *68*(5), 524-531. https://doi.org/10.1007/s42860-020-00096-4

Sequences which were edited are marked in italics.

Fig. S1. Simultaneous thermal analysis (STA) of kaolin KBE-1.

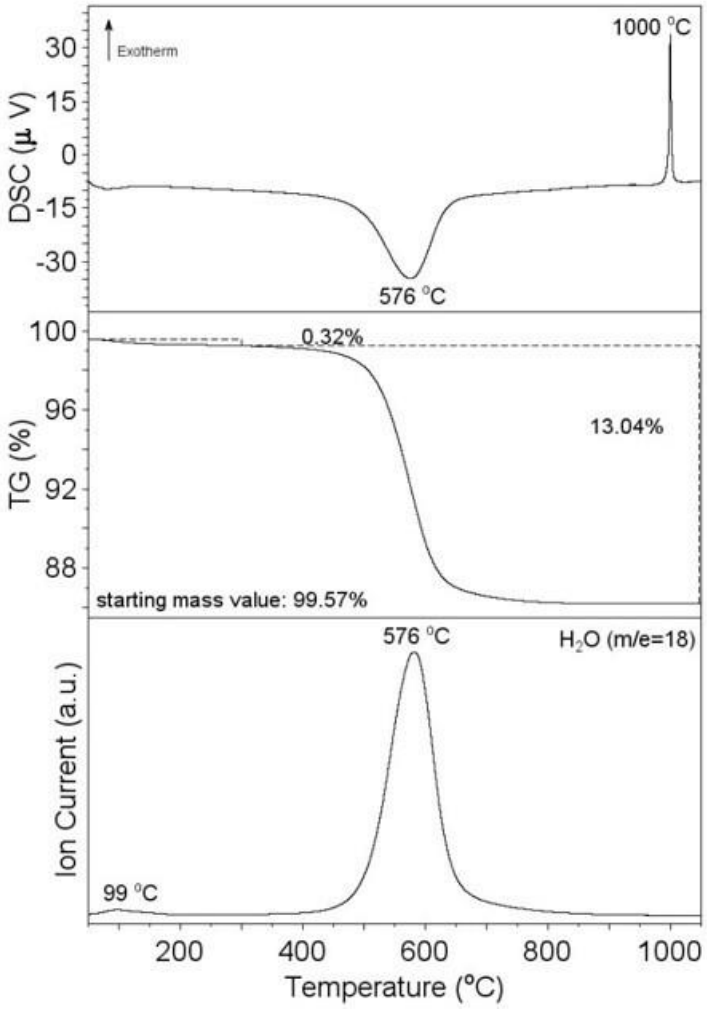

Temperature	°C
after DHD[a]	200
Onset DHX[b]	480
DHX	555
Offset DHX	615
prior to Recrystallization	900

[a]Dehydration

[b]Dehydroxylation

Fig. S2. Solubility of KBE-1 in NaOH (10.79 mol/L, 4 mol/L, 0.01 mol/L) as a function of calcination temperature.

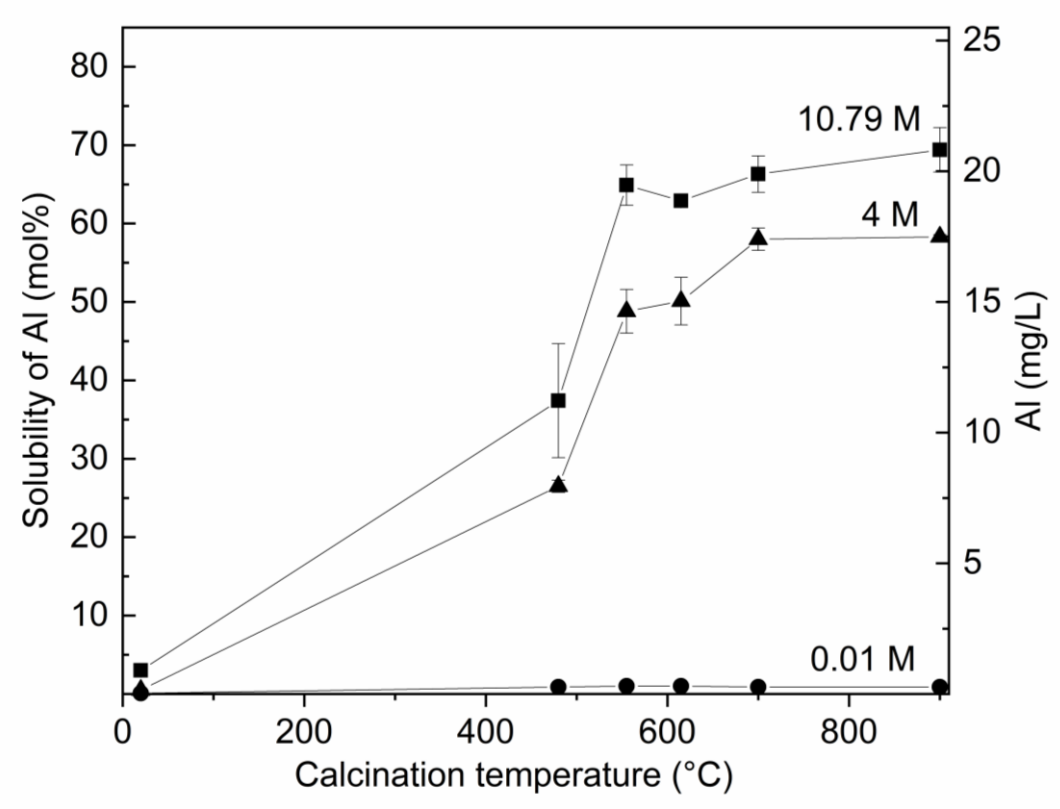

Supplementary Material to Chapter 6

The following electronic supplementary data was published online in addition to:

Werling, N., Kaltenbach, J., Weidler, P. G., Schuhmann, R., Dehn, F., & Emmerich, K. (2022). Solubility of Calcined Kaolinite, Montmorillonite, and Illite in High Molar NaOH and Suitability as Precursors for Geopolymers. Clays and Clay Minerals 70, 270–289. https://doi.org/10.1007/s42860-022-00185-6

Sequences which were edited are marked in italics.

Fig. S3. Solubility of Si of Certaosil WG (all NaOH concentrations, reaction time 24 h).

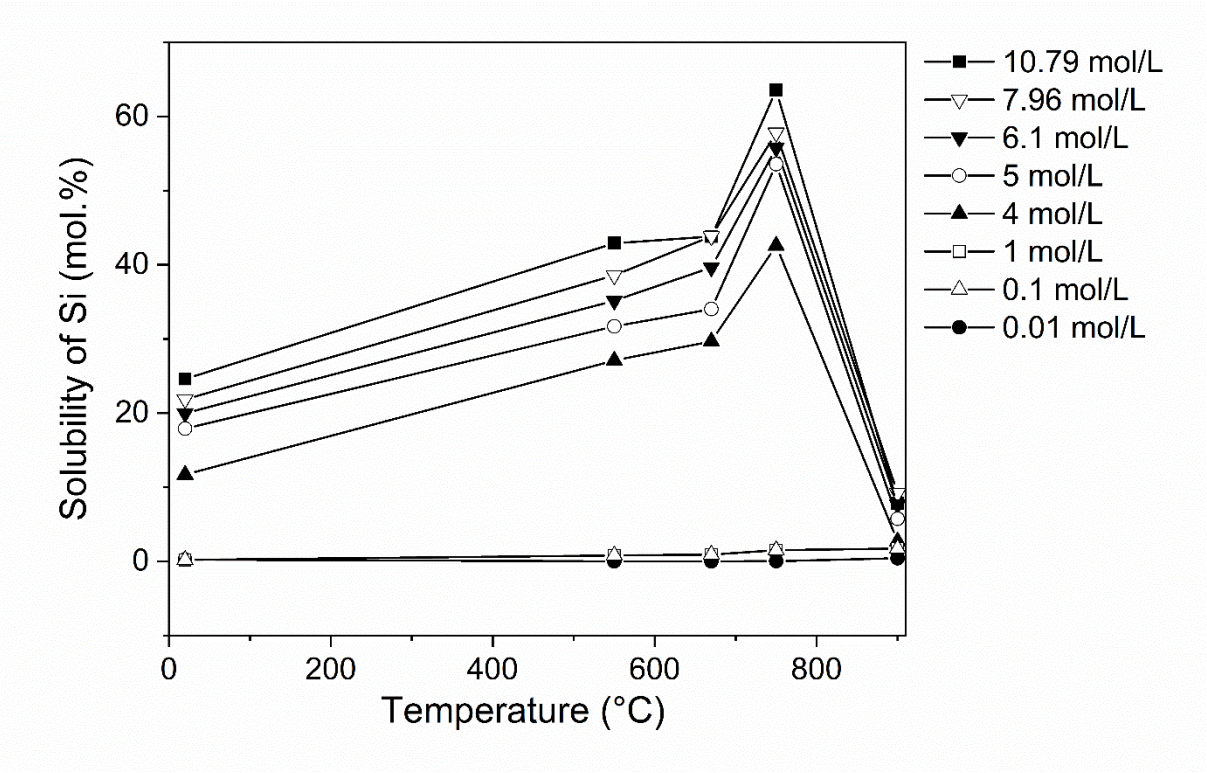

Fig. S4. Solubility of Si of Arginotec INX (all NaOH concentrations, reaction time 24 h).

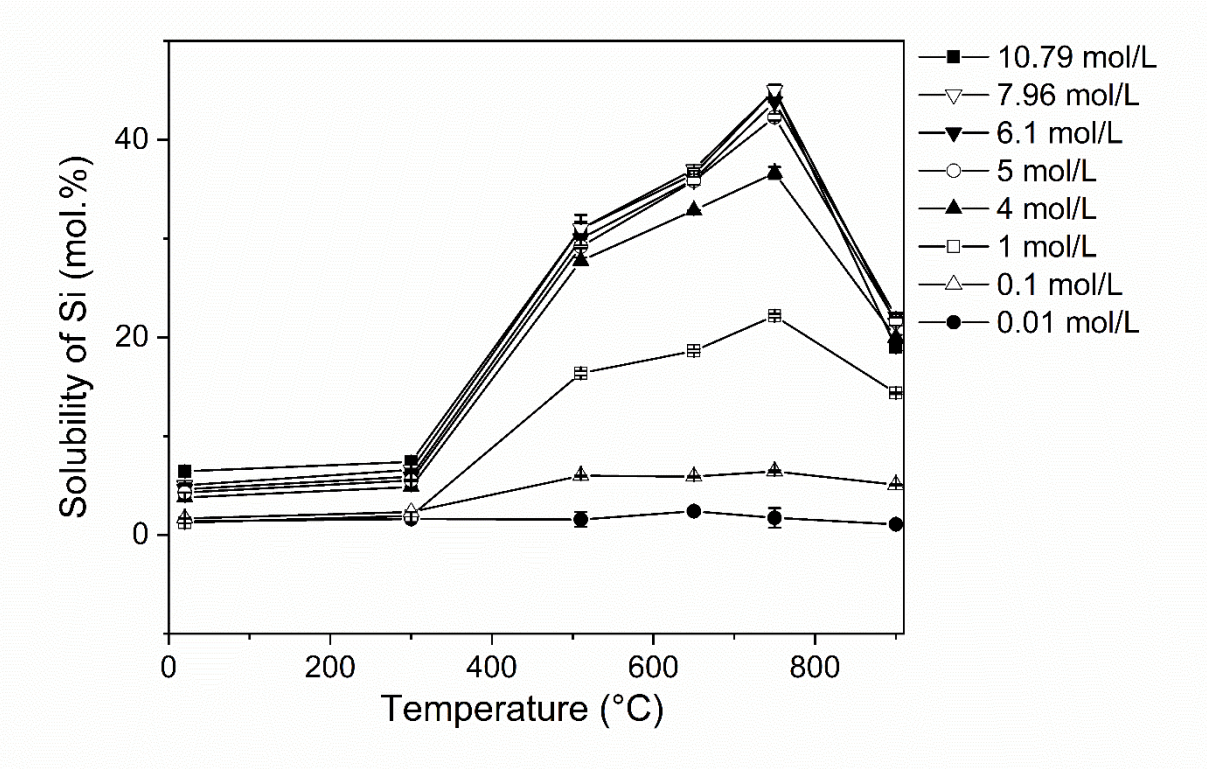

Fig. S5. Total dissolved Si of Ceratosil WG (reaction time 24 h).

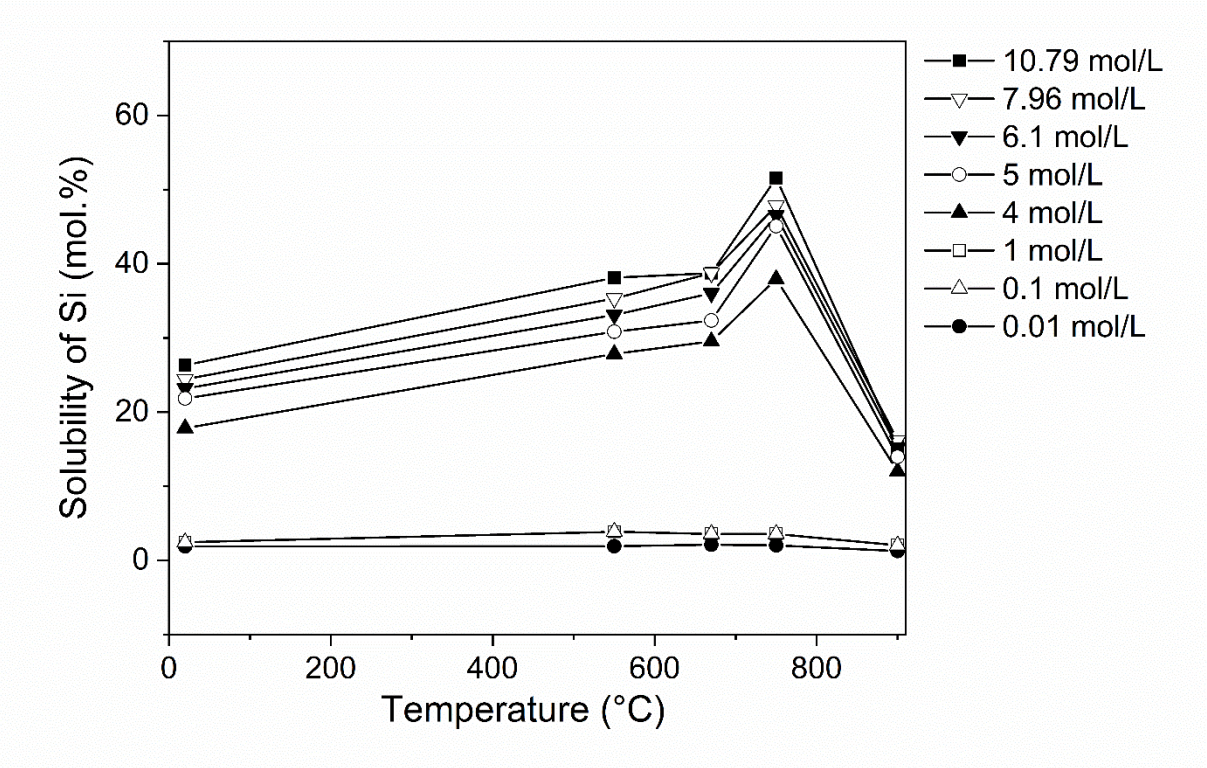

Fig. S6. Total dissolved Al of Ceratosil WG (reaction time 24 h).

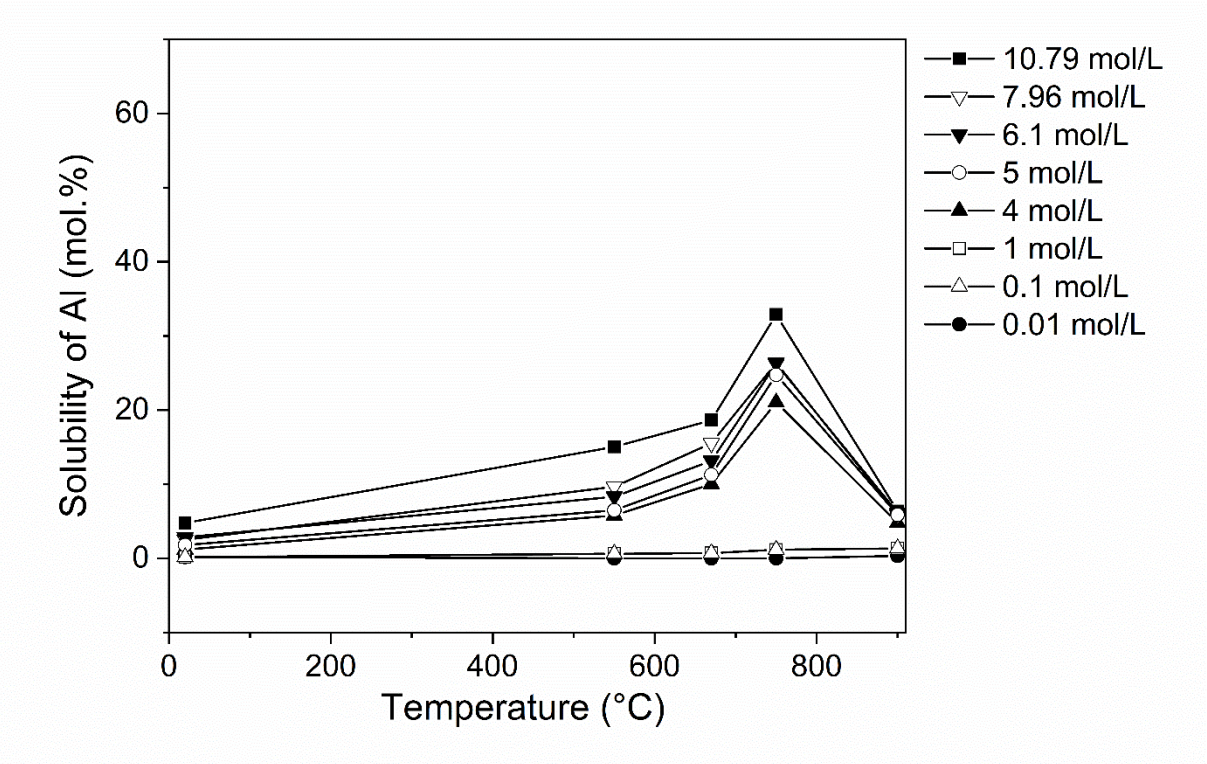

Fig. S7. Total dissolved Si of Arginotec INX (reaction time 24 h).

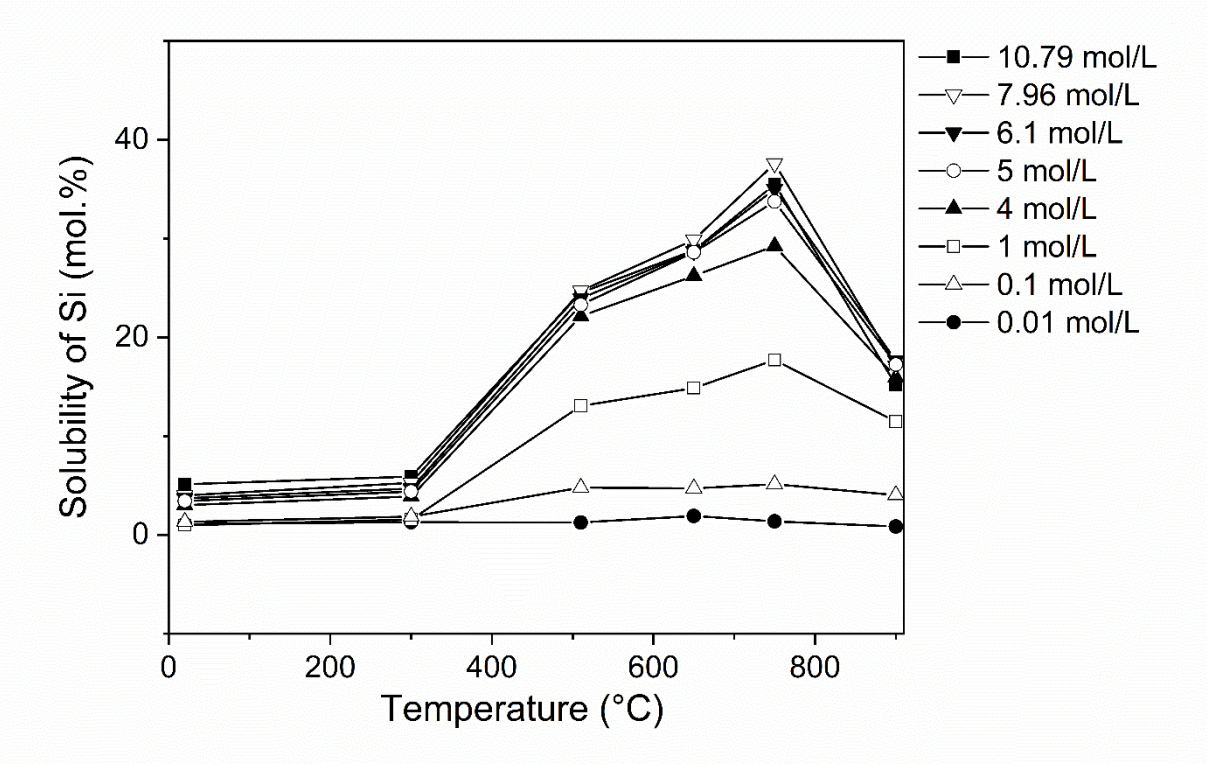

Fig. S8. Total dissolved Al of Arginotec INX (reaction time 24 h).

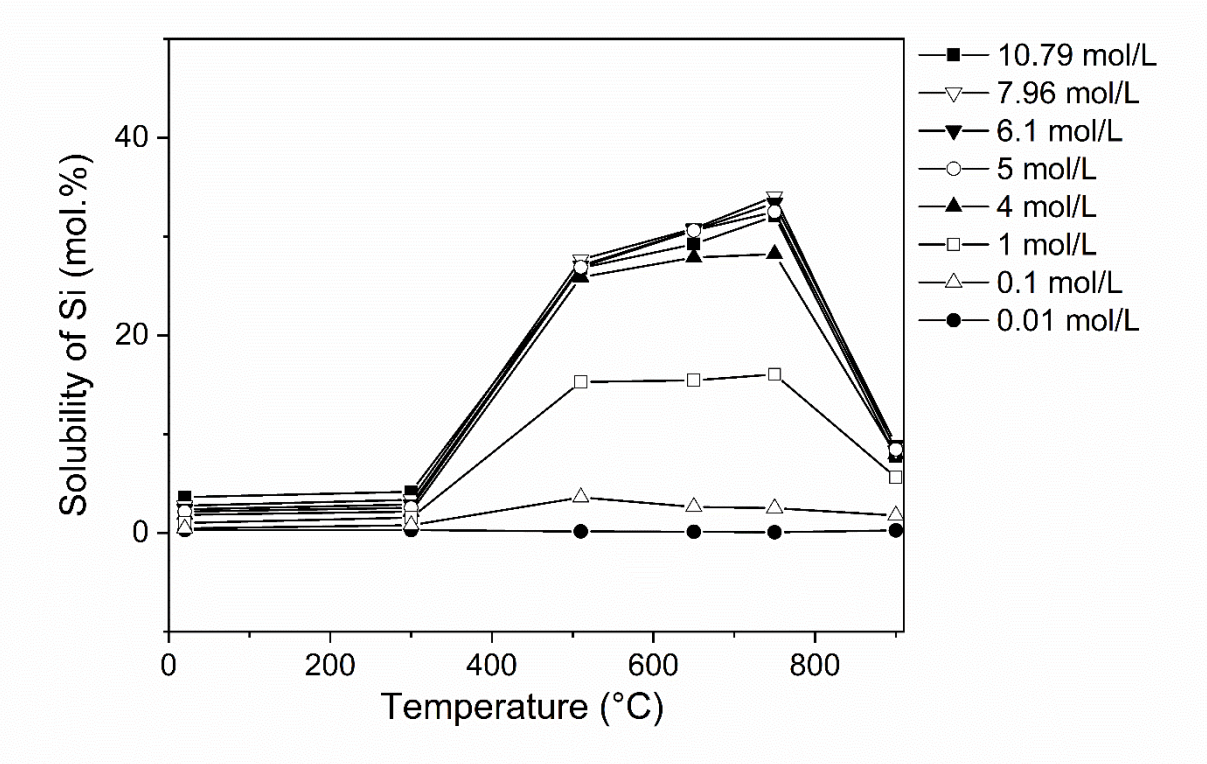

Fig. S9. Qualitative phase analysis of KBE-1 after calcination at different temperatures.

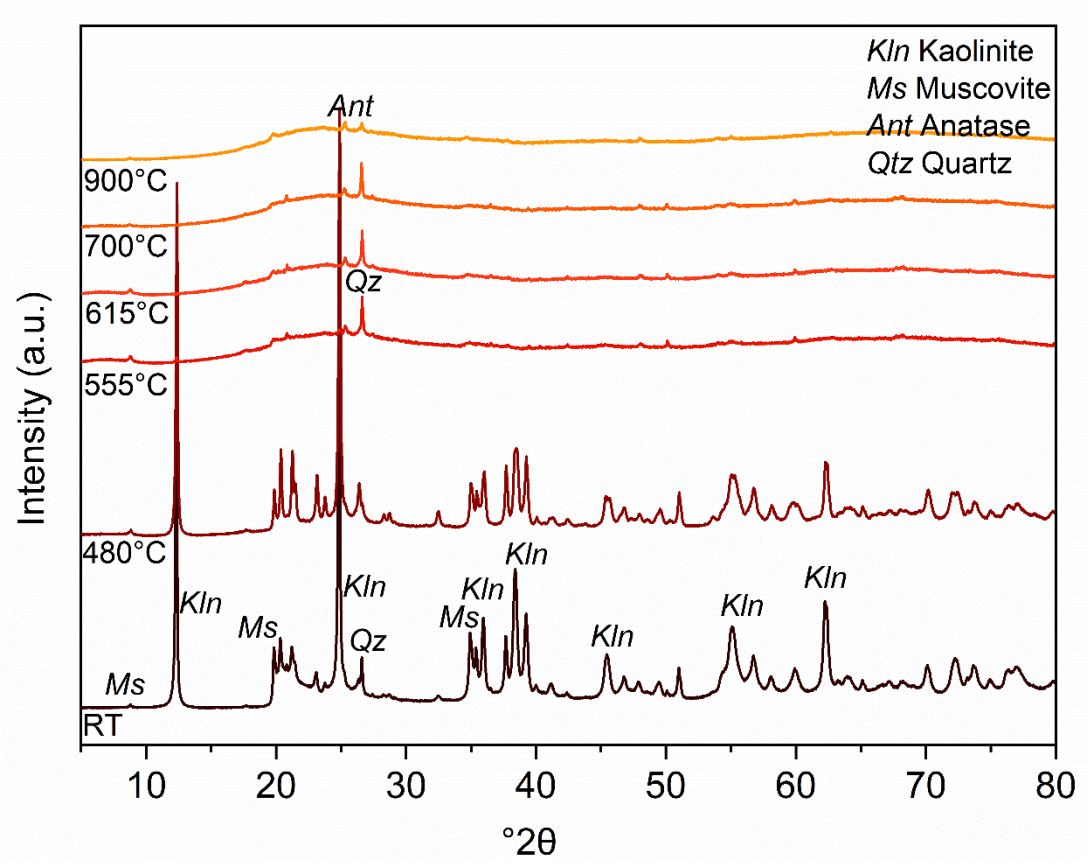

Fig. S10. Qualitative phase analysis of Ceratosil WG after calcination at different temperatures.

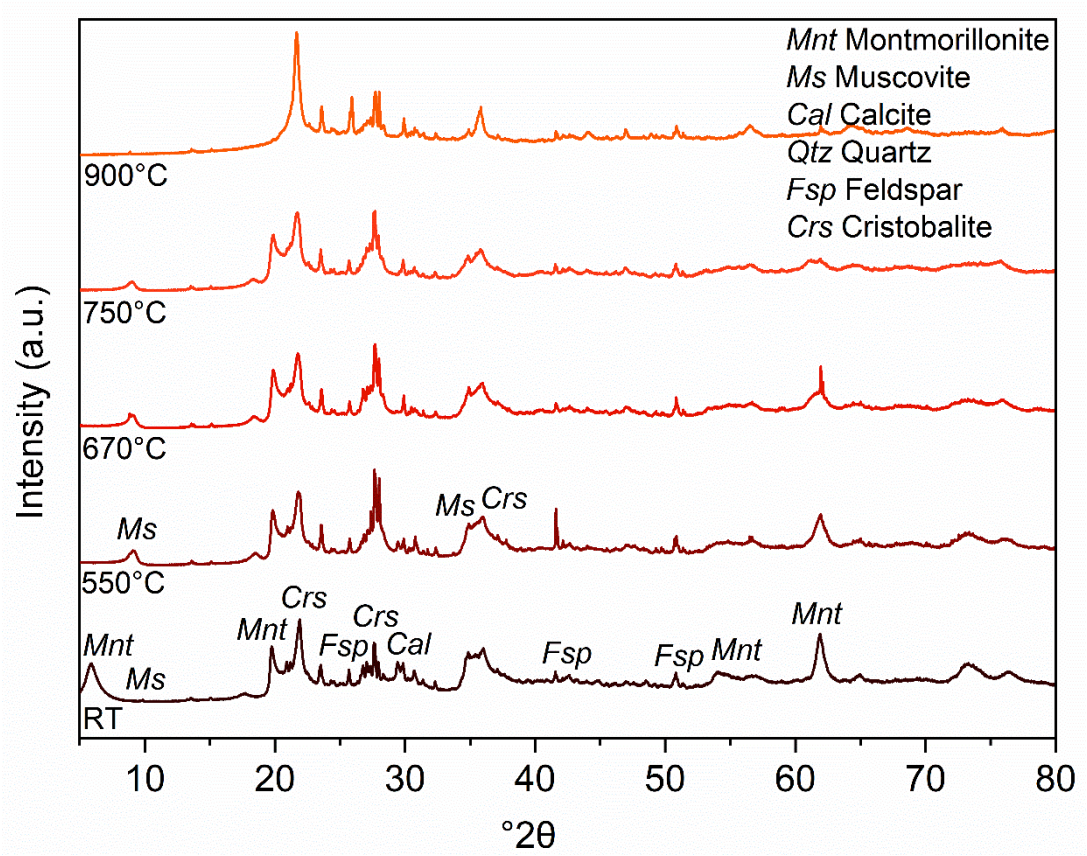

Fig. 11. Qualitative phase analysis of Arginotec INX after calcination at different temperatures.

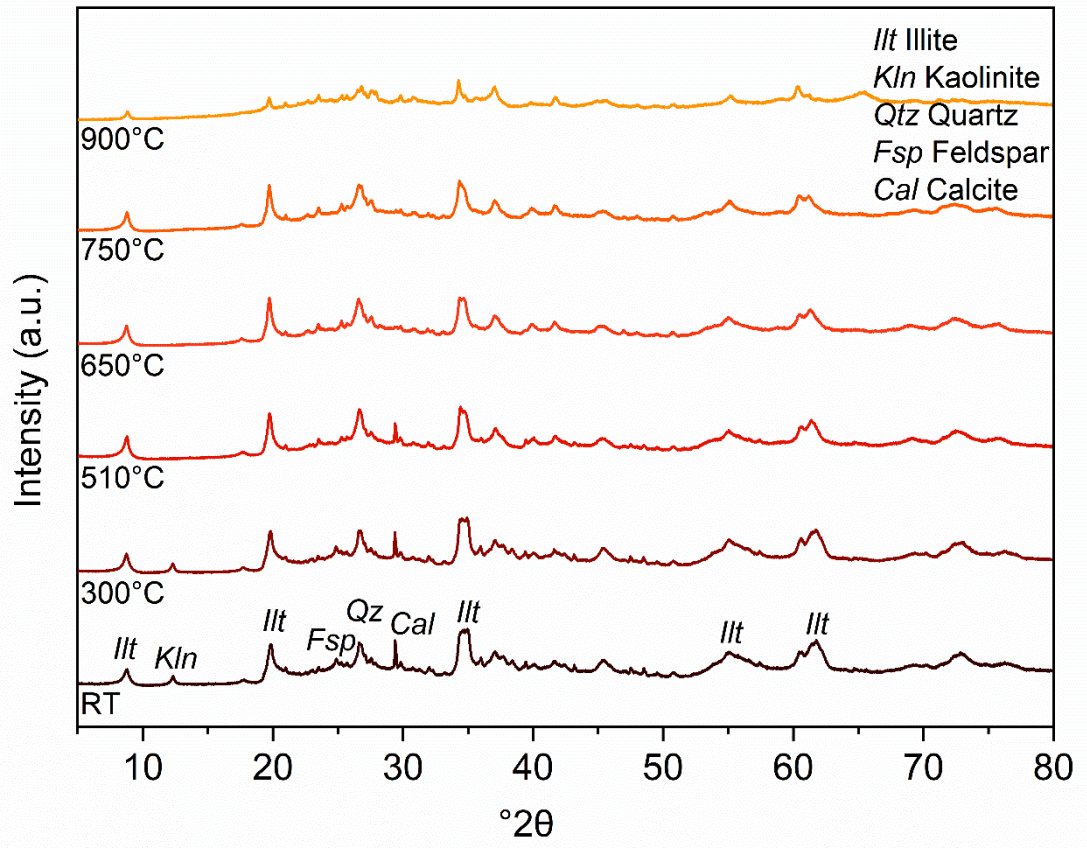

Fig. S12. Differentiation between cristobalite and opal-C (according to Elzea et al., 1994).

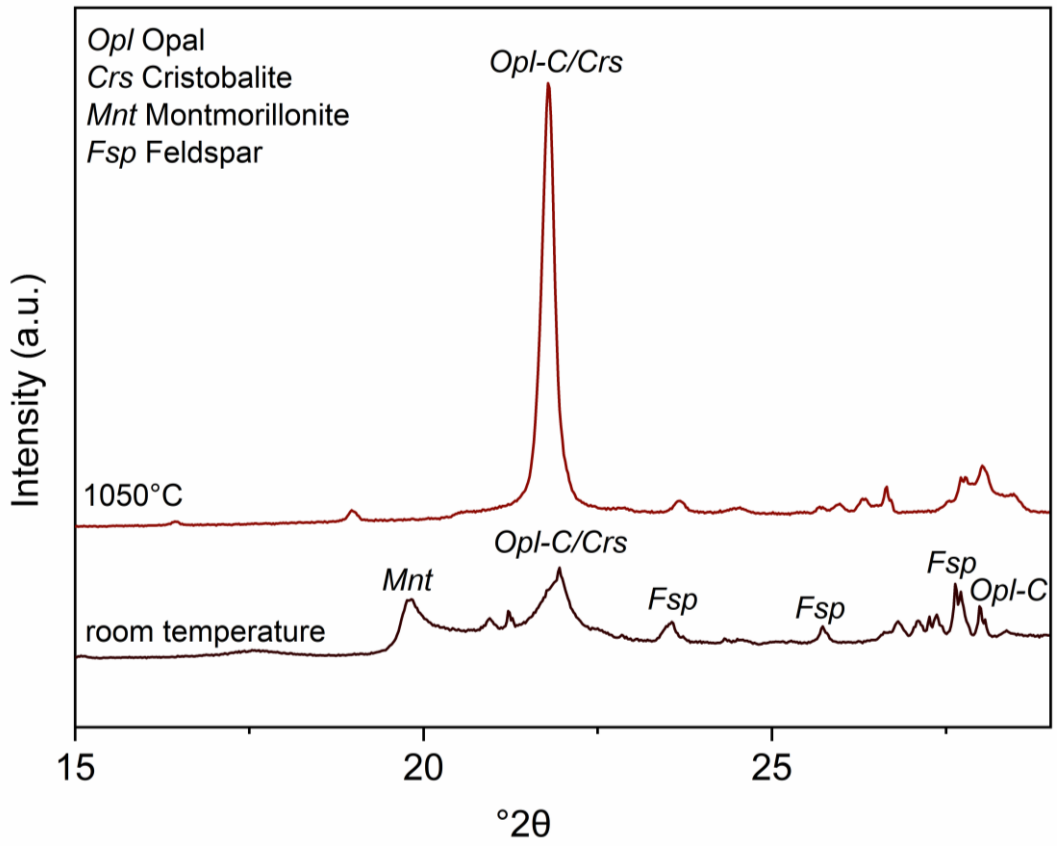

Fig. S13. Qualitative phase analysis of residues (KBE-1 700°C, Ceratosil WG 750°C, and Arginotec INX 750°C) after alkaline treatment in 10.79 mol/L NaOH (7 d reaction time).

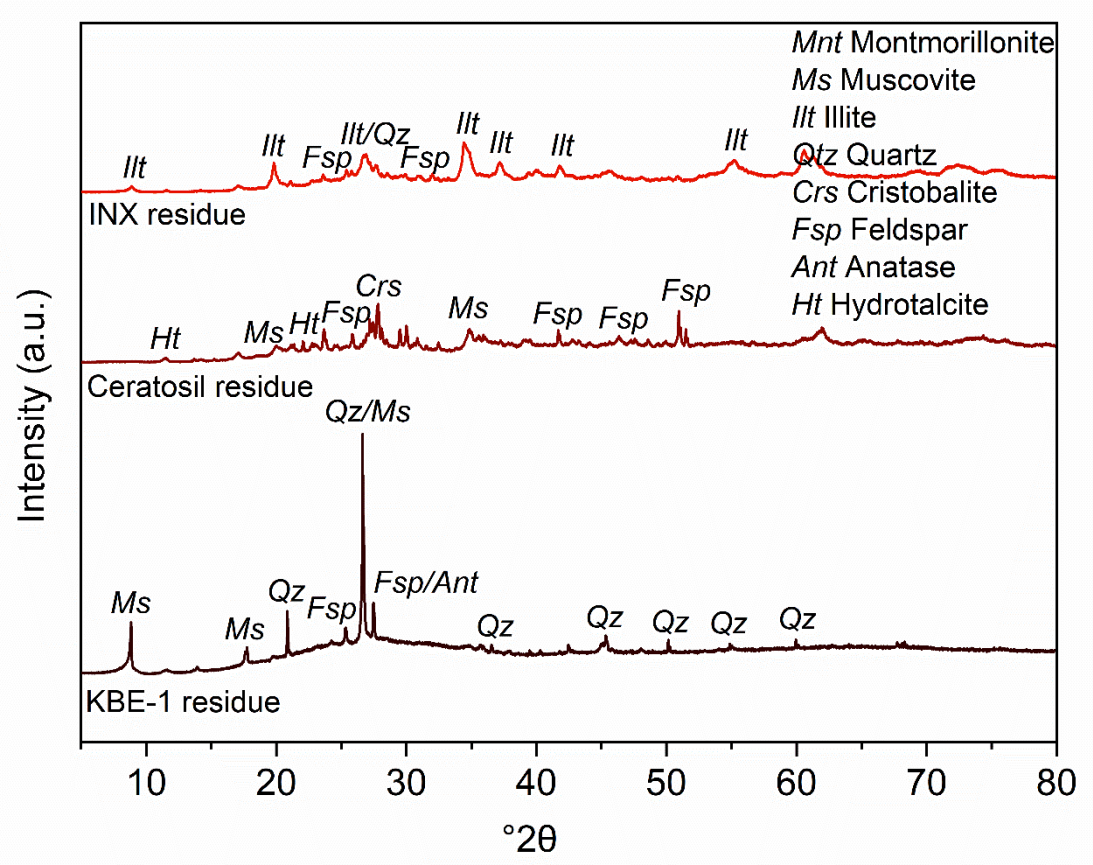

Fig. S14. Solubility of Si of KGa-2 (all NaOH concentrations, reaction time 24 h).

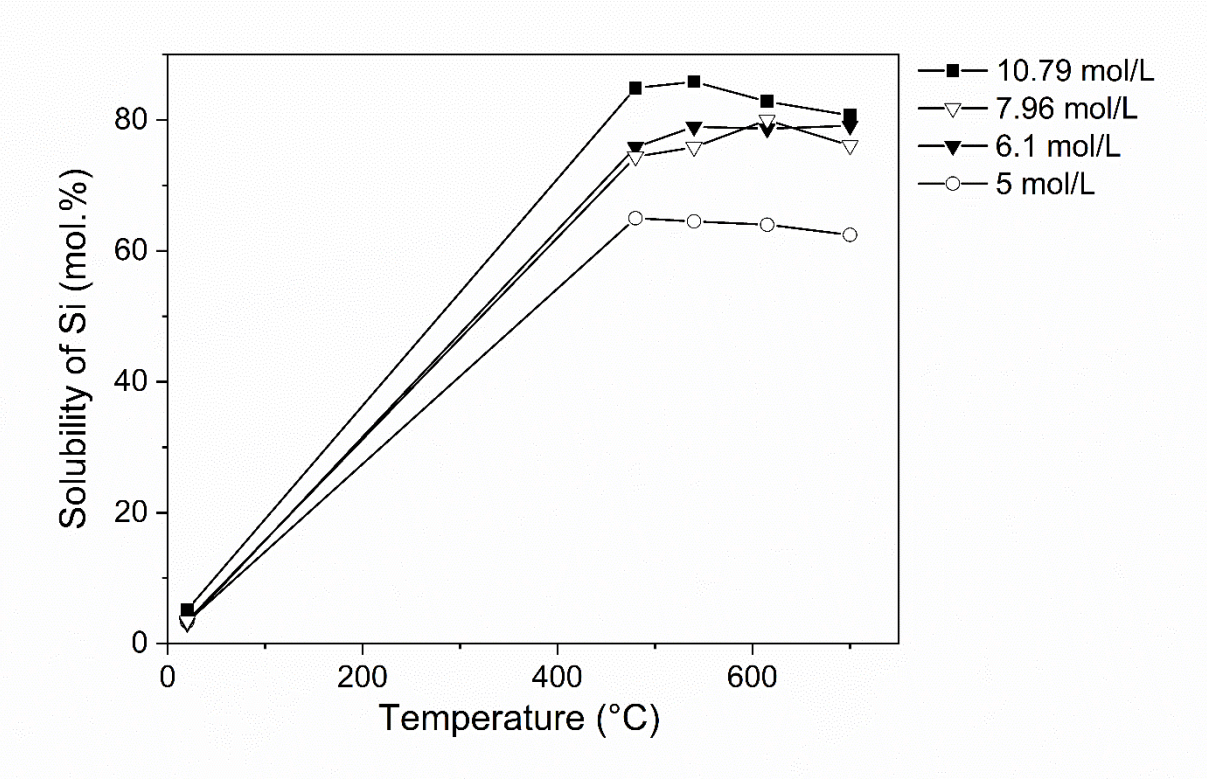

Fig. S15. Solubility of Al of KGa-2 (all NaOH concentrations, reaction time 24 h).

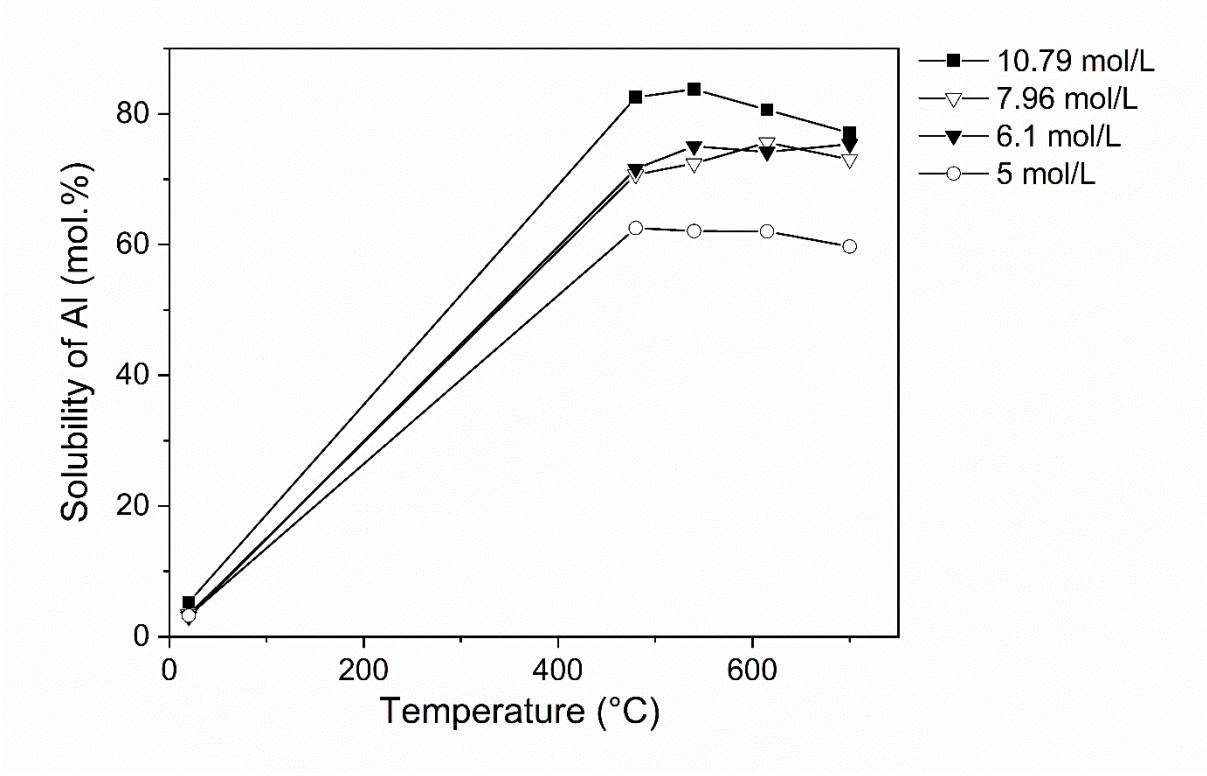

Fig. S16. Solubility of Si of Volclay (all NaOH concentrations, reaction time 24 h).

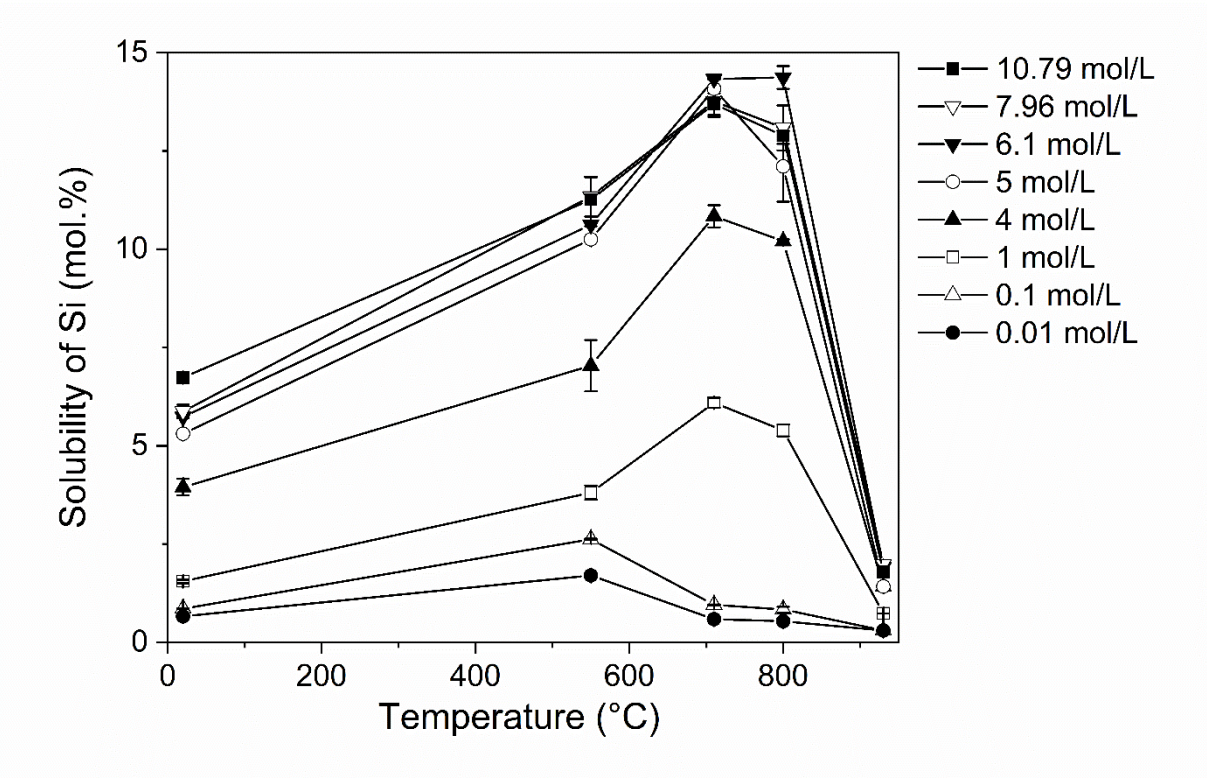

Fig. S17. Solubility of Al of Volclay (all NaOH concentrations, reaction time 24 h).